Coulomb blockade and transfer of electrons one by one

H. Pothier

THESE DE DOCTORAT DE L'UNIVERSITE PARIS 6

Spécialité:

Physique des Solides

présentée par Hugues POTHIER

pour obtenir le titre de DOCTEUR DE L'UNIVERSITE PARIS 6

Sujet de la thèse:

BLOCAGE DE COULOMB ET TRANSFERT D'ELECTRONS UN PAR UN

Soutenue le 16 septembre 1991

devant le jury composé de MM:

J. BOK
C. COHEN-TANNOUDJI
M. DEVORET
K. VON KLITZING
B. PANNETIER

à Katrin, Marjorie, Nathalie, Noëlle et Véronique

REMERCIEMENTS

J'ai eu le bonheur de faire ce travail de thèse dans le groupe de "Quantronique", avec Michel Devoret, Daniel Esteve et Cristian Urbina. Ils m'ont consacré une grande partie de leur temps, et m'ont transmis, outre leur savoir et leur savoir-faire, leur enthousiasme et leur esprit critique. Je les en remercie très sincèrement.

Je remercie Pief Orfila qui, par ses compétences techniques et son esprit d'initiative, a été l'artisan de la réussite des expériences.

Je remercie Emmanuel Turlot d'avoir guidé mes premiers pas au laboratoire.

Philippe Lafarge est depuis un an mon compagnon de tournevis, de potentiomètre et de clavier. L'expérience de la boîte à électrons ("single electron box") que je présente ici est aussi en grande partie la sienne. Travailler en sa compagnie m'a été très agréable.

Edwin Williams nous a apporté ses connaissances, ses astuces et son acharnement lors de cette même expérience. Je l'en remercie.

La partie théorique de cette thèse doit beaucoup à la collaboration avec Hermann Grabert et Gert Ingold de l'Université d'Essen.

La collaboration avec Valérie Anderegg, Bart Geerligs et Hans Mooij a été le véritable point de départ de nos expériences. L'expérience du "turnstile" est le résultat le plus tangible de cette collaboration. Mais ils nous ont aussi appris à fabriquer des échantillons; en nous communiquant régulièrement leurs résultats, et grâce a de nombreuses discussions, ils ont eu une très large part à ce travail.

En plus des compétences scientifiques, je tiens également à remercier Morvan Salez qui, pendant l'année qu'il a passé dans le groupe de Quantronique, y a fait régner une atmosphère constante de bonne humeur.

Je remercie Pierre Bergé de m'avoir accueilli dans le Service de Physique du Solide et de Résonance Magnétique, et Daniel Beysens pour m'avoir permis de continuer ce travail au sein du Service de Physique de l'Etat Condensé. Parmi les physiciens que j'y ai cottoyé et avec qui j'ai eu l'occasion de discuter, je tiens à remercier plus particulièrement Christian Glattli et Marc Sanquer.

J'ai eu la chance de participer pendant ces trois années à plusieurs conférences, et

de visiter plusieurs laboratoires. Chaque discussion, chaque visite m'a un peu plus ouvert les yeux. Je tiens à remercier plus particulièrement Dima Averin, Per Delsing, Klaus von Klitzing, John Martinis, Yuri Nazarov, Jurgen Niemeyer et Stefan Verbrugh.

Lors de la rédaction de cette thèse, j'ai bénéficié des remarques et des conseils fournis de Michel Devoret, Daniel Esteve, Cristian Urbina et Hermann Grabert. Andrew Cleland a bien voulu en plus rectifier mon anglais parfois (souvent?) approximatif. Madame Gaujour a mis son talent dans plusieurs des dessins qui illustrent cette thèse. Je les en remercie vivement.

Mon frère aîné Jacques a eu l'idée de comparer le fonctionnement de notre premier circuit transférant les électrons un par un avec un de ces tourniquets auxquels les utilisateurs du métro parisien (ou New-Yorkais) sont habitués. Merci donc au parrain du "turnstile"!

Je remercie particulièrement Julien Bok, Claude Cohen-Tannoudji, Klaus von Klitzing et Bernard Pannetier d'avoir accepté de faire partie du jury de ma thèse. Leur temps est précieux, et j'apprécie d'autant plus l'intérêt et l'attention qu'ils ont bien voulu porter à mon travail.

Enfin, je suis très reconnaissant envers tous ceux qui m'ont montré que leurs talents de physicien n'excluaient pas leur intérêt pour l'archéologie, l'architecture, la peinture, les enfants ou la clarinette.

TABLE OF CONTENTS

1. INTRODUCTION

Striking photographs of artificial arrangements of a few xenon atoms (Eigler and Schweizer, 1990) and studies of single Rydberg atoms (Goy *et al.*, 1983) recently illustrated the ability of physicists to deal with individual elementary constituents of matter. The trapping of single electrons with electronic and magnetic fields (Van Dyck *et al.*, 1986) had demonstrated before that electrons could also be isolated in vaccuum chambers. In the present work, single electrons are manipulated one by one in the solid state. The metallic circuits we have fabricated are the first genuine "electronic" devices, in the sense that they deal with single electrons at the macroscopic level. They are based on the combination of two well-known ingredients: the quantum tunneling effect and classical electrostatics. Spectacular consequences of such a combination were predicted in 1984 and 1986 (Zorin and Likharev, 1984; Averin and Likharev, 1986): firstly, the tunneling of electrons through a small-capacitance tunnel junction should be suppressed at low temperatures and low voltages because tunneling of a single electron would increase by too large an amount the electrostatic energy of the junction. These authors called this effect the Coulomb blockade of tunneling. Secondly, they predicted the existence of voltage oscillations across a current biased small-capacitance junction. Despite substantial experimental efforts, the Coulomb blockade of tunneling had never been clearly observed in circuits containing only one junction before our work. The reason for this failure is that, in practice, the biasing circuit cannot be made perfect enough to forbid quantum fluctuations of the junction capacitor charge larger than the electron charge e. The starting point of our work is a thorough understanding of how these fluctuations suppress the Coulomb blockade. From this understanding a different approach of the problem emerged. The key concept lies in the fact that the charge on an isolated piece of metal ("island") must correspond to an integer number of electron charges. This quantization of the macroscopic charge results in the quenching of the charge fluctuations and thus leads to Coulomb blockade.

To see this, let us start from the beginning and examine what happens when a battery charges a capacitor. The charge Q on the surface of the metal electrodes of the capacitor arises from the very small displacement of the electrons with respect to the fixed metal ions.

The variable Q is therefore continuous, and is not constrained to be an integer number of elementary charges e. However, if one opens a switch placed between the capacitor and the battery, a metallic island is created. Just as an isolated ion carries a well defined number of electrons, the charge of this island, disconnected from any charge reservoir, corresponds to an integer number of electrons which remains constant. An intermediate situation is achieved when the switch is replaced by a tunnel junction (see Fig. 1.1) with high tunnel resistance R_T. We have called this circuit a "single electron box" (see Fig. 1.2). In the single electron box, electrons are able to tunnel in and out of the island through the junction. The charge which tunnels through the junction can only be an integer number of electron charges. The instantaneous charge of the island, in units of e, is thus constrained to be an integer number n. If one wishes to control this number, its thermal fluctuations have to be suppressed. This is achieved by lowering the temperature until the typical energy k_BT of the fluctuations is much lower than the energy $e^2/2(C + C_S)$ required to charge the island with one electron (C and C_S are the capacitances of the junction and of the capacitor, respectively). Under this condition, the number of electrons in the island will anchor itself to the integer n_{min} which minimizes the electrostatic energy of the whole circuit. In fact, in addition to being subject to thermally induced fluctuations, n is also subject to quantum fluctuations. However, these fluctuations are negligible if $R_T \gg R_K$, where $R_K = h/e^2 \approx 25.8$ kΩ is the resistance quantum. In practice, the conditions needed to observe the anchoring phenomenon can be achieved by fabricating circuits with tunnel junctions with $R_T \approx 100$ kΩ and areas of the order of $(100\ \text{nm})^2$, which results in capacitances below 1 fF. The capacitance C_S can be made smaller than 1 fF by designing a micron size island and avoiding large metallic islands in the neighbourhood. With capacitances of this magnitude, the condition $e^2/2(C + C_S) \gg k_BT$ is satisfied at dilution refrigerator temperatures ($T \approx 50$ mK).

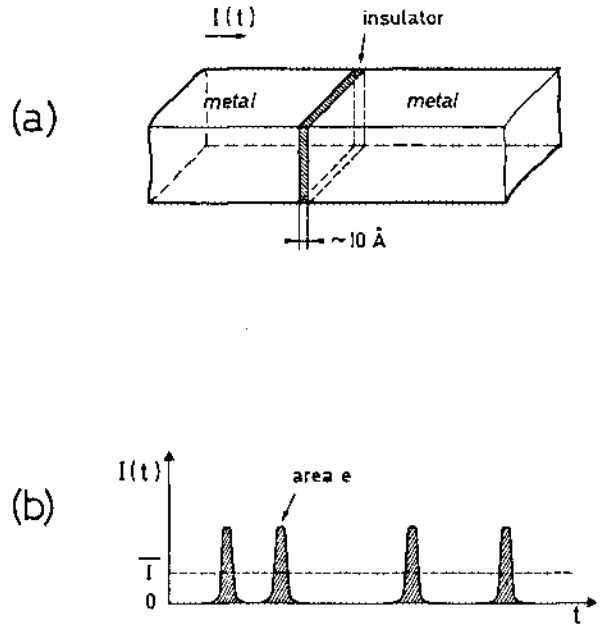

Fig. 1.1 (a) *Tunnel junction: a tunnel junction consists of two pieces of metal separated by a thin insulating layer. This insulator is a tunnel barrier for electrons. The current* I(t) *through such a tunnel junction is proportional to the voltage applied to it (provided the voltage is much lower than the Fermi energies of the metals). The ratio between the voltage and the current defines the "tunnel resistance"* R_T *of the junction. It is generally believed (Averin and Likharev, 1986) that if* R_T *is much larger that the quantum of resistance* $R_K = h/e^2 \simeq 25.8\ \mathrm{k}\Omega$, *the electrons are localized on either side of the junction tunnel barrier. The electrons tunnel through the barrier as separate entities, and this quantum mechanical process occurs in less than* 10^{-15} s. *The current through such a tunnel junction as a function of time* (b) *is then composed of peaks of area e, each one corresponding to the tunneling of a single electron through the tunnel barrier (Fig. 1.1). The time between peaks is a random variable whose average value determines the value of the current. The current noise resulting from this Poisson process is called shot noise; its spectrum at low enough temperature* ($k_B T \ll eR_T I$) *is given by* $S_I(\omega) = eI$. *While this spectrum was measured as early as 1922, the individual peaks have never been observed.*

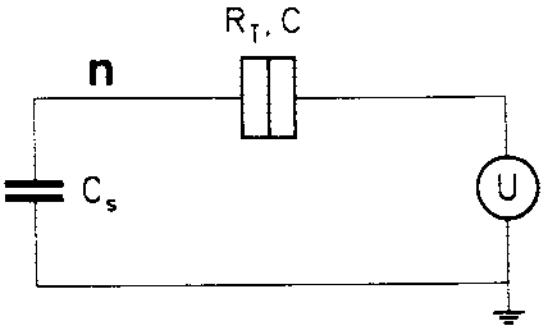

Fig. 1.2 *Single electron box. This basic circuit contains a metallic "island", which is the electrode between the dielectric of the capacitor and the insulating layer of the junction. The number* n *of extra electrons on the island is controlled by a voltage source* U. *The island capacitance is the sum of the junction capacitance* C *and of the capacitance* C_S. R_T *is the junction tunnel resistance.*

ORGANIZATION OF THIS WORK

In chapter 2, we examine how the circuit connected to a small-capacitance tunnel junction influences the tunneling rate of electrons. We show that the tunneling through one junction can be blocked only if the junction is placed in an environment with a high impedance, such as the one provided by i) a small capacitor, ii) another small junction or iii) a very large ohmic resistance (compared to R_K). We show that the simplest way to observe Coulomb blockade of tunneling is in circuits containing a metallic island, such as the electron box and, more generally, in circuits with several junctions connected in series. The case of a large resistor is the most difficult to implement experimentally (Cleland *et al.*, 1990).

The experimental setup, including our filtering and measurement techniques, is presented in chapter 3, together with the computer programs we have used to calculate planar capacitances and to simulate the behaviour of one-dimensional arrays of junctions. We also describe the nanolithography techniques that we used to fabricate the devices.

We describe in chapter 4 the experiment on the electron box, which is the first device containing only one junction to display the Coulomb blockade of tunneling. Furthermore, in this device, we controlled the charge of an island at the level of the single electron charge by applying a capacitively-coupled gate voltage.

At this point, the question naturally arises whether one can also control a current electron by electron. We have designed and operated two devices which achieve this controlled transfer: the "turnstile" and the "pump". Here the transfer is clocked by external signals applied to gates. This is the central subject of chapter 5. At the end of this chapter, applications of pumps and turnstiles to metrology are discussed: circuits manipulating charges in the quantum limit are candidates for a new representation of the ampere, in the same way as Josephson junction arrays provide a representation of the volt and quantum Hall samples a representation of the ohm. The limits in precision of present day single-electron devices are discussed: the most serious source of error to the regular transfer of single electrons is the possibility of simultaneous tunneling through several junctions. This is discussed in appendix 3.

Two papers are included in appendices 4 and 5. Paper 1 (ref. Devoret *et al.*, 1990a) deals with the influence of the electromagnetic environment on the tunneling rate through a tunnel junction. It gives the extension of the calculation of chapter 2 to finite temperatures. The results of paper 1 were developed in later publications (Devoret *et al.*, 1990b; Grabert *et al.*, 1991a&b). Paper 2 describes the first device with which we transferred electrons one by one: a "turnstile", that we operated in collaboration with Geerligs, Anderegg, Holweg and Mooij of T.U. Delft (Geerligs *et al.*, 1990a). This complements chapter 5, where the experimental results were obtained using a different sample. The turnstile and the pump have also been discussed in other publications (Anderegg *et al.*, 1990; Devoret *et al.*, 1991; Pothier *et al.*, 1991a&b; Urbina *et al.*, 1991a&b).

2. LOCAL VERSUS GLOBAL RULES: EFFECT OF THE ELECTROMAGNETIC ENVIRONMENT ON THE TUNNELING RATE OF A SMALL TUNNEL JUNCTION

The environment of a tunnel junction determines the Coulomb blockade of tunneling through it. The understanding of the role of the environment is essential for the design of circuits using the Coulomb blockade of tunneling and for the simulation of their behaviour. The calculations of this chapter show that the tunnel rates in the circuit we designed are given by a simple expression, known as the "global rule". They are used in the SETCAD program presented in section 2.2.2 and are the basis for the chapters 4 and 5.

Historically, the Coulomb blockade of tunneling through a tunnel junction placed in a circuit was described using two simplified approaches. The first one was to assume that, since tunneling occurs fast, only the part of the circuit which is very close to the junction determines the blockade (Likharev and Zorin, 1985): the rest of the circuit "does not have time" to be involved. The radius around the junction which participates was called the "electromagnetic horizon". This radius was thought by some to be determined by the speed of light and the traversal time of tunneling (Büttiker and Landauer, 1986). For others, it was thought to be the distance associated with a "quantum time" $\hbar/\Delta E$, where ΔE is the thermal energy $k_B T$ or eV (Delsing *et al.*, 1989; Nazarov, 1989). Whatever it may be, a local energy change of the system therefore determines the blockade: this gives the local rule (Geigenmüller and Schön, 1989). The second way is to consider the junction and the circuit as a whole coherent unit, and the blockade of tunneling through the junction depends on the energy change of the whole circuit when one electron tunnels: this is the global rule (Geigenmüller and Schön, 1989; Likharev *et al.*, 1989).

Cleland *et al.* (1990) first approached the solution of the problem by considering the quantum fluctuations of the junction capacitor charge due to the electromagnetic environment of the junction. Using a semiclassical picture of tunneling across a junction whose capacitor charge is fluctuating, they found that Coulomb blockade only occurs when the quantum fluctuations of the junction charge are much less than one electron charge.

Here, we present a calculation of the single electron tunneling rate through a junction

connected to an environment of impedance $Z(\omega)$ in the limit of zero traversal time (the case of finite traversal time, which is relevant in semiconductor circuits with Schottky barriers, has been considered by Nazarov (1991)). We treat the environment and the electronic degrees of freedom quantum mechanically, and use the Fermi Golden rule to compute the probability that an electron tunnels and induces an excitation of the environment. These inelastic tunneling channels are the dominant ones only if the fluctuations of the junction charge are much below e. Coulomb blockade occurs when the elastic channel has a vanishing probability: tunneling can then only occur at a bias voltage V large enough to provide an energy eV sufficient to excite the environmental modes. We will finally see in this chapter that although their derivations were not correct, the local and global rules do correspond to two limiting cases of this more general theory taking into account the influence of the environment of the junction.

We first present the general formalism to describe the environment (2.1) and distinguish two types of environment: low-pass and high-pass. For both, we give the hamiltonian of the circuit (2.2.1 and 2.3.1) and calculate the tunneling rate (2.2.2 and 2.3.2) as a function of the impedance of the environment. In the case of a single mode environment, the probabilities of the different channels can be explicitely written down, and the rate has a transparent expression (2.2.2.1). Finally, we conclude on the observability of the Coulomb blockade of tunneling in the low-pass and high-pass cases (2.1.3 and 2.2.3) and summarize the different expressions of the rate (2.4).

2.1. DESCRIPTION OF THE DEGREES OF FREEDOM OF THE CIRCUIT

The circuit embedding the junction consists of the biasing circuits and possibly of other junctions. Since we compute the single electron tunneling rate at the second order in the tunneling hamiltonian, the other junctions can be treated as pure capacitors. Higher order processes ("co-tunneling") are considered in appendix 3. The external circuit is thus an electrical dipole described by a voltage source V is series with an impedance $Z(\omega)$ (see Fig. 2.1). We call the environmental mode those of the circuit consisting of the junction capacitance in parallel with $Z(\omega)$. These modes constitute a set of harmonic oscillators.

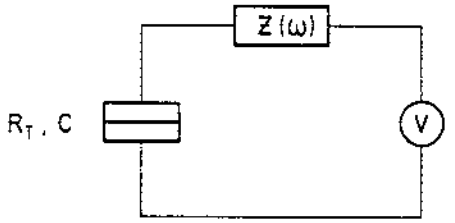

Fig. 2.1 *Small tunnel junction in a linear circuit. Using Thevenin's theorem, the electromagnetic environment of the junction reduces to an impedance* $Z(\omega)$ *in series with a voltage source* V.

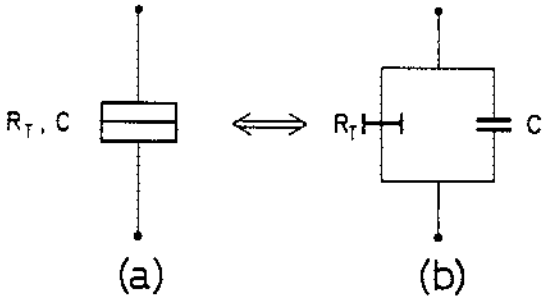

Fig. 2.2 *A tunnel junction* (a) *is symbolized by a double box. It consists of two basic electrical elements* (b)*: a pure tunnel element of tunnel resistance* R_T *(symbolized by a double T) and a capacitance C.*

The electronic degrees of freedom in the junction electrodes, described by quasiparticle states populated according to a Fermi distribution, are assumed to be entirely decoupled, in absence of tunneling, from the electromagnetic degrees of freedom.

2.1.1. Description of the tunnel junction

The tunnel junction is modelled by a capacitor in parallel with a pure tunnel element (Fig. 2.2): the capacitance is the geometrical capacitance between the two electrodes of the junction (denoted in what follows as "left" and "right"), and the pure tunnel element has a tunnel resistance R_T. In the one dimensional model of the tunnel junction, the matrix element t associated with the tunneling through the barrier is related to R_T by

$$\rho_L \rho_R t^2 = R_K/(4\pi^2 R_T) \tag{2.1.1}$$

where ρ_L and ρ_R are the densities of states at the Fermi level on the left and right electrodes, and $R_K = h/e^2$ is the quantum of resistance (Cohen *et al.*, 1962). We assume that the matrix element t is independent of the energy of the incident quasiparticle. This approximation accounts for the linear dependence of the current as a function of the applied voltage in metallic junctions. We will make use of this model in what follows.

2.1.2. The low-pass and high-pass environments

We distinguish two different types of environment differing in the behaviour of their impedance at zero frequency: we call them "low-pass" and "high-pass".

If $Z(\omega)$ does not diverge near $\omega = 0$, there is no capacitance (either a pure capacitor or another junction) in series with the junction: the junction is not connected to an island in the sense described in chapter 1, and tunneling is not expected to be blocked if the circuit always remains in thermal equilibrium. A blockade of tunneling could only result from the dynamics of the environment. In the following, we call an environment which satisfies

$$\lim_{\omega \to 0} \omega Z(\omega) = 0$$

a "low-pass environment". In particular, if $Z(\omega) = 0$ for all frequencies, the charge on the

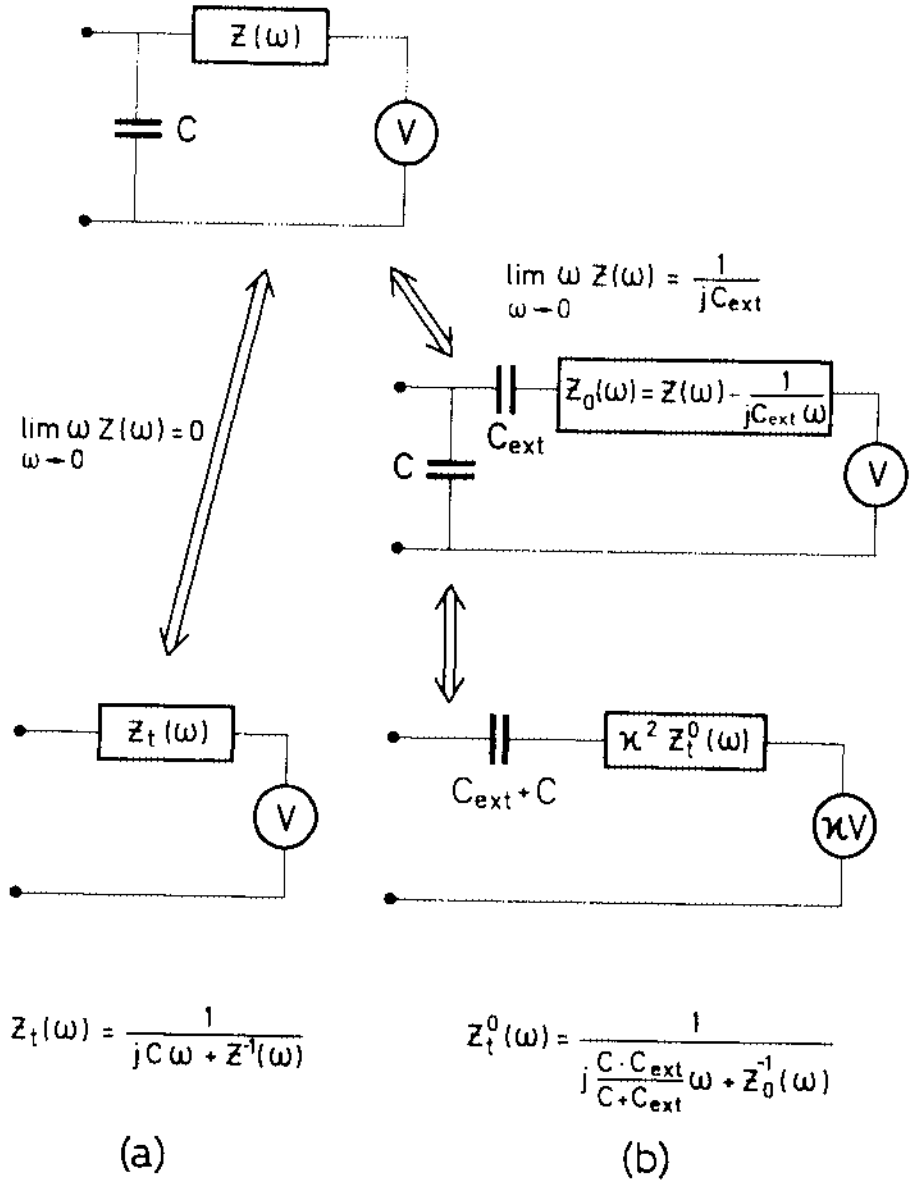

Fig. 2.3 *The circuit seen by the pure tunnel element can be of two types:*
(a) *low-pass: the circuit conducts at dc. It is then equivalent to the impedance* $Z_t(\omega)$ *(defined as the parallel combination of the junction capacitance* C *and the impedance* $Z(\omega)$*) in series with a voltage source* V.
(b) *high-pass: the circuit does not conduct at dc. One electrode of the tunnel junction thus forms an island of capacitance* $C + C_{ext}$. *The rest of the environment acts as a reduced voltage source* κV *and an impedance* $\kappa^2 Z_t^0(\omega)$ *where* $\kappa = C_{ext}/(C + C_{ext})$.

junction does not change after a tunnel event because it is always equal to $q = CV$: there is no Coulomb blockade of tunneling in a perfectly voltage biased junction.

The opposite limit, where $Z(\omega)$ is infinite at all frequencies, corresponds to an ideal current bias. This case was treated by Likharev: he predicted the Coulomb blockade of tunneling. If $Z(\omega)$ diverges only at $\omega = 0$, which we call a "high-pass environment", the electrons tunneling through the junction charge an island: we showed in section 1.3 that the charge doesn't fluctuate thermally (if $k_B T << e^2/2C$) or quantum mechanically (if $R_T >> R_K$) on this island except for particular values of the voltage bias, and tunneling is expected to be blocked even when the junction is in thermal equilibrium. Therefore, the low-pass and the high-pass cases will be treated separately.

2.1.3. The electromagnetic environment of the pure tunnel element

Using Thevenin's and Norton's theorems, we reduce the circuit connected to the pure tunnel element by an effective impedance $Z_{eff}(\omega)$ in series with an effective voltage source V_{eff}.

If the impedance $Z(\omega)$ is such that

$$\lim_{\omega \to 0} \omega Z(\omega) = 0,$$

(low-pass environment) this effective impedance is

$$Z_{eff}(\omega) = Z_t(\omega) = (jC\omega + 1/Z(\omega))^{-1} \tag{2.1.2}$$

and the effective voltage source is $V_{eff} = V$ (Fig. 2.3a).

If, on the contrary, the impedance $Z(\omega)$ is such that

$$\lim_{\omega \to 0} \omega Z(\omega) \neq 0,$$

(high-pass environment) we define a capacitance C_{ext} by

$$1/(jC_{ext}) = \lim_{\omega \to 0} \omega Z(\omega)$$

and an impedance $Z_0(\omega) = Z(\omega) - 1/(jC_{ext}\omega)$. Then

$$Z_{eff}(\omega) = 1/\left[j\left(C + C_{ext}\right)\omega\right] + \kappa^2 Z_t^0(\omega) \tag{2.1.3}$$

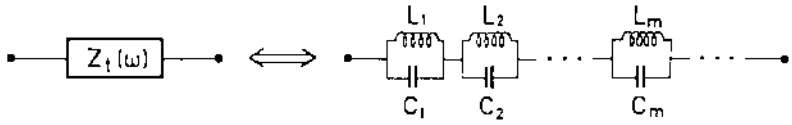

Fig. 2.4 *Decomposition of a low pass environment impedance* $Z_t(\omega)$ *into an infinite collection of* LC *oscillators.*

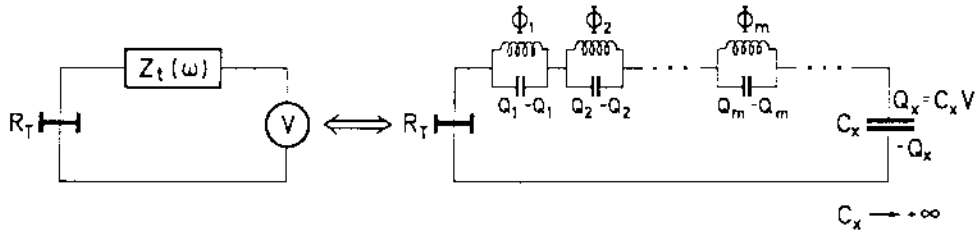

Fig. 2.5 *Quantum mechanical operators used in the hamiltonian description of the environment of the pure tunnel element:* Φ_m *is the flux in the inductor* L_m, Q_m *is the charge on the capacitor* C_m. *The voltage source is modelled by an infinite capacitor* C_x, *charged by* Q_x.

where

$$Z_t^0(\omega) = (j\frac{CC_{ext}}{C+C_{ext}}\omega + 1/Z_0(\omega))^{-1}$$

and $\kappa = C_{ext}/(C+C_{ext})$ (see Fig. 2.3b). The voltage source is also reduced into $V_{eff} = \kappa V$. The impedance $Z_t(\omega)$ or $Z_t^0(\omega)$ has no poles at $\omega = 0$ or $\omega = \infty$. Since it is the Fourier transform of a causal response function, and since the function

$$z(\omega) = Z_t(\omega) - \lim_{\omega \to 0}(Z_t(\omega))$$

is a complex function of the real variable ω, the function $z(p)$, where the complex variable p replaces ω, is analytical and regular in the half plane where $\mathrm{Im}(p) \leq 0$ (see Abragam, 1961). Therefore,

$$z(\omega) = \lim_{\epsilon \to 0^-}(z(\omega + i\epsilon)).$$

When modellizing an impedance, it must be taken care that this latter relation, equivalent to the Kramers-Krönig relations, is satisfied. For example, the correct expression for the impedance of a parallel LC circuit is:

$$Z_{LC}(\omega) = \frac{jL\omega}{1-LC\omega^2} + \frac{\pi}{2C}\left(\delta(\omega - (LC)^{-1/2}) - \delta(\omega + (LC)^{-1/2})\right)$$

The real part of the impedance $Z_t(\omega)$, properly written to satisfy the Kramers-Krönig relations, defines completely the impedance, and can be written as:

$$\mathrm{Re}\,(Z_t(\omega)) = \lim_{\Delta\omega \to 0}\left(\sum_{m=1}^{\infty}\frac{\pi}{C_m}\delta(\omega - m\Delta\omega)\right),$$

where the parameters C_m are real. Note that there is no term at $m = 0$ because $Z_t(\omega)$ has no pole at $\omega = 0$. Since $\mathrm{Re}\,(Z_t(\omega))$ is an even function, it can also be written as:

$$\mathrm{Re}\,(Z_t(\omega)) = \lim_{\Delta\omega \to 0}\left(\sum_{m=1}^{\infty}\frac{\pi}{2C_m}(\delta(\omega - w_m) - \delta(\omega + \omega_m))\right), \qquad (2.1.4)$$

where $\omega_m = m\Delta\omega$. Each term of the sum is the real part of the impedance of a parallel LC circuit of capacitance C_m and inductance $L_m = \left(C_m\omega_m^2\right)^{-1}$. Therefore, $Z_t(\omega)$ can be treated as an infinte collection of LC oscillators (see Fig. 2.4).

2.2. LOW-PASS ENVIRONMENT

2.2.1. The hamiltonian of the circuit

We make the hypothesis that in absence of tunneling the circuit can be described by two independent types of degrees of freedom: the quasiparticle operators in both junction electrodes ("left" and "right", corresponding respectively to the bottom and top electrodes of Fig. 2.5). Quasiparticle states are supposed to be populated according to Fermi distributions in both electrodes. We call μ_L and μ_R the electrochemical potentials of both electrodes. In order to describe the junction in its electromagnetic environment, we define a flux $\Phi(t)$:

$$\Phi(t) = \int_{-\infty}^{t} dt' \ \left(\mu_L(t') - \mu_R(t')\right)/e$$

The voltage source is described by a huge capacitor C_X charged with Q_X^t through a very large inductance L_X placed in parallel with C_X, such that

$$\lim_{C_X \to \infty} \frac{Q_X^t}{C_X} = V.$$

When n_t quasiparticles have tunneled from the right to the left (from the top to the bottom in Fig. 2.5), the charge of this capacitor is $Q_X = Q_X^t - n_t e$.

We call $Q_m^t(t) = -\int_{-\infty}^{t} \Phi_m(t')/L_m \ dt'$ the charge that went through the inductor L_m, the current Φ_m/L_m being the current in inductor L_m from the left to the right in Fig. 2.5. Then $Q_m^t = Q_m + n_t e$. Since $\dot{Q}_m^t = -\Phi_m/L_m$, the electromagnetic part of the circuit can be described in Hamilton's formalism with the variables Φ_m and Q_m^t. It is obtained by summing the electric and magnetic energies stored in all the capacitors and inductances of the circuit. It reads:

$$H\left(\Phi_m, Q_m^t\right) = \sum_m \left(\frac{\Phi_m^2}{2L_m} + \frac{\left(Q_m^t - n_t e\right)^2}{2C_m} \right) + \frac{\left(Q_X^t - n_t e\right)^2}{2C_X}$$

This hamiltonian accounts for the classical equations of the circuit:

$$\dot{\Phi}_m = \frac{\partial H}{\partial Q_m^t} = \frac{Q_m}{C_m};$$

$$\dot{Q}_m^t = -\frac{\partial H}{\partial \Phi_m} = -\frac{\Phi_m}{L_m}.$$

The flux Φ_X through L_X is conjugated to Q_X^0. The fluxes Φ_m and the flux Φ_X are related to the flux through the tunnel element by:

$$\Phi = \sum_m \Phi_m + \Phi_X \tag{2.2.1}$$

The conjugated variables Φ_m and Q_m^t are in a quantum treatement of the circuit conjugated operators, and their commutator is

$$\left[\Phi_m, Q_m^t\right] = i\hbar.$$

The hamiltonian of the circuit reads then:

$$H_{em} = \sum_m \left(\frac{\Phi_m}{2L_m} + \frac{\left(Q_m^t - n_t e\right)^2}{2C_m} \right) + \frac{\left(Q_X^0 - n_t e\right)^2}{2C_X}. \tag{2.2.2}$$

With the sign conventions chosen for the charges and the currents, fluxes are position-like operators and charges are momentum-like operators: in particular,

$$\Phi_m = \sqrt{\frac{\hbar Z_m}{2}} \left(c_m + c_m^\dagger\right) \tag{2.2.3}$$

$$Q_m^t = \sqrt{\frac{\hbar}{2Z_m}} \left(\frac{c_m - c_m^\dagger}{i} \right) \tag{2.2.4}$$

where c_m is the bosonic annihilation operator of a photon in the harmonic oscillator m.

Quasiparticles are described by the hamiltonian:

$$H_{qp} = \sum_{k_L} \epsilon_{k_L} n_{k_L} + \sum_{k_R} \epsilon_{k_R} n_{k_R} \tag{2.2.5}$$

where k_L indexes states in the left electrode and k_R in the right electrode; $n_{k_L} = a_{k_L}^\dagger a_{k_L}$; $n_{k_R} = a_{k_R}^\dagger a_{k_R}$ where $a_{k_L}^\dagger$ and a_{k_L} are the fermionic quasiparticle creation and annihilation operators in the left electrode, $a_{k_R}^\dagger$ and a_{k_R} in the right one; ϵ_{k_R} and ϵ_{k_L} denote the kinetic energies of quasiparticle states k_R and k_L. The number of quasiparticles n_t that went through the tunnel element is related to the total numbers $n_L = \sum_{k_L} a_{k_L}^\dagger a_{k_L}$ and $n_R = \sum_{k_R} a_{k_R}^\dagger a_{k_R}$ of quasiparticles in the left and right electrodes:

$$n_t = \frac{1}{2}\left(n_R - n_L\right).$$

The tunneling hamiltonian is written in the usual way (Cohen et *al.*, 1962):

$$H_t = \sum_{L,R} t a^\dagger_{k_L} a_{k_R} + \text{h.c.} \tag{2.2.6}$$

The relation between t and R_T is given by (2.1.1). The total hamiltonian is:

$$H = H_{qp} + H_{em} + H_t. \tag{2.2.7}$$

In this hamiltonian, quasiparticles are charged: the number n_t of quasiparticles which have tunneled through the tunnel element interact with the charges of all the capacitors of the circuit. This is no longer the case in the base deduced from the former one by the unitary transformation defined by the operator $U = e^{ien_t\Phi/\hbar}$, where a wave function $|\Psi\rangle$ transforms into $|\Psi\rangle' = U|\Psi\rangle$, and where the hamiltonian is deduced from the former one by:

$$H \rightarrow UHU^{-1}.$$

This unitary transformation transforms H_{em} into

$$H_{EM} = \sum_m \left(\frac{\Phi_m}{2L_m} + \frac{(Q^t_m)^2}{2C_m} \right) + \frac{(Q^0_X)^2}{2C_X} \tag{2.2.8}$$

where Q^t_m must now be interpreted as the charge of the junction in the former basis:

$$'\langle\Psi| Q^t_m |\Psi\rangle' = \langle\Psi| e^{-ien_t\Phi/\hbar} Q^t_m e^{ien_t\Phi/\hbar} |\Psi\rangle = \langle\Psi| Q_m |\Psi\rangle .$$

and Q^0_X as the charge of the capacitor C_X in the former basis. Therefore, in what follows, we will write Q_m for Q^t_m and Q_X for Q^0_X.

H_{qp} remains unchanged in the unitary transformation:

$$H_{qp} \rightarrow H_{QP} = H_{qp}$$

The unitary transformation transforms H_t into

$$H_T = \sum_{L,R} t a^\dagger_{k_L} a_{k_R} \exp(ie\Phi/\hbar) + \text{h.c.} \tag{2.2.9}$$

The effect of the hamiltonian H_T is to "kick" the electromagnetic environment states: according to relation (2.2.1), the operator $\exp(ie\Phi/\hbar)$ shifts the charge the charge of each oscillator and the charge Q_X^0 on the "source" capacitor C_X by $-e$. These shifts can possibly excite the electromagnetic degrees of freedom.

We assume that the environment is in its ground state $|G\rangle\,|Q_X\rangle$ before each tunnel event (or is in thermodynamic equilibrium at finite temperature, see 2.2.2.4). This is only valid if the characteristic relaxation time of the environment τ is much shorter than the time between tunnel events e/I, where I is the dc current through the tunnel element. Since the current I is at most V/R_T, this condition reads

$$V \ll \frac{eR_T}{\tau}$$

After a tunnel event from the left electrode to the right electrode, the environment is in a state described by:

$$|N\rangle\,|Q_X - e\rangle = |\ N_1\ N_2\ \ldots\ N_m\ \ldots\ \rangle\,|Q_X - e\rangle$$

The initial and final quasiparticle states are denoted by:

$$|\ I\ > = |\ \ldots\ k_{L-1}\ k_L\ k_{L+1}\ \ldots\ > |\ \ldots\ k_{R-1}\ k_{R+1}\ \ldots\ >$$

and

$$|\ \mathcal{F}\ > = |\ \ldots\ k_{L-1}\ k_{L+1}\ \ldots\ > |\ \ldots\ k_{R-1}\ k_R\ k_{R+1}\ \ldots\ >$$

The complete initial and final states of the system are of the form:

$$|\ i\ > = |\ I\ > |\ G\ > |Q_X\rangle\,;$$

$$|\ f\ > = |\ \mathcal{F}\ > |\ N\ > |Q_X - e\rangle$$

We compute the probability per unit time that an electron tunnels from left to right by using Fermi's Golden Rule

$$P_{l\to r} = \sum_{i,f} \frac{2\pi}{\hbar}\ |<\ i\ |\ H_T\ |\ f\ >|^2\ \delta(E_i - E_f) \qquad (2.2.10)$$

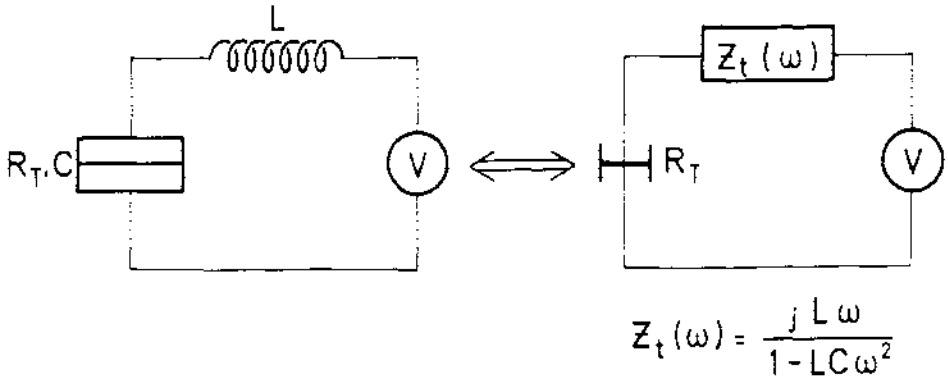

Fig. 2.6 *Tunnel junction biased by a voltage source* V *through an inductor* L. *The circuit seen by the tunnel element is the parallel combination* $Z_t(\omega)$ *of the capacitance* C *of the junction and of the impedance* L.

All the oscillators are in their ground state before the tunnel event. The conservation of energy forbids transition to states where the energy of the environmental state is higher than eV. The total tunnel probability is therefore reduced by the existence of this excited states. This contributes to the Coulomb blockade of tunneling. The calculation at zero temperature is done in detail in the following section; the finite temperature is developed in paper 1.

2.2.2. Tunneling rate calculation

2.2.2.1. The basic calculation: one junction in series with an inductance at zero temperature

Let us consider the circuit of Fig. 2.6, where the environment reduces to an inductance L and a voltage source V. Following section 2.1,

$$Z_t(\omega) = \frac{jL\omega}{1-LC\omega^2} + \frac{\pi}{2C}\left(\delta(\omega-\omega_1) - \delta(\omega+\omega_1)\right)$$

The circuit has only one mode, of pulsation $\omega_1 = (LC)^{-1/2}$. The system state is given by

the number N of photons in this mode, by the charge Q_X on the capacitor modelling the voltage source, and by the quasiparticle occupation numbers. The initial oscillator state is $|0>$ and all quasiparticle states below the Fermi energy are occupied in both electrodes. Since $\Phi = \Phi_1 + \Phi_X$, and since Φ_1 acts only on the oscillator state and Φ_X only on the charge on the source capacitor Q_X,

$$\exp(ie\Phi/\hbar)\,|0\rangle\,|Q_X\rangle = \exp(ie\Phi_1)\,|0\rangle\exp(ie\Phi_X)\,|Q_X\rangle$$

Since

$$\exp(ie\Phi_1/\hbar)\mid 0>=\exp(-r/2)\sum_{N=0}^{+\infty}\frac{(i\sqrt{r})^N}{\sqrt{N!}}\,|N\rangle \tag{2.2.11}$$

where

$$r=\frac{\pi Z}{R_K}=\frac{e^2/2C}{\hbar\omega_1}$$

with

$$Z=\sqrt{\frac{L}{C}},$$

the oscillator has a probability of absorbing any number of photons (Fig. 2.7). The probability of absorbing N photons is given by

$$r^N\exp(-r)/N!$$

The projection of the translated ground state wave function onto the wave functions of the oscillator states with N photons is therefore determined by r. If $r \ll 1$, the dominant component of the translated state is the ground state itself; if $r \gg 1$, the dominant component of the translated state are the states with energy near $e^2/2C$.

The oscillator energy in the state $|N\rangle$ is $(N+1/2)\hbar\omega_1$; in the ground state, it is $\hbar\omega_1/2$. Since

$$\exp(ie\Phi_X)\,|Q_X\rangle = |Q_X - e\rangle$$

the final source energy is $(Q_X-e)^2/2C_X$ and the initial same energy is $Q_X^2/2C_X$. We now take the limit where Q_X and C_X go to infinity in such a way that $V = Q_X/C_X$ and find that the work performed by the source is given by

$$\lim_{Q_X,C_X\to\infty}\left(\frac{(Q_X-e)^2}{2C_X}-\frac{Q_X^2}{2C_X}\right)=-eV. \tag{2.2.12}$$

Thus, the energy difference of the entire system between the final and initial states is $E_f - E_i = (E_{\mathcal{F}} - E_{\mathcal{I}}) + N\hbar\omega_1 - eV$ where $E_{\mathcal{F}} - E_{\mathcal{I}}$ is the energy given to the quasiparticles (at zero temperature, $E_{\mathcal{F}} - E_{\mathcal{I}} \geq 0$).

The only allowed transitions are those conserving the global energy of the circuit. Therefore the transition to the state with N photons is forbidden if $eV < N\hbar\omega_1$. At voltages multiple of $\hbar\omega_1/e$ a new channel for conduction opens. If $r \ll 1$, all the weight of the translated oscillator state is in the ground state, which is at the same energy than the initial state: the dominant conduction chanel is "opened" as soon as V is finite, which corresponds to the absence of blockade of tunneling. On the other hand, if $r \gg 1$, the dominant conduction channels open only at voltages around $e/2C$, which corresponds to a blockade of tunneling at lower voltages.

If $eV > N\hbar\omega_1$, the excess energy $eV - N\hbar\omega_1$ is absorbed by quasiparticles. We make the asumption that the density of states ρ_L and ρ_R in the electrodes are constant. The number of combinations of states in the left and the right electrodes such that $\epsilon_{k_L} + \epsilon_{k_R} = eV - N\hbar\omega$ is directly proportional to $eV - N\hbar\omega$. Therefore, the tunneling rate from left to right in a low-pass environment Γ_L reads:

$$\Gamma_L = \frac{1}{2R_T C} e^{-r} \sum_{N \leq rV/(e/2C)} \frac{r^N}{N!} \left(\frac{V}{e/2C} - \frac{N}{r} \right) \tag{2.2.13}$$

and the current is given by $I = e\Gamma_L$ since the tunneling rate from right to left is zero at zero temperature. The corresponding current-voltage characteristic and its derivative are shown in Fig. 2.8.

Note that the transition probability corresponding to the elastic channel $N = 0$ is finite. This means that when the electron tunnels, the source can perform the work eV instantaneously and without exciting the oscillator. This seems paradoxical in a classical approach since the source is usually much farther than the junction "electromagnetic horizon", which is the speed of light multiplied by the tunneling time (10^{-15} s). The solution to this paradox is that the system behaves quantum mechanically: the junction and the source are in a coherent state. When this state changes both junction and source are affected at the same time. This elastic tunneling is similar to the recoilless emission of a γ ray by an atom in a crystal (Mössbauer effect).

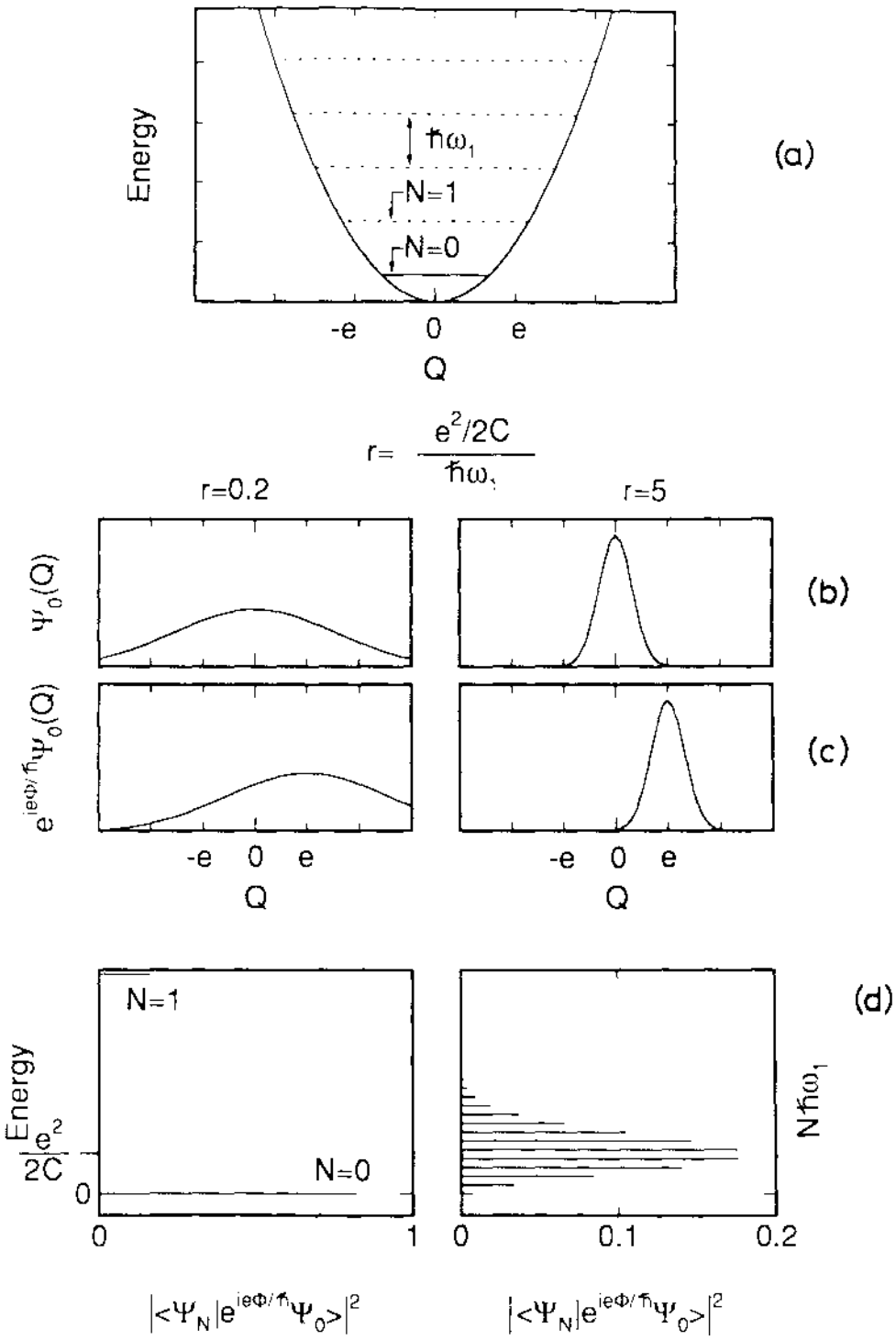

Fig. 2.7 *Effect of the tunnel hamiltonian* H_T *on the environmental oscillator 1 with energy level spacing* $\hbar\omega_1$ (a). *Initially the oscillator is in its ground state* $N = 0$ (b). *After a tunnel event, the wave function* $\Psi_0(Q)$*of the oscillator is shifted by* e (c). *Depending on the ratio* r *of the charging energy* $e^2/2C$ *and the energy level spacing* $\hbar\omega_1$, *the main component of* $e^{ie\Phi/\hbar}\Psi_0$ (b) *is state* $N = 0$ $(r \ll 1)$ *or the state whose energy is closest to* $e^2/2C$ $(r \approx N)$.

2.2.2.2. General calculation at zero temperature

At zero temperature, the environment ground state has no photon present,

$$|G\rangle = |\ 0\ 0\ ...\ 0\ \rangle\ ,$$

and $E_G = 0$. After a tunneling event, the energy ϵ_L of the hole created in the left electrode and the energy ϵ_R of the electron created in the right one are positive. The kinetic energies of all the other quasiparticles remain unchanged. Using the Fermi statistics of quasiparticles and Eq. (2.2.10) we express the total tunneling rate Γ_L, where now there are an arbitrary number of environmental modes available:

$$\Gamma_L = \sum_N \frac{2\pi}{\hbar} \int_0^{+\infty} d\epsilon_L \int_0^{+\infty} d\epsilon_R \rho_L \rho_R \left|\langle i \left| H_T \right| f \rangle\right|^2 \times \delta\left(\frac{Q_X^2}{2C_X} - \left(\epsilon_L + \epsilon_R + E_N + \frac{(Q_X - e)^2}{2C_X}\right)\right) \quad (2.2.14)$$

Since $E_N \geq E_G$, $\epsilon_L + \epsilon_R \leq eV$, we introduce $E' = -\epsilon_L + eV (\geq 0)$ and $E'' = \epsilon_R (\leq E')$. Making use of equation (2.2.12), the argument of the delta function reads $(E' - E'' - E_N)$. Noting now that in equilibrium $\langle \Phi \rangle = \langle \Phi_X \rangle$ and that $\langle Q_X \left| \exp(ie\Phi_X) \right| Q_X - e \rangle = 1$, we define $\varphi = \Phi - \Phi_X$ and obtain:

$$\Gamma_L = \frac{2\pi \rho_L \rho_R t^2}{\hbar} \int_0^{eV} dE' \int_0^{E'} dE''\ P\left(E' - E''\right) \quad (2.2.15)$$

where

$$P(E) = \sum_N \left|\langle G \left| \exp\left(ie\varphi/\hbar\right) \right| N \rangle\right|^2 \delta\left(E - E_N\right) \quad (2.2.16)$$

Note that the function $P(E)$ is normalized:

$$\int_{-\infty}^{+\infty} P(E)\ dE = 1 \quad (2.2.16')$$

We now calculate the Fourier transform of $P(E)$: the relations

$$\delta\left(x\right) = \frac{1}{2\pi} \int_{-\infty}^{+\infty} e^{ixu} du$$

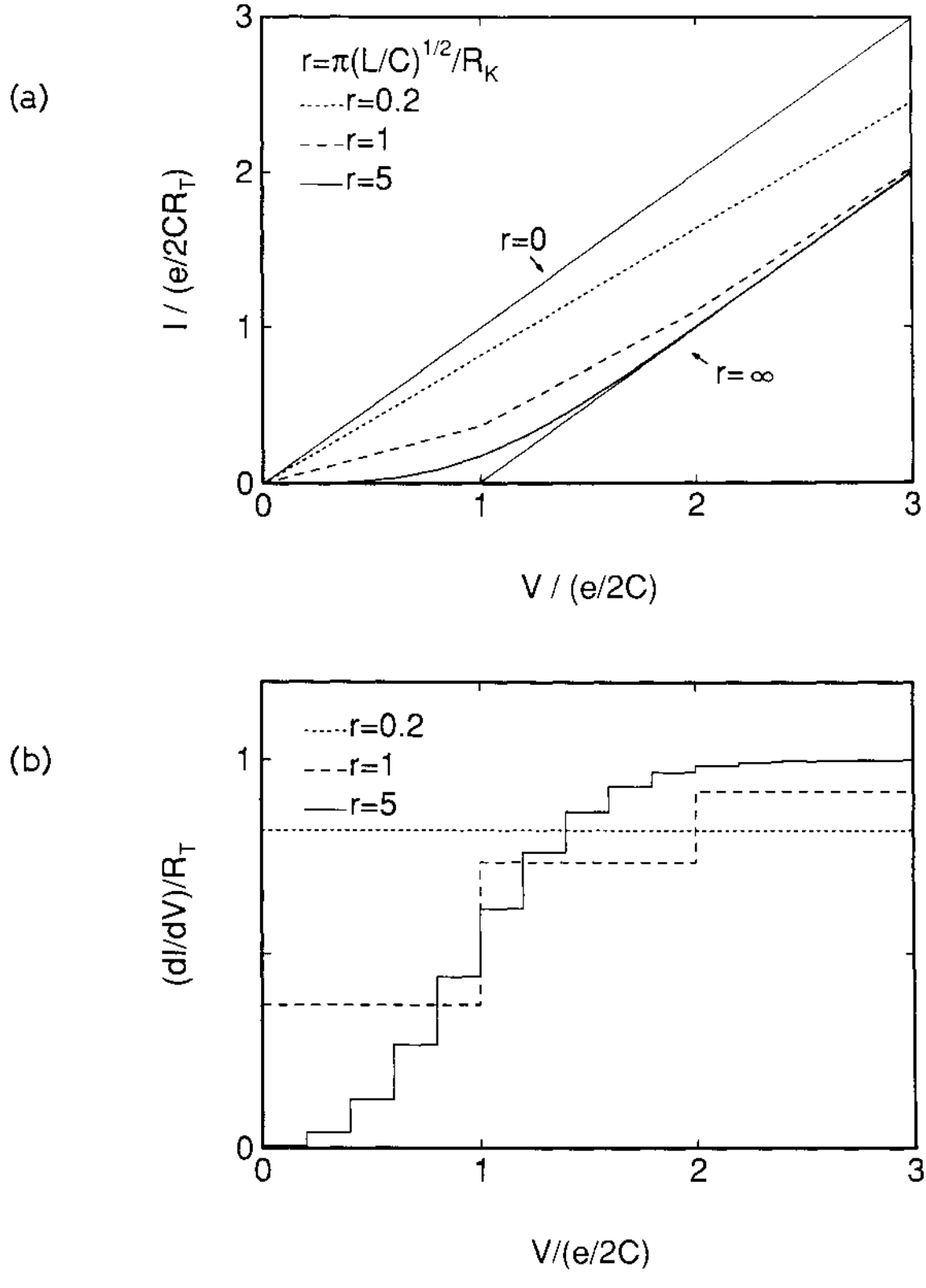

Fig. 2.8 I − V *characteristic* (a) *and its derivative* (b) *for a tunnel junction biased with a voltage* V *through an inductance* L *for the values of* $r = \pi(L/C)^{1/2}/R_K$ *of* Fig. 2.7: $r = 0.2$ *(dotted line) and* 5 *(full line); we have also represented* $r = 1$ *(dashed line), and in* (a) *the* $r \to 0$ *and* $r \to \infty$ *limits with thin continuous lines.*

where

$$c_m(t) = c_m e^{-i\omega_m t},$$
$$Z_m = \sqrt{\frac{L_m}{C_m}},$$

and

$$\omega_m = \frac{1}{\sqrt{L_m C_m}}.$$

By making use of Eq. (2.1.4), we finally arrive at:

$$R(t) = \frac{2}{R_K}\int_0^\infty \frac{d\omega}{\omega}\mathrm{Re}\left[Z_t(\omega)\right]e^{-i\omega t} \tag{2.2.20}$$

and

$$J(t) = -2i\int_0^t dt' \int_0^\infty d\omega \frac{\mathrm{Re}(Z_t(\omega))}{R_K} e^{-i\omega t'}, \tag{2.2.21}$$

where $R_K = h/e^2$.

Expressions (2.2.15), (2.2.17), (2.2.18) and (2.2.20) when combined, provide the relation between the impedance $Z_t(\omega)$ and the $I-V$ characteristic of the junction. We combine (2.2.17) and (2.2.18) to write

$$P(E) = \frac{1}{2\pi\hbar}\int_{-\infty}^{+\infty} dt\, \exp\left(J(t) + \frac{iEt}{\hbar}\right), \tag{2.2.22}$$

and write (2.2.15) as

$$\begin{aligned}\Gamma_L &= \frac{1}{e^2 R_T}\int_0^{eV} dE' \int_0^{E'} dE'' P(E'-E'') \\ &= \frac{1}{e^2 R_T}\int_0^{eV} dE \int_0^{E} dE'\ P(E').\end{aligned} \tag{2.2.23}$$

The current is simply given by $I = e\Gamma_L$.

This formula can be implemented on a computer equipped with Fast Fourier Transform and integration algorithms. Some care must be taken, however, if $Z_t(\omega)$ does not vanish for $\omega \to 0$. This point is discussed further in section 2.2.2.3.

$$e^{\frac{i}{\hbar}(E_G - E_N)t} \langle G | X | N \rangle = \left\langle G \left| e^{\frac{i}{\hbar} H_{osc} t} X e^{-\frac{i}{\hbar} H_{osc} t} \right| N \right\rangle$$

$$= \langle G | X(t) | N \rangle$$

$$\sum_N |N\rangle \langle N| = 1$$

(where X is an operator; here $X = \exp(ie\varphi/\hbar)$) lead to

$$P(E) = \int_{-\infty}^{+\infty} \frac{dt}{2\pi\hbar} e^{iEt/\hbar} \tilde{P}(t) \tag{2.2.17}$$

with

$$\tilde{P}(t) = \langle G | \exp(ie\varphi(t)/\hbar) \exp(-ie\varphi(0)/\hbar) | G \rangle \tag{2.2.17'}$$

We now make use of the Glauber identity (see Cohen-Tannoudji, 1973)

$$\langle G | \exp(A) \exp(B) | G \rangle = \exp\left\{ \frac{1}{2} \left\langle G \left| (A+B)^2 + [A,B] \right| G \right\rangle \right\},$$

where A and B are operators linear in the bosonic creation c_m and annihilation $c_m^\dagger$ operators of the set of harmonic oscillators describing $Z_t(\omega)$, and get

$$\tilde{P}(t) = exp[J(t)], \tag{2.2.18}$$

where

$$J(t) = R(t) - R(0) \tag{2.2.18'}$$

with

$$R(t) = (e^2/\hbar^2) \langle G | \varphi(t) \varphi(0) | G \rangle . \tag{2.2.18''}$$

We now use the relation (2.2.1) which reads

$$\varphi = \Phi - \Phi_X = \sum_m \Phi_m$$

and obtain

$$\varphi(t) = \sum_m \sqrt{\frac{\hbar Z_m}{2}} \left(c_m(t) + c_m^\dagger(t) \right), \tag{2.2.19}$$

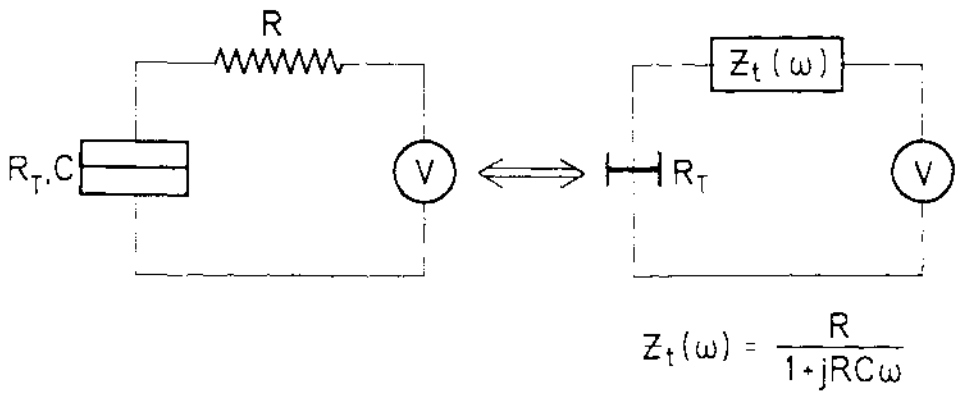

Fig. 2.9 *Tunnel junction biased by a voltage source* V *through a resistance* R. *The circuit seen by the tunnel element is the parallel combination* $Z_t(\omega)$ *of the capacitance* C *of the junction and of the resistance* R.

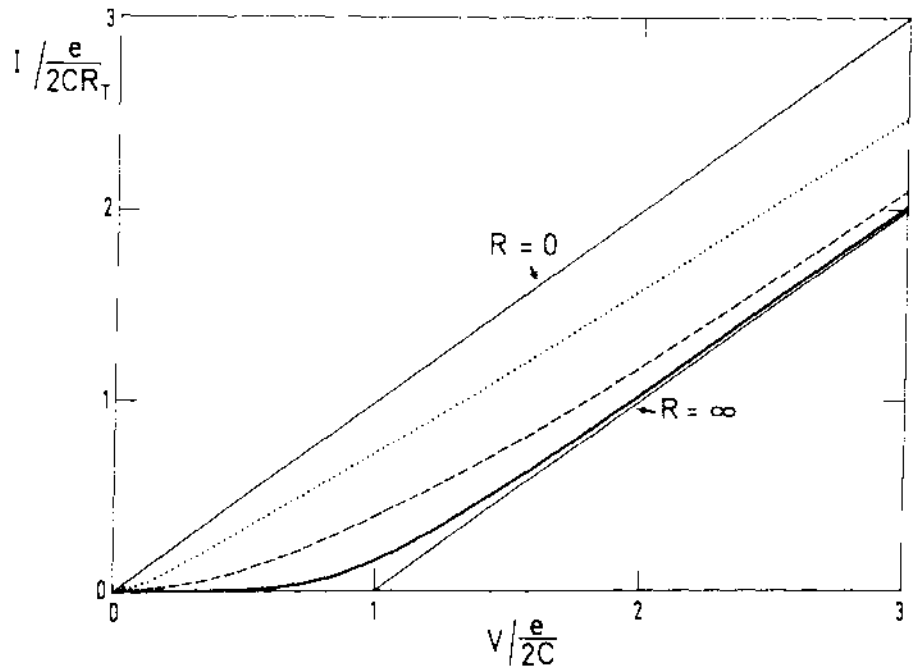

Fig. 2.10 *The* I − V *characteristic of a tunnel junction biased with voltage* V *through a resistance* R *for* $r = 2R/R_K = 0.05$ *(dotted line),* 0.5 *(dashed line) and* 5 *(full line). We have also represented the* $R \to 0$ *and* $R \to \infty$ *limits with thin continuous lines.*

Discussion: asymptote of the current voltage characteristic at large voltages

At very large voltages all the modes of the environment can be excited, hence all the charging energy of the junction $e^2/2C$ will be left in the environment. This appears in the relation

$$\int_{-\infty}^{+\infty} EP(E)dE = \frac{e^2}{2C}.$$

Using this relation and the normalization (2.2.16') of $P(E)$, we integrate expression (2.2.23) by parts and find

$$I = \frac{1}{R_T}\left(V - \frac{e}{2C} + \int_{eV}^{+\infty}\left(\frac{E}{e} - V\right)P(E)dE\right) \qquad (2.2.24)$$

Since at very large frequencies the impedance $Z_t(\omega)$ describing $Z(\omega)$ in parallel with the junction capacitance behaves like a capacitance, it follows that $P(E) \sim 1/E^3$ when $E \to +\infty$ and the integral in (2.2.24) vanishes as 1/V. Therefore

$$I = \frac{V}{R_T} - \frac{e/2C}{R_T} + O\left(\frac{1}{V}\right) \qquad (2.2.24')$$

This corresponds to a voltage offset in the current-voltage characteristic at high voltage, in agreement with the predictions of the "local rules" (Geigenmüller and Schön, 1989). We will show in section 2.2.2.3 that, for a low impedance environment, the asymptote yielding the "local rules" voltage offset is reached below the limit $V = (R_T/R)(e/C)$ over which the present theory does not apply (see section 2.2.1: the relaxation time for the environment is here $\tau = RC$).

Relevant frequencies

One can also show that $P(E)$ obeys the integral equation

$$EP(E) = \int_0^E dE' P(E') \frac{\mathrm{Re}(Z_t(E - E'))}{R_K/2} \qquad (2.2.25)$$

(Falci *et al.*, 1991). This equation indicates that the relative value of the current at a voltage V depends only on $Z(\omega)$ at frequencies lower than $eV/\hbar$. There is however a normalisation factor that depends on the impedance at all frequencies: the integral of $P(E)$ over all energies is normalised to unity. Therefore, the absolute current at a given

bias voltage depends on the value of the impedance at all frequencies. However, if we assume that $Z_t(\omega)$ is small compared with R_K at all frequencies, we can make a linear expansion in expression (2.2.18) and get

$$\begin{aligned} P(eV) &= \frac{R_T}{e}\frac{d^2I}{dV^2} \\ &\approx \frac{1}{e}\left[\left(1-\int_0^\infty \frac{d\omega}{\omega}\frac{\mathrm{Re}\left(Z_t(\omega)\right)}{R_K/2}\right)\delta(V) \right. \\ &\qquad \left. + \frac{\mathrm{Re}\left(Z_t(eV/\hbar)\right)}{R_K/2}\frac{1}{V}\right] \end{aligned} \tag{2.2.26}$$

This expansion is valid only when the integral on the right hand side converges. It shows that in a low impedance environment the second derivative of the current at a non zero voltage V is determined by the value of the impedance at frequency ω such that $\hbar\omega = eV$.

The above calculation of the the tunneling rate in a normal metal junction is readily adapted to the superconducting state in which charge carriers are Cooper pairs: this is developed in appendix 1.

2.2.2.3. Application to a purely resistive environment

Let us consider the case of Fig. 2.9 where the environment reduces to a pure resistance R and a voltage source V. The impedance in series with the junction is $Z(\omega) = R$. Since $\lim_{\omega\to 0}\omega Z(\omega) = 0$, the total impedance is then

$$Z_t(\omega) = \frac{R}{1+jRC\omega}$$

and

$$J(t) = \frac{-2i}{R_K}\int_0^t dt' \int_0^\infty d\omega \frac{R}{1+\omega^2R^2C^2}\exp(-i\omega t'),$$

or, introducing the reduced variables $r = 2R/R_K$, $\tau = RC$, $x = t/\tau$, $y = t'/\tau$, $z = \omega\tau$, we write

$$J(x) = -ir\int_0^x dy \int_0^\infty dz \frac{1}{1+z^2}\exp(-izt).$$

Then one has to calculate

$$\Gamma_L = \frac{\hbar}{2\pi e^2 R_T \tau} \int_0^{eV\tau/\hbar} du \int_0^u dv \int_{-\infty}^{+\infty} dx \, \exp\{J(x) + ivx\}. \tag{2.2.27}$$

A problem arises if one calculates expression (2.2.27) numerically, since the finite value of $Z_t(0)$ makes $J(x)$ diverge for $x \to \infty$. This divergence causes the function I(V) to be non-analytic at V=0 except for integer values of r. However, after some algebra, one can show that Eq. (2.2.27) is equivalent to

$$\Gamma_L = \frac{\hbar}{2\pi e^2 R_T \tau} \frac{\exp(-r\mathcal{C})}{\Gamma(r)} \times \int_0^{eV\tau/\hbar} du \int_0^u dv \; [r(v) \otimes s(v) + s(v)] \tag{2.2.28}$$

where

$$r(v) = \int_{-\infty}^{+\infty} dx e^{ixv} \times \left\{ exp\left[r \int_0^{\infty} \frac{dz}{z} e^{-izx} \left(\frac{1}{1+z^2} - e^{-z} \right) \right] - 1 \right\} \tag{2.2.28'}$$

and

$$s(v) = v^{r-1} e^{-v} \Theta(v) \tag{2.2.28''}$$

where the symbols $\otimes$,Γ,Θ,$\mathcal{C}$ denote the convolution product, the gamma and the Heaviside functions, and Euler's constant ($\mathcal{C} = 0.577...$) respectively. We have plotted in Fig. 2.10 the function I(V) for values of r equal to 0.05, 0.5 and 5. Although the curves are now smooth, as expected since the environment consists of an infinite number of oscillators, they are built from the non analytic function s(v) which diverges at v = 0 for all r less than unity, i.e. when the resistor R is below half of the resistance quantum R_K. Therefore, whereas the current at a given voltage depends on the impedance at all frequencies, the finiteness of the slope of the $I - V$ characteristic at the origin is only determined by $Z(0)/(R_K/2)$.

Asymptotic behaviour

If the impedance R if much smaller than R_K (which is the case in most experiments) we can use the expansion (2.2.26) at large energies (Ingold *et al.*, 1991):

$$P(E) \approx \frac{2\hbar^2}{R R_K C^2} \frac{1}{E^3}$$

and substitute it in (2.2.24). We then find

$$I \underset{V\to\infty}{\sim} \frac{1}{R_T}\left(V - \frac{e}{2C} + \frac{R_K}{4\pi^2 R}\frac{(e/C)^2}{V}\right).$$

Therefore, the "local rules" result $I = (1/R_T)(V - e/2C)$ is reached when

$$V \gg \left(R_K/4\pi^2 R\right)(e/C).$$

More precisely, the tangent to the $I-V$ characteristic taken at $V \gg \left(R_K/4\pi^2 R\right)(e/C)$ intersects the V axis at

$$V_g = \frac{e}{2C}\left(1 - \frac{2R_K}{\pi^2 R}\frac{e/2C}{V}\right)$$

The tangent extrapolates to $e/2C$ with an error of 1% when taken at

$$V_{1\%} = 100\left(2R_K/\pi^2 R\right)(e/2C).$$

Since the present theory is only valid when $V \ll (R_T/R)(e/C)$ (see section 2.2.1), this prediction applies only if $R_T \gg 10R_K$. Experimentally, the offset in the $I-V$ characteristic at large voltages was observed in single junctions by Geerligs *et al.* (1989), but only with low tunnel resistance junctions.

2.2.2.4. Calculation at finite temperature

The calculation is carried out in paper 1 and applications to simple situations were described by Ingold and Grabert (1991). The rate from left to right at finite temperature is:

$$\Gamma_L = \frac{1}{e^2 R_T}\int_{-\infty}^{+\infty} dE \int_{-\infty}^{+\infty} dE' f(E)\left[1 - f(E')\right] P(E' - E - eV) \qquad (2.2.28)$$

where $P(E)$ has the same definition as in (2.2.22), $f(E) = \left(1 + \exp\left(-\beta E\right)\right)^{-1}$ is the Fermi function, and where $J(t)$ is now given by

$$\begin{aligned} J(t) \;&= \int_0^{+\infty} \frac{d\omega}{\omega}\frac{\mathrm{Re}\left[Z_t(\omega)\right]}{R_K} \\ &\times \left(\coth\left(\frac{1}{2}\beta\hbar\omega\right)\left[\cos(\omega t) - 1\right] - i\sin(\omega t)\right) \end{aligned} \qquad (2.2.28')$$

The current from left to right is the product of e and of the difference between the rates from left to right and from right to left. Note that the phase φ introduced in this paper differs from the flux φ in what precedes by a factor equal to the flux $\hbar/e$. Also this phase is not the phase conjugated to the charge of the junction, but the difference between the phase of the junction and the phase of the source. It thus only describes the fluctuating part of the junction phase.

2.2.3. Observability of the Coulomb blockade of tunneling on a junction in a low-pass electromagnetic environment

In a low-pass circuit, the Coulomb Blockade of tunneling only occurs if the charge fluctuations are small enough. This is only the case in a very high impedance environment: in order to have the current significantly decreased at the gap voltage $e/2C$, the impedance must be higher than the quantum of resistance R_K at all frequencies below $e^2/2Ch$. If $C = 1$ fF, this frequency is 20 GHz. Experimentally, this requires a large ohmic resistor within a few millimeters from to the junction to avoid stray capacitance.This is of great difficulty since it has to be both a high impedance and a cold conductor. Cleland *et al.* succeeded partially this experimental tour de force (Cleland *et al.*, 1990) by fabricating on-chip NiCr and CuAu resistors within a few millimeters from the junction. They observed a partial Coulomb blockade of tunneling on the single junction. We will demonstrate in the following section that the case of many junctions in series or that of a junction in series with a true capacitor are much simpler from the technological point of view because the Coulomb blockade of tunneling occurs even without any impedance implemented on chip.

2.3. HIGH-PASS ENVIRONMENT

2.3.1. Hamiltonian of the circuit

The circuit seen by the pure tunnel element is now the island capacitance $C_i = C+C_{ext}$ in series with an impedance $\kappa^2 Z_t^0(\omega)$ and a voltage source κV where $\kappa = C_{ext}/(C + C_{ext})$ (Fig. 2.11). Note that in the low-pass environment Z_t describes the junction capacitance C in parallel with the impedance $Z(\omega)$, whereas here $Z_t^0(\omega)$ describes the series capacitance CC_{ext}/C_i in parallel with the non-diverging part $Z_0(\omega)$ of $Z(\omega)$. Therefore the description of a single junction is applicable but we have to add the degree of freedom of the capacitance C_i: we call q the charge of this capacitance and ψ its conjugate flux. q and ψ obey the commutation relation $[\psi, q] = i\hbar$. The hamiltonian describing the electromagnetic degrees of freedom has an extra term $q^2/2C_i$ and the phases are now related through $\Phi = \psi + \sum_m \Phi_m + \Phi_X$. Therefore, since ψ, Φ_m and Φ_X commute, the operator $a_{k_L}^\dagger a_{k_R} \exp(ie\Phi/\hbar)$ couples a state with a charge state $|q\rangle$ on C_i to a charge state $|q - e\rangle$. Note that the charge Q_X and the capacitance C_X describing the voltage source now obey the relation $Q_X/C_X = \kappa V$. With those definitions, the initial and final states coupled by the hamiltonian for tunneling from left to right are:

$$|i\rangle = |I\rangle\,|G\rangle\,|Q_X\rangle\,|q\rangle\,;|f\rangle = |\mathcal{F}\rangle\,|N\rangle\,|Q_X - e\rangle\,|q - e\rangle$$

2.3.2. Calculation of the rate

The change of energy between the initial and the final state now reads:

$$\begin{aligned} E_i - E_f &= \left(E_I + E_G + \frac{Q_X^2}{2C_X} + \frac{q^2}{2C_i}\right) - \left(E_{\mathcal{F}} + E_N + \frac{(Q_X - e)^2}{2C_X} + \frac{(q-e)^2}{2C_i}\right) \\ &= (E_I - E_{\mathcal{F}}) + (E_G - E_N) + \kappa eV + \frac{e\,(q - e/2)}{C_i} \end{aligned} \tag{2.3.1}$$

The fluctuating part of the flux on the junction (see section 2.2.2.4) is now $\varphi = \Phi - \Phi_X - \psi$; noting that $\exp(ie\psi)\ |q\rangle = |q - e\rangle$, we write the rate for tunneling from left to right as in

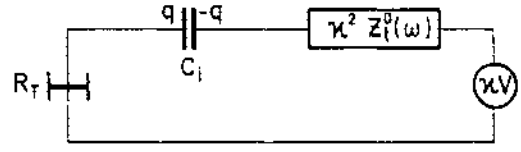

Fig. 2.11 *High-pass environment: the environment has one more degree of freedom than a low pass environment, namely the charge* q *of the island capacitor* $C_i = C + C_{ext}$. *The eigenvalues of* q *are integers because* q *changes only when electrons tunnel through the tunnel element.*

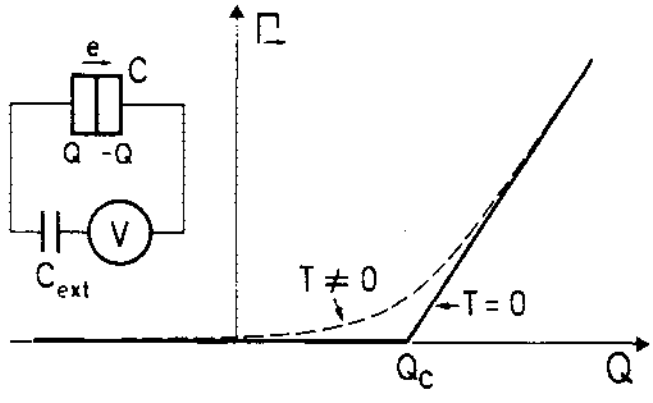

Fig. 2.12 *The "global rules" for the high-pass environment: tunneling is blocked, i.e. the tunneling rate* Γ *is zero, when the junction charge is below the critical charge* Q_c *determined by the external capacitance* C_{ext} *(see* Fig. 2.3*) and the junction capacitance* C. *The critical charge is* $Q_c = (e/2)\,(1 - C_{ext}/C)^{-1}$.

section 2.2.2.4:

$$\begin{aligned}\Gamma_H &= \frac{1}{e^2 R_T}\int_{-\infty}^{+\infty} dE \int_{-\infty}^{+\infty} dE'\ f(E)\,[1-f(E')] \\ &\quad \times P\left(\kappa, E-E'+\kappa eV+\frac{e\,(q-e/2)}{C_i}\right) \\ &= \frac{1}{e^2 R_T}\int_{-\infty}^{+\infty} dE\ \frac{E}{1-exp(-\beta E)} P\left(\kappa, -E+\kappa eV+\frac{e(q-e/2)}{C_i}\right) \qquad (2.3.3)\end{aligned}$$

where

$$P(\kappa, E) = \frac{1}{2\pi\hbar}\int_{-\infty}^{+\infty} dt\ \exp\left(\kappa^2 J(t) + \frac{iEt}{\hbar}\right) \qquad (2.3.3')$$

and $J(t)$ has the same definition than in section 2.2.2.4:

$$\begin{aligned}J(t) &= \int_0^{\infty} \frac{d\omega}{\omega} \frac{\mathrm{Re}\left[Z_t^0(\omega)\right]}{R_K} \\ &\quad \times \left(\coth\left(\frac{1}{2}\beta\hbar\omega\right)\left[\cos(\omega t)-1\right] - i\sin(\omega t)\right) \qquad (2.3.3'')\end{aligned}$$

$J(t)$ does not describe the phase fluctuations on the tunnel junction as it did in section 2.2.2.2, but on the series capacitance CC_{ext}/C_i. In other words, the environment only feels one capacitor, and has no means of knowing that there are actually two capacitors in series. Mathematically, this corresponds to a different definition of $Z_t(\omega)$ in the low-pass as opposed to high-pass environment in Eq. (2.1.2) and (2.1.3).

At zero temperature, the expression (2.3.3) simplifies into

$$\begin{aligned}\Gamma_H(V) &= \frac{1}{e^2 R_T}\int_0^{\kappa eV + e(q-e/2)/C_i} dE \int_0^{E} dE'\ P(\kappa, E') \\ &= \Gamma_L\left(\kappa eV + \frac{e\left(q-\frac{e}{2}\right)}{C_i}\right)\end{aligned}$$

which is very similar to Eq. (2.2.23).

Thus, the tunneling rate $\Gamma_H(V)$ calculated in the high-pass case is equal to the rate $\Gamma_L\left(\kappa eV + e(q-e/2)/C_i\right)$ calculated in the low-pass case with the reduced impedance $\kappa^2 Z_t^0(\omega)$, $Z_t^0(\omega)$ being given by the impedance of the parallel combination of the series capacitance CC_{ext}/C_i and the impedance $Z_0(\omega)$. We now deduce the observability of Coulomb blockade in the case of the high-pass environment.

2.3.3. Observability of the Coulomb blockade of tunneling in a high-pass environment

The non-diverging part of the environment impedance is characterized by an impedance $\kappa^2 Z_t^0(\omega)$ which, as in the case of a low-pass environment, is compared to R_K to distinguish two limiting regimes: the very high impedance regime, for which we obtained the Coulomb blockade of tunneling in low-pass environments; and the very low impedance regime, for which the Coulomb blockade is completely washed out in the case of a low-pass environment at voltages of the order of e/C, and only appears at voltages much larger than e/C. In the following, we make use of the relation between Γ_H and Γ_L to derive an expression for the Coulomb gap in a high-pass environment.

Coulomb gap

At zero temperature $\Gamma_L(E)$ is zero for $E < 0$. Therefore, whatever the impedance $Z_t(\omega)$, $\Gamma_H(V)$ is zero for $V < (e - 2q)/C_{ext}$. This is what we call the Coulomb gap. It is an important result based on energy conservation which can be obtained from the representation of the circuit in Fig. 2.11: the energy of the state of the circuit after tunneling is at least the electrostatic energy corresponding to a charge κe having passed through the source V and to an increase of the charge of the island between the junction and the capacitor by $e(e-2q)/C_{ext}$. The tunneling is therefore blocked at low voltages for a topological reason, the presence of a metallic island in the circuit. However, as we will show in the appendix 2, there is a finite current even through a series of tunnel junctions below the Coulomb gap which is obtained by perturbations theory at orders larger than two. We call the higher-order processes "co-tunneling" processes. The calculations in this chapter give the tunneling rate through only one junction, whatever the external impedance. Simple expressions are derived in the following for the two limiting cases of a very low impedance and a very large impedance.

2.3.3.1. Very low impedance

If $\kappa^2 Z_t^0(\omega) << R_K$, the function $P(E)$ reduces to a delta function $\delta(E)$. The rate then reads:

$$\Gamma_H = \frac{1}{e^2 R_T} \frac{\Delta E}{1 - \exp(-\beta \Delta E)} \tag{2.3.4}$$

where

$$\Delta E = \kappa e V + \frac{e(q - e/2)}{C_i} \tag{2.3.4'}$$

(Likharev *et al.*, 1989). Although this energy difference depends on the whole system including the source, it is possible to formulate it in terms of the average value Q of the junction charge before the tunnel event, which corresponds to the junction charge one would obtain using classical electrostatics:

$$Q = \frac{C C_{ext}}{C + C_{ext}} \left(V + \frac{q}{C_{ext}} \right)$$

$$\Delta E = \frac{e}{C} (Q - Q_c) \tag{2.3.5}$$

where the "critical charge" Q_c is:

$$Q_c = \frac{e}{2} \frac{1}{1 + \frac{C_{ext}}{C}} \tag{2.3.5'}$$

and C_{ext} is the capacitance in series with the junction.

This critical charge is always below $e/2$: tunneling is possible for $Q_c \leq Q \leq e/2$, which would not be the case if the "local rules" would apply. At zero temperature, the rate is then (Fig. 2.12):

$$\begin{aligned} \Gamma_H &= 0 \qquad \text{for } Q \leq Q_c \\ \Gamma_H &= \frac{1}{R_T C} \frac{Q - Q_c}{e} \quad \text{for } Q > Q_c \end{aligned} \tag{2.3.6}$$

For example in a linear array of N identical tunnel junctions of capacitance C, the critical charge is $Q_c = (e/2)(1 - 1/N)$ for each junction. The Coulomb gap is therefore $(N - 1)(e/2C)$. At large bias voltages, the rate is at equilibrium the same through all junctions and the current is given by the rate through any junction:

$$I = e\Gamma_H = (1/NR_T)(V - V_c).$$

(the tunneling rate in the opposite direction is negligible).

Those very simple expressions, called the "global rules" (Geigenmüller and Schön, 1989), will be fundamental in the description of the circuits of chapters 4 and 5 since they correspond to the experimental case where a true capacitance or other junctions are in series with the junction, and where the circuit does not contain any large impedance added on the chip. In these setups, connection leads present in the microwave range an impedance ~100 Ω, low compared to the impedance quantum, and the present calculation applies. In particular, we asked at the end of chapter 1 how long it takes for the system to go from the a state with n extra electrons in the island to the state with $n+1$ electrons (when this is of course energetically favourable). The answer is typically $R_T C$, which for usual experimental parameters is of the order of 0.1 ns.

Asymptotes of the $I-V$ characteristic

As with a low-pass environment, the local rules apply in the limit of very large bias voltages. Hence, in a linear array of tunnel junctions, the asymptote at large voltage corresponds to the voltage offset of the local rules $e/2C_{tot}$, where C_{tot} is the total capacitance of array. In the particular case of N identical junctions in series, the offset of the asymptote is Ne/C. It differs from the offset at intermediate voltages which we found to be given by the global rules by $(N-1)e/C$. These two offsets were measured experimentally by Geerligs *et al.* (1990b) on four samples with double junctions. They found a factor of 1.5 between the two offset voltages instead of the expected factor 2. We attribute this discreapancy to a measurement if the large scale asymptotes at a too low voltage (see section 2.2.2.3).

2.3.3.2. Very high impedance

If $Z_t^0(\omega) >> R_K$, we found in paper 1 that on a junction in a low-pass environment the rate Γ_L is zero for $V \leq e/2C$ and is $(V - e/2C)/eR_t$ for $V > e/2C$. Therefore, in a high-pass environment of high impedance, the rate is zero for

$$\kappa V + \frac{q - e/2}{C_i} \leq \kappa^2 \frac{e}{2CC_{ext}/C_i} \tag{2.3.7}$$

(κ^2 results from the transposition of the calculation in the low-pass case with an effective impedance $\kappa^2 Z_t$). This condition can be re-written as

$$V \leq \frac{e}{2C} + \frac{e-2q}{2C_{ext}} \tag{2.3.8}$$

On the contrary, if

$$V > \frac{e}{2C} + \frac{e-2q}{2C_{ext}} \tag{2.3.9}$$

the rate is given by (2.3.4) where

$$\Delta E = eV - \frac{e}{2C} - \frac{e(e-2q)}{2C_{ext}} = \frac{e}{C}\left(Q - \frac{e}{2}\right) \tag{2.3.10}$$

As in the case of a very low impedance, we can define a "critical charge" equal to $Q_c = e/2$ and write the rate as in the Eq. (2.3.6). Therefore, at zero temperature, tunneling is blocked when the charge on the tunnel junction is below $e/2$: this corresponds to the "local rules". Measuring this extra blockade of tunneling due to the environment is even more difficult than on one junction in a low-pass circuit because the coupling to the impedance $Z_t^0(\omega)$ is reduced by a factor κ^2.

2.4. CONCLUSION

We have distinguished two types of environments of a tunnel junction, low-pass (containing no capacitors or junctions in series) and high-pass (containing at least one capacitor or another junction in series), and calculated in both cases the junction tunneling rate. We have given simple expressions in two limiting cases: zero and infinite external impedance, for which the tunneling rate can be expressed as a function of the charge Q of the junction and of a "critical charge" Q_c: at finite temperature, this is given by formulas (2.3.4) and (2.3.5). At zero temperature, they simplify to (2.3.6): we recall these equations

$$\begin{aligned} \Gamma &= 0 && \text{for} \quad Q \leq Q_c \\ \Gamma &= \frac{1}{R_T C}\frac{Q - Q_c}{e} && \text{for} \quad Q > Q_c. \end{aligned}$$

We summarize these results in the following table:

	$Z_t(\omega) \ll R_K$	general case	$Z_t(\omega) \gg R_K$
low pass	$Q_c = 0$	Cf. Eq. (2.2.28)	$Q_c = \frac{e}{2}$
high pass	$Q_c = \frac{e}{2}\frac{1}{1+\frac{C_{ext}}{C}}$	Cf. Eq. (2.3.3)	$Q_c = \frac{e}{2}$

When $Z_t(\omega) \ll R_K$, the "global rules" apply: the critical charge depends on all the capacitances of the circuit. However, when $Z_t(\omega) \gg R_K$, the "local rules" apply: the critical charge is $e/2$. The local rules also apply in the case $Z_t(\omega) \ll R_K$ at voltages much higher than $\left(R_K/4\pi^2 R\right)(e/C)$ (where R is the dc resistance of the environment). We described the asymptotic behaviour of the current-voltage characteristic in sections 2.2.2.3 (low-pass) and 2.3.3.1 (high-pass).

In all of the devices we fabricated, the environment of the junction was always high-pass (many junctions in series or a junction in series with a capacitor) and low impedance, and we operated the device at voltages much below $\left(R_K/4\pi^2 R\right)(e/C)$. Hence, we will always use in what follows the global rules expressions (2.3.4) and (2.3.5) with

$$Q_c = \frac{e}{2}\frac{1}{1+\frac{C_{ext}}{C}}, \tag{2.4.1}$$

C_{ext} being the external capacitance seen by the junction considered.

3. EXPERIMENTAL TECHNIQUES

This chapter is devoted to the experimental techniques that were employed in the experiments that are described in chapters 4 and 5.

The realisation of circuits which exhibit charging effects requires the fabrication of tunnel junctions of nanometric dimensions ($\sim 100 \times 100$ nm^2). We used a scanning electron microscope (SEM) for the lithography and the technique of the shadow mask evaporation for the metal deposition. This is described in section 3.1.

In circuits exhibiting charging effects, not only the junction capacitances need to be small: so does the capacitance to ground of the islands between them needs also to be small. Moreover, it is important, as we shall see, to capacitively couple gate lines to these islands, while avoiding cross-talk between these lines. All this requires a precise design of the planar electrodes which define the circuit. For this purpose we wrote a computer program which calculates the capacitance matrix of an arbitrary set of planar electrodes. This program is described in section 3.2.1. Another important design tool is a simulation program that predicts the behavior of a circuit with a given set of parameters. This is achieved by our SETCAD program which is described in section 3.2.2. It has greatly helped us in understanding the roles of the various parameters in our circuits.

Experiments were carried out at low temperatures using a dilution refrigerator. The low noise electrical measurement techniques are described in section 3.3.

3.1. FABRICATION OF JUNCTIONS

Junctions were fabricated by making overlap two aluminium thin films, using the method of the suspended bridge (Niemeyer, 1974; Dolan and Dunsmuir, 1988). The aluminium has the advantages of evaporating at a relatively low temperature, and of having a good quality oxide. The details of the procedure were inspired by those of Geerligs in Delft (Geerligs, 1990) and Delsing in Göteborg (Delsing, 1990).

The tunnel junctions for experiments on charging effects must have high tunnel resistance ($R_T >> R_K$) and small capacitance ($C << e^2/2k_BT$). In a junction where the

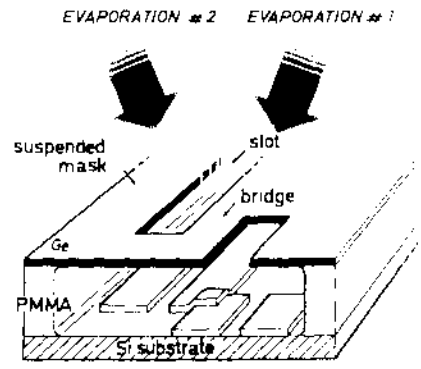

Fig. 3.1 *Junction fabrication with the method of "shadow mask evaporation": two evaporations at different angles through a suspended mask produce two films with an overlap of nanometric dimensions. This overlap constitutes the junction.*

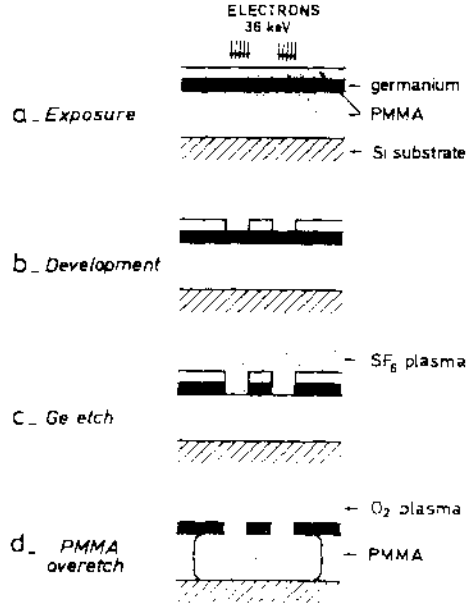

Fig. 3.2 *Fabrication steps of the suspended mask:* (a) *a PMMA resist covering a thin layer of germanium and a spacer of PMMA is exposed to the electron beam;* (b) *the regions exposed are dissolved in the developer;* (c) *the germanium is etched by a* SF_6 *plasma through the windows opened in the upper layer by the development;* (d) *the lower layer of PMMA is etched in an oxygen plasma, first at* μb *pressure and high power in order to etch vertically into the layer, then at* mb *pressure and low power in order to etch under the germanium, thus defining a bridge like the one of* Fig. 3.1.

tunnel barrier is 1 nm thick, the area needs to be around 0.01 μm^2 to obtain a capacitance of 1 fF. The shape of the electrodes is fixed by lithography. The minimal dimensions achievable with a particular lithographic technique is of the order of the wave length of the radiation. Although UV radiation (200 nm) has been successfuly used by Martinis (Martinis *et al.*, 1990) to make single junctions with them, this technique is not suitable to fabricate complex devices. X-rays (30 nm) and electron-beams (10 nm) are in fact the only available nanolithographic tools. We used the electron beam of a Scanning Electron Microscope (SEM).

Alignment at the 100 nm scale can be a serious problem. With the method of "shadow mask evaporation" (Dolan and Dunsmuir, 1988), the two electrodes are self-aligned: the principle is to take advantage of the shadow of a suspended bridge on the substrate to define separate conductors (Fig. 3.1). The junction is formed by the partial overlap of two metallic layers evaporated at two different angles through a suspended mask. An intermediate oxidation step creates the insulating barrier.

The mask with a nanometric suspended bridge is made by SEM lithography. The bridge is made out of germanium, a tough material that evaporates at a relatively low temperature. The mask far from the bridge lies on a resist layer of PMMA (plexiglass) 200 nm thick. The pattern was defined by writing with the SEM on a thin PMMA layer on top of the germanium; the developped pattern is later transfered to the germanium. The fabrication of the mask therefore requires three layers (Fig. 3.2a): an underlying PMMA spacer, a thin germanium film and a thin PMMA layer for e-beam patterning.

3.1.1. Wafer preparation

We fabricated our samples on oxidized 2-inch silicon wafers. The wafers were first cleaned in a bath of pure nitric acid, then rinsed in deionised water. After the spinning of the first 200 nm thick PMMA spacing layer, 20 nm of germanium were Joule-evaporated at the rate of 0.1 nm/s. Finally, the upper PMMA layer was spun, with a thickness of only 60 nm, in order to reduce the broadening due to back-scattered electrons.

The wafer, covered with the three layers, was then cut into 8 mm $\times$ 8 mm chips, which

were treated one by one during the steps that are described below.

3.1.2. Electron-beam patterning

The electron beam patterning (Fig. 3.2a) was done with a JEOL 840A scanning electron microscope, in which the deflecting coils were controlled by a real-time Hewlett-Packard 1000 computer through digital to analog converters (DAC) (Fig. 3.3). The whole pattern, from the junction bridges up to the millimeter-size connection pads, was exposed in the SEM. We thus avoided using any optical lithography for the coarse features of the pattern. Hence, no alignment was needed during the lithography.

The computer program for patterning

The patterns are defined on a 4092×4092 pixels grid. A pattern is decomposed into square and trapezoidal boxes. The coordinates of the corners of the boxes, the values of two iteration steps dX and dY, the number of repetitions n and the relative charge dose d for each box, are stored in a file. A typical pattern file corresponding to the design of the electron pump of Fig. 5.13 is given in Appendix 2. The program calculates the coordinates of a sequence of points inside each box so as to define a scan from one box edge to the opposite one. This scanning is performed in steps of size dX in the X direction and dY in the Y direction; the time between steps is calculated in order to obtain after n identical scans d times the standard charge dose for the box. The standard charge dose is 2 pC/μm^2. It is necessary to be able to change the values of the iteration steps dX and dY and the number of repetitions n because the time step of the computer is coded on only 8 bits.

The polymerization of the PMMA at a given point of the chip is due to the back-scattered electrons from several neighbouring points of the scan. As a consequence, the narrowest boxes need a higher relative dose d because fewer neighboring points contribute there to the exposure.

The exposure

Since the grid used for the definition of a pattern is only 4092×4092 pixels, we use

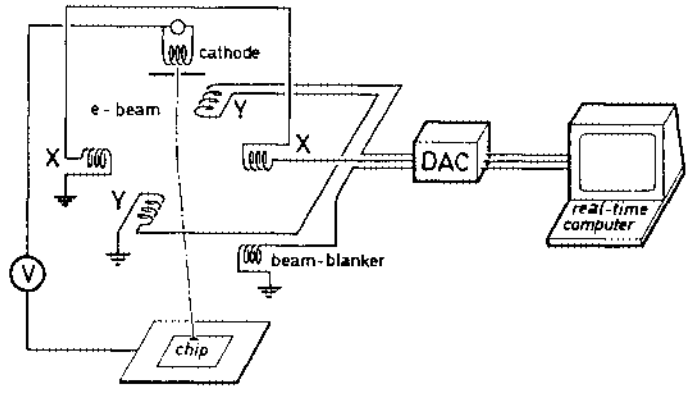

Fig. 3.3 *Electron beam (e-beam) patterning set-up: a computer with a real time operating system controls the currents in the deflecting and blanking coils of a Scanning Electron Microscope (SEM).*

four different magnifications of the SEM to define all the features, large and small, of a design. At the 100 nm scale, the field of exposure is 18 μm $\times$ 24 μm (magnification $\times$5000). After the finest pattern was exposed, the SEM magnification was successively lowered to $\times$1000, $\times$180 and $\times$30. Small shifts of the center of the image occur when changing the magnification (a few μm between $\times$5000 and $\times$1000, and $\times$1000 and $\times$180; tens of μm between $\times$180 and $\times$30), but these are reproducible and were systematically compensated for.

The electrons are accelerated by a voltage of 36 kV. The electron beam is brought into focus using two spots of silver paint placed on opposite edges of the chip. The current is 13 pA for the two smallest scales. Since little precision was needed for the coarse features at magnifications $\times$180 and $\times$30, a higher current of 10 nA was used at these magnifications to save time. The exposure of the pattern of an entire device took less than half an hour.

3.1.3. Development. Etching

The development (Fig. 3.2b) was done in a solution of MIBK(1) - propanol-2(3) during 45 seconds at 20°C. The time for the development proved to be very temperature-dependent. The sample was then etched (Fig. 3.2cd) in three steps in a reactive ion etching (RIE) reactor:

etch of	gas	flow (sccm)	pressure (mb)	rf power (W)	sample holder polarization (V)	time (min)
Ge	SF_6	5	$2\ 10^{-3}$	10	85	1/2
PMMA	O_2	5	$2\ 10^{-3}$	50	175	3
PMMA	O_2	20	0.1	10	65	10

(sccm stands for standard cube centimeter per second).

In the two first steps, laser interferometry was used to detect the end of the etch: too long an etch would broaden the lines and increase the capacitance of the junctions.

The last etch was intended to dig under the germanium bridge, where the two electrodes of the junction should overlap. If this etch is stopped too early, the lift-off removes the junctions; if it is stopped too late, the germanium bridge collapses. After this last step,

the sample was ready for evaporation.

3.1.4. Evaporation of aluminium. Lift-off

We used two types of evaporation systems: a Joule-effect evaporator and an electron-beam evaporator. In the Joule-effect installation, we pumped down to 5.10^{-7} mb with a diffusion pump and evaporated at 1.5 nm/s. A liquid nitrogen cooled trap was placed in the chamber in order to lower the water vapor partial pressure. In the electron-gun evaporation system, a turbo-molecular pump could reach 5.10^{-8} mb, and the evaporation rate was 0.4 nm/s. The sample was mounted on a tiltable holder and was cooled to around 5°C during the process.

The thickness of the aluminium films was 30 nm for the first layer and 50 nm for the second one. The first layer was oxidized in pure oxygen, at a pressure of a few millibars, at room temperature, for 15 mn to 45 mn depending on the required R_T.

The PMMA-germanium mask was then lifted-off by placing the sample in a $50°C$ bath of acetone for 20 minutes. The junctions were immediatly tested with 1 MΩ resistors in series with a hand-held multimeter. We found that we had to be extremely careful when handling with the junctions: electrostatic discharges could very easily destroy them. All the wires were therefore grounded before measurements. We often observed that our junctions became shorts after a period of a few hours. We interpreted this as a rearrangement of the aluminium films at the atomic level.

3.2. DESIGN OF DEVICES

3.2.1. Calculation of planar capacitances

In order to design islands with specified capacitance we wrote a program called C2D (Capacitances in 2 Dimensions) to calculate the capacitance matrix of a set of planar electrodes. The principle of this program is to minimise the electrostatic energy of a set of conductors $\alpha, \beta, ...$, polarized at potentials $V_\alpha, V_\beta, ...$, with respect to the distribution of charges on all those conductors. Each conductor is divided into square pixels (indexed by

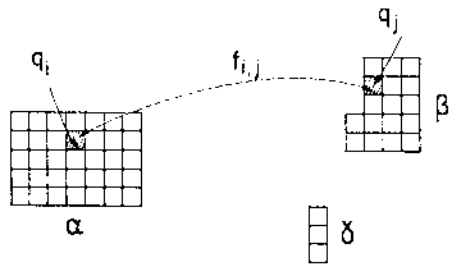

Fig. 3.4 *Representation of the planar conductors for the calculation of their capacitance matrix. The conductors are defined on a grid. The interaction between pixels* i *and* j *depends on the product of their charges and of a parameter* $f_{i,j}$ *depending on the distance.*

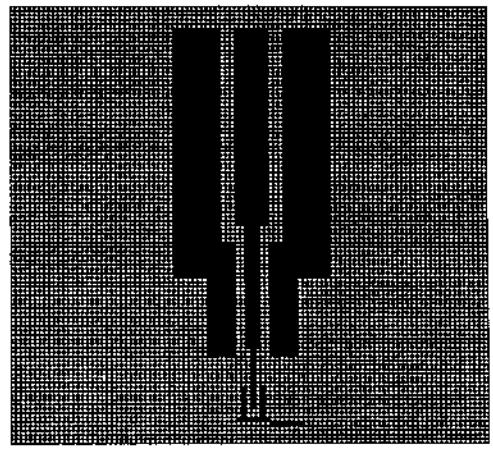

Fig. 3.6 *Interdigitated capacitor: the capacitance* C_0 *between the long guarded finger and the island with two fingers is ten times larger than the cross-talk capacitance* C_x *to the neighbouring rectangular island. For a spacing of* 0.2μm, *we found* $C_0 = 0.105$ fF *and* $C_x = 0.010$ fF.

i) of area l^2 uniformely charged with a charge q_i (Fig. 3.4). We call $\alpha(i)$ the conductor to which pixel i belongs. For a given charge distribution, the electrostatic energy of the system of conductors can be written as

$$E = \frac{1}{4\pi\epsilon}\left(\sum_{i,j} f_{i,j} q_i q_j\right) - \sum_i q_i V_{\alpha(i)},$$

where

$$\epsilon = \epsilon_0 \frac{\epsilon_r + 1}{2}$$

accounts for the fact that half of the space is empty and the other half is the substrate (whose thickness can be taken as infinite at the micrometer scale of the conductors), whose dielectric constant is ϵ_r, and where $f_{i,j}$ is the interaction potential between the two uniformely charged square pixels i and j. The first term in E is the electrostatic interaction between all pairs (i,j) of charged pixels. The electrostatic interaction energy associated with the charged pixels i and j depends only on the product of their charges $q_i q_j$ and on the distance r_{ij} between their centers. If the pixels were reduced to points, this distance dependence would simply be $f_r = r_{ij}^{-1}$. Here, pixels are squares of finite dimension and we took into account the first correction, which is the quadrupolar one: $f_{ij} = r_{ij}^{-1} + \frac{1}{12} r_{ij}^{-3}$. This correction is independent of the orientation of the squares with respect to the line joining their centers. We calculated the f_{ij} for the first, second and third neighbouring pixels even more carefully by dividing the pixels themselves into smaller pixels and calculating the interaction potential in a self-consistent way. The self-energy of a square pixel ($r_{ij} = 0$) was calculated analytically.

At each step of the calculation, the charge of all the pixels is modified sequentially, each pixel correction δq_i being given by

$$\delta q_i = -\kappa \frac{\partial E}{\partial q_i} = -\kappa \left\{ \frac{1}{4\pi\epsilon}\left(\sum_j f_{ij} q_j\right) - V_{\alpha(i)} \right\}$$

where κ is a convergence parameter. When the iterative calculation has converged, the charge is summed on all the pixels of each capacitor:

$$q_\alpha = \sum_i q_i$$

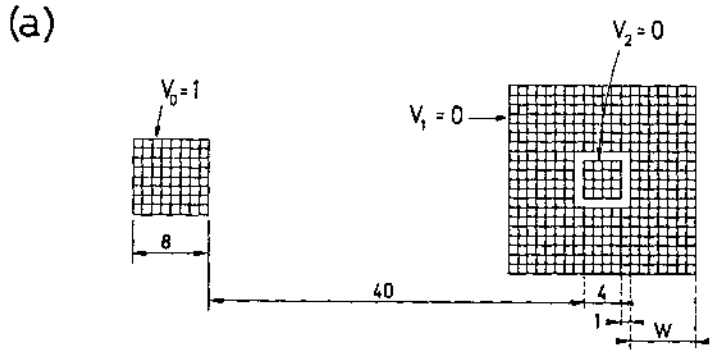

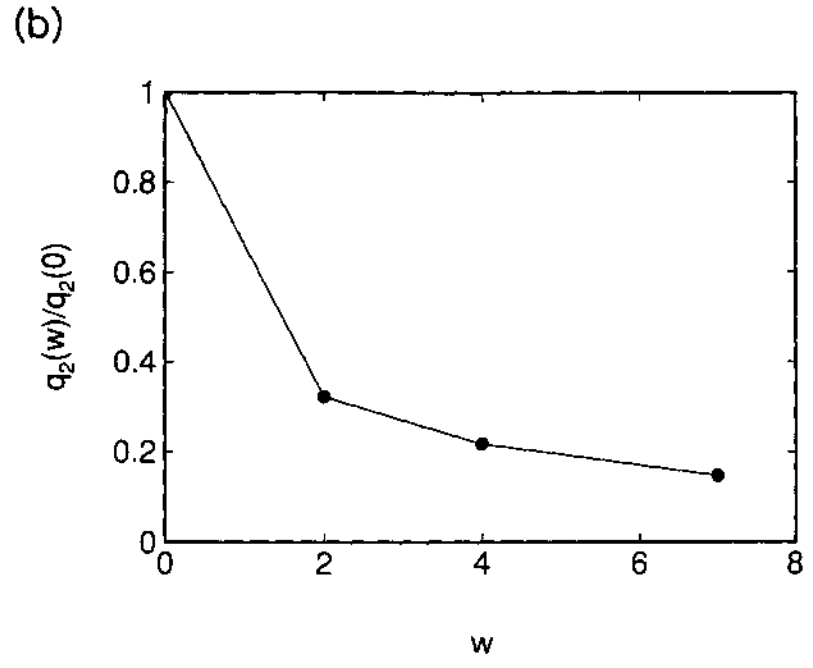

Fig. 3.5 *Effect of a planar guard electrode* (1) *of width* w *at potential* V_1 *on the cross-talk between two electrodes* (0) *and* (2) *at potentials* V_0 *and* V_2. (a) *The figure corresponds to the case* $w = 7$. (b) *Numerical calculation of the charge induced by* (2) *on* (0)*: the guarding effect is imperfect and decreases slowly with* w.

where the summation is carried out on the pixels i of the conductor α. Since

$$q_\alpha = \sum_\beta C_{\alpha\beta} (V_\beta - V_\alpha)$$

we finally arrive at the capacitances $C_{\alpha\beta}$ between conductors α and β.

This program showed that guarding lines in two dimensions are never perfect (see Fig. 3.5). We made a compromise between the necessity of guarding and the requirement of small capacitances to ground, and obtained cross-talks nearly ten times smaller than the desired couplings. The best way to design a planar capacitor is to make interdigitated fingers as in Fig. 3.6. The capacitances we calculated agreed with the measured capacitances within the experimental accuracy.

3.2.2. Simulation of small junction circuits

The detailed prediction of the behaviour of circuits containing more than one junction is rather complicated: the current results from the combination of tunnel events through all the junctions, and the rate of each tunnel event depends not only on the precise values of the gates and bias voltages, but also on the charge configuration of all the islands, which is determined by the history of the system. In order to find the right design parameters for the devices we fabricated, and in order to make comparisons with experimental measurements, we wrote a program called SETCAD (Single Electron Tunneling Computer Aided Design), which simulates the charge dynamics in linear arrays of small tunnel junctions. The parameters of the simulation are the junctions and gates capacitances, the voltages applied to the gates and across the array, and the temperature. The tunnel resistance R_T of a junction of capacitance C is fixed by forcing the same $R_T C$ product to all the junctions since it depends only on the parameters of the oxidation process.

Use of SETCAD

The SETCAD program can be used in two modes: i) the display mode, where the islands and junctions charges are displayed after each tunnel event. The voltages can be

modulated automatically or interactively; ii) the calculation mode, where the current is calculated as a function of the dc value of one voltage (gate or bias); a modulation can be added to one or several voltages.

Principle of the SETCAD program

The global rules of Eq. (2.3.4) are used to calculate the tunneling rates. According to Eq. (2.3.5), the tunneling rate through one junction is proportionnal to the difference between this junction's charge and its critical charge. Both are calculated in the SETCAD program with the inverse capacitance matrix C^{-1} of the array, deduced from the junction and gate capacitances. To second order in R_T/R_K, the co-tunneling rates are calculated using Eq. (A.1.1), and the energies are calculated from the junction charges according to Eq. (2.3.5).

C^{-1} is calculated at the beginning of the program, when the capacitance values are introduced. The critical charges are deduced as simple linear combinations of the matrix elements of C^{-1}. At each step of the simulation the program calculates the electrical potential of each island as a product of C^{-1} and the column vector of the effective charges of the islands (the effective charge on one island is the sum of the number of extra electrons on it and of the charge induced by the gate attached to it). The difference between the electrical potentials of two neighbouring islands gives the charge on the junction between them.

According to the tunneling rates calculated for all the junctions, the program randomly chooses whether or not a tunnel event occurs, and, if one occurs, through which junction (or junctions in the case of co-tunneling) and in which direction the electron tunnels. The number of extra electrons on the two islands next to this junction are then changed by one. The time variable is then iterated and the new values of the voltages are calculated for the next step.

3.3. MEASUREMENT TECHNIQUES

Samples were mounted in a copper box thermally anchored to the mixing chamber

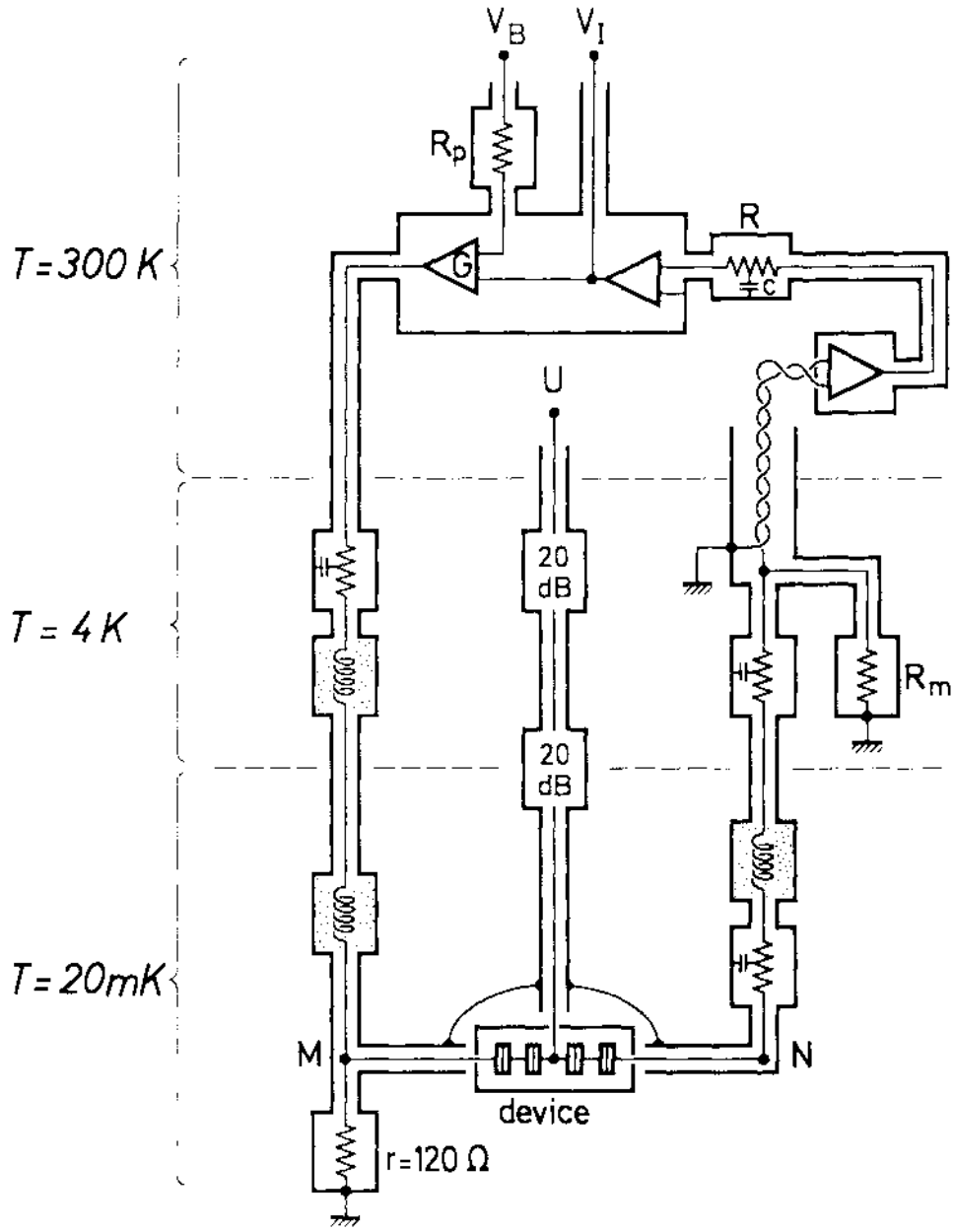

Fig. 3.7 *Wiring of the experimental set up. The current through the device under study was measured by recording the voltage drop across the cold resistor* R_m. *This voltage was sent to room temperature through a twisted pair. A feed-back loop at room temperature compensates the voltage drop across* R_m.

of a dilution refrigerator. Measurements were performed between 300 mK and 20 mK. Since the critical temperature for superconductivity in aluminium is 1.2 K, a magnetic field of 0.5 T was applied parallel to the surface of the sample with a superconducting coil in order to bring the aluminium in the normal state. The wiring of the experiment is showed in Fig. 3.7. A voltage dividing bridge (R_p, r) provides a voltage bias. Current was determined by measuring the voltage drop across a nominally 10 MΩ resistor cooled to 4 K. The resistance R_m of this resistor was measured at 4 K and found to be 12.07 MΩ. The voltage across this resistor was connected to a battery-powered PAR 113 amplifier with a twisted-pair in a grease-filled tube. Two types of microwave filters were used on the bias and measurement lines: distributed RC filters and lossy inductive filters. Distributed RC filters (Fig. 3.8a) were made with resistive films (60 Ω/square, 50×2 mm^2) pressed between insulating Mylar films by two brass blocks. The distributed filter was enclosed in a brass box. Lossy inductive filters (Fig. 3.8b) consisted of a manganin wire spiral immersed in copper powder. Attenuation at 4 K for both types of filters was found to be better than 60 dB at 1 GHz. Gate lines were coaxial lines with 40 dB total attenuation provided by two thermally anchored Radiall microwave-frequency attenuators.

When a current I flows through the device, the voltage V_N is $R_m I$ and the voltage across the junction $V_M - R_m I$. We used a feed-back loop so that $V_M - V_N = V_B/1000$. The time-response of the loop was around 1 s. The circuit was therefore floating at the voltage V_N. No correction was applied to the gate voltages to compensate with the variations of V_N which were small.

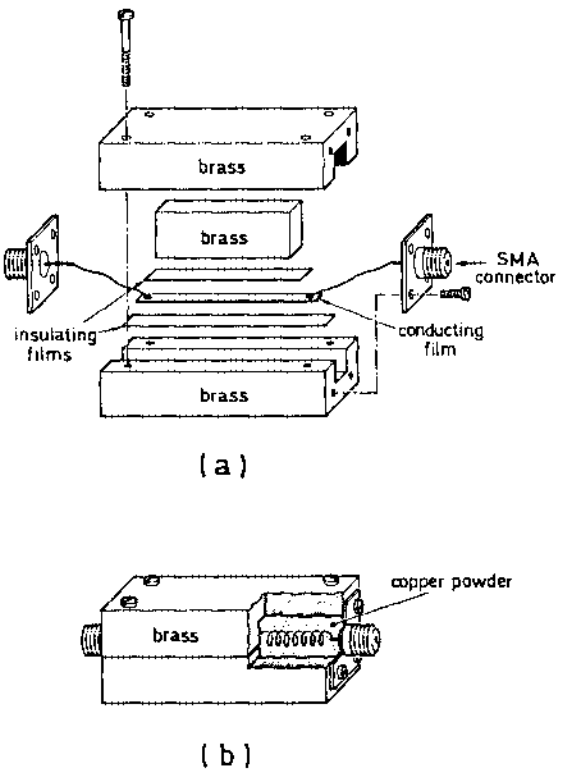

Fig. 3.8 *Microwave filters:*

(a) *exploded view of a distributed RC filter: the current through the filter passes through a conductive resistive film pressed against metallic surfaces connected to ground.*

(b) *cut-away view of a lossy inductive filter: the copper powder provides skin depth losses.*

4. OBSERVATION OF THE COULOMB BLOCKADE OF TUNNELING IN A "SINGLE ELECTRON BOX"

4.1. THERMAL EQUILIBRIUM AVERAGES

The essence of the Coulomb blockade of tunneling through a junction in a high-pass low impedance environment is that tunneling is blocked when the charge Q on the tunnel junction is below a critical charge Q_c, determined by the external capacitance and the capacitance of the junction (see chapter 2). As a result, when charging with a voltage source U a junction of capacitance C in series with a capacitance C_S (Fig. 1.3), tunneling is blocked as long as $\tilde{Q} = C_S U < e/2$. At this point $Q = Q_c$ and one electron can enter the island. From the definition of Q_c, the energy of the entire circuit is the same before and after the tunnel event which occurs when the charge of the junction is exactly Q_c. The tunneling of one electron is then reversible: after one electron has entered the island, the junction charge is equal to $-Q_C$. $\langle Q \rangle$ is related to the thermal average $\langle n \rangle$ of the number n of extra electrons on the island:

$$\langle Q \rangle = \frac{C}{C_i} \left[\langle n \rangle (-e) + \tilde{Q} \right] \tag{4.1.1}$$

where $C_i = C + C_S$.

$\langle n \rangle$ is an odd function of the bias voltage U. Moreover, $\langle n \rangle - C_S U/e$ is a periodic function of $C_S U$ with period e. This is explained in Fig. 4.1 by considering two electrically equivalent dipoles from which we can deduce the translation property:

$$\langle n \rangle_{U+e/C_s} = \langle n \rangle_U + 1 \tag{4.1.2}$$

At zero temperature, n has no fluctuations i.e. $\langle n \rangle$ is the integer n_{min} minimizing the total energy. Using these properties and the fact that $\langle n \rangle$ is an increasing function of U, we obtain the result that n_{min} is a staircase function of U (Fig. 4.2a). At finite temperature this staircase becomes rounded. The distribution of n is given by a Boltzmann law:

$$\langle n \rangle = (1/Z) \sum_{n=-\infty}^{+\infty} n \exp(-\beta E_n) \tag{4.1.3}$$

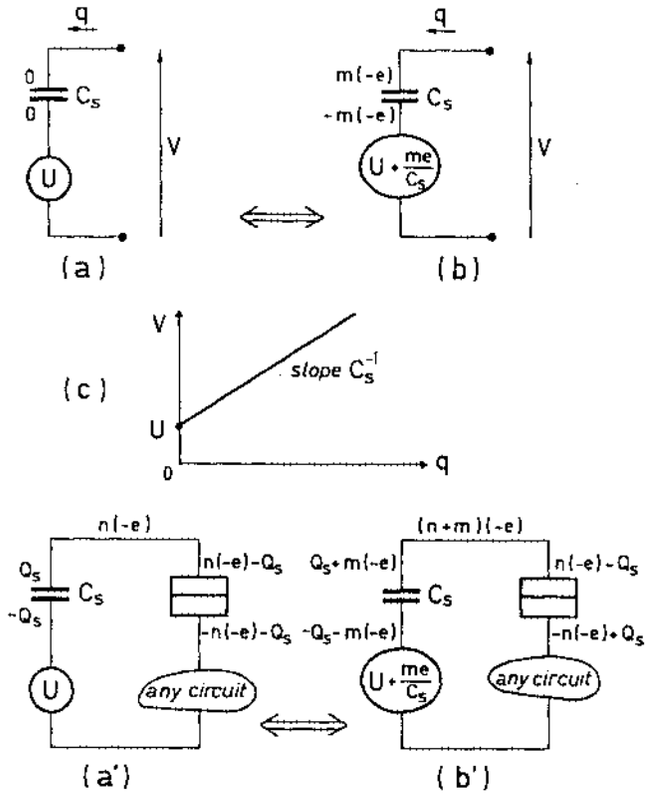

Fig. 4.1 *The voltage response to a charge signal of dipoles* (a) *and* (b) *are the same* (c), *so they are electrically equivalent. When they are connected to a tunnel junction in series with an arbitrary circuit, the charges relaxes the same way in both cases* (a' and b'). *We call* Q_s *the equilibrium charge on* C_s *in (a'): the equilibrium charge on* C_s *in* (b') *is therefore* Q_s—me. *If the charge of the island is* n(—e) *in* (a'), *the junction charge in* (a') *and, by equivalence, also in* (b'), *is* $n(-e) - Q_s$. *The final island charge in* (b') *is therefore* (n + m)(—e). *Thus,* $U \to U + m(e/C_s) \Rightarrow n \to n + m$.

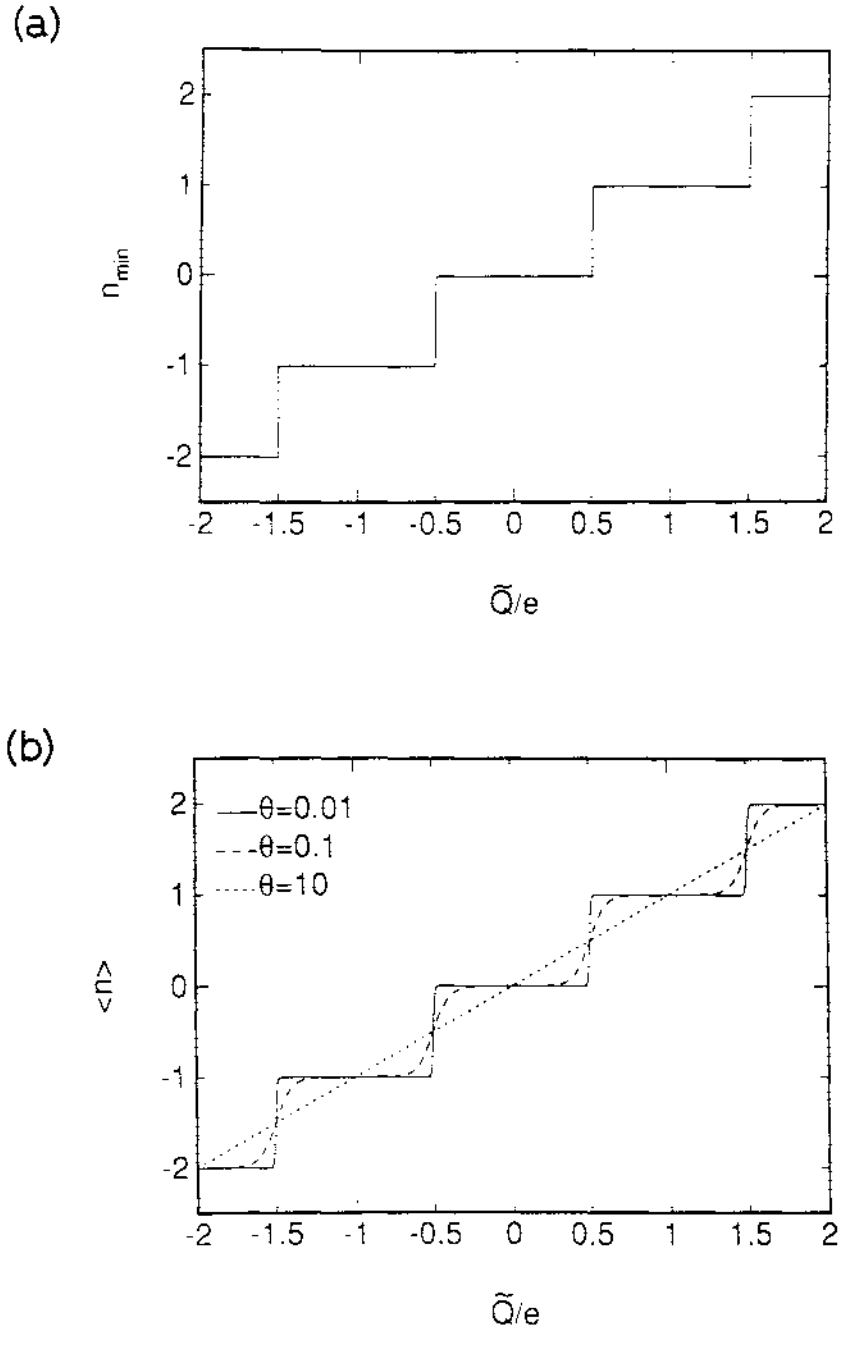

Fig. 4.2 (a) *Number of extra electrons* n_{min} *on the island that minimizes the energy of the electron box (see* Fig. 1.2), *plotted as a function of the polarization charge* $\tilde{Q} = C_S U$ *in units of* e. (b) *Variations of the island average electron number* $\langle n \rangle$ *for* $\theta = k_B T (C_S + C) / e^2 = 0.01$ *(solid lines),* 0.1 *(dashed lines) and* 10 *(dotted line).*

where $\beta = (k_B T)^{-1}$, $E_n = (C_S U - ne)^2/(2C_i)$ and

$$Z = \sum_{n=-\infty}^{+\infty} \exp(-\beta E_n)$$

The energy E_n is the n-dependent part of the electrostatic energy of the whole circuit. The variations of $\langle n \rangle$ are given in Fig. 4.2b for various temperatures. This expression has already been considered by Glazman and Schekhter (1989) in the context of quantum dots.

The function $\langle Q \rangle$ versus $\tilde{Q}$ is therefore a sawtooth function, with zero mean value. As the temperature increases, this function becomes progresssively rounded. The dependance of $\langle Q \rangle / e$ on $\tilde{Q}/e$ is plotted in Fig. 4.3 for various temperatures. In the limit where $C_S \ll C$ which was considered by Büttiker (1987) in the context of Bloch oscillations, the oscillations shown in Fig. 4.3 are analogous to the SET oscillations (Averin and Likharev, 1986) of Q versus It for a junction biased with a current I. We showed in chapter 2 that, when the island is connected to the outside world through only one junction, the tunneling rate when U is increased above $e/2C_S$ is given by $\Gamma_L = (Q - Q_c)/(eR_T C)$ in a low impedance environment. If the experimental parameters are such that $(R_T C)^{-1} \approx 0.1$ ps, the tunneling can be considered instantaneous as long as $C(dU/dt)/e << 1$ GHz. In this case, the system will always remain in thermodynamic equilibrium. We make the ergodic hypothesis, i.e. we assume that the time-averaged value $\bar{Q}$ of Q corresponds to its thermodynamic value $\langle Q \rangle$. We therefore have access to $\langle Q \rangle$ versus $\tilde{Q}$ by measuring $\bar{Q}$ versus $\tilde{Q}$ with an averaging time constant much larger than 1 ns.

Experimentally, the measurement of $\langle Q \rangle$ requires measuring a charge with sub electron accuracy, without increasing noticeably the capacitance of the island to ground. Furthermore, the disturbance of the island charge by the back-action of the measuring apparatus has to be negligible on the same scale. These requirements are not met by off-the-shelf electrometers: their sensitivity is at most 100 e/$\sqrt{\text{Hz}}$, and any wire going from the island to the electrometer would increase the capacitance of the island by many picofarads. Hence we used an on-chip "SET transistor" (SET standing for Single Electron Tunneling) to measure $\langle Q \rangle$ (Lafarge *et al.*, 1991). It consists of two small tunnel junctions biased below the Coulomb gap. Its sensitivity was first demonstrated experimentally by Fulton and Dolan (Fulton and Dolan, 1987).

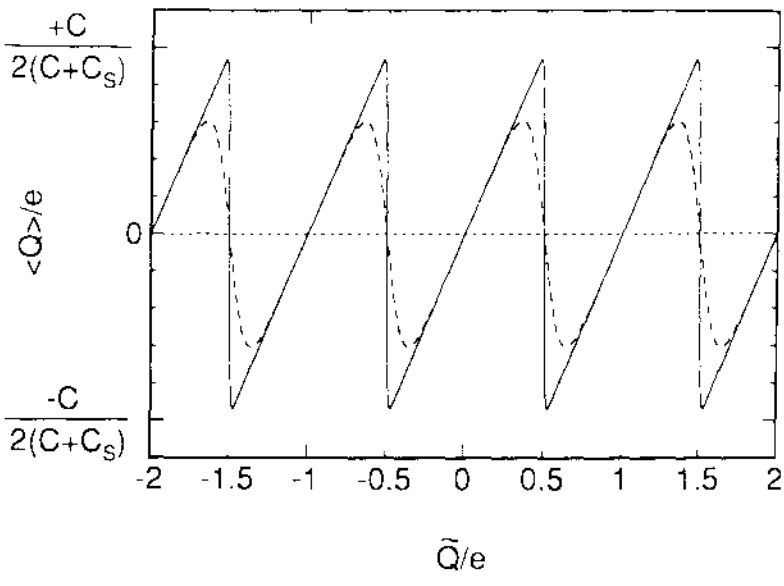

Fig. 4.3 *Variations, in the single electron box, of the junction average charge* $\langle Q \rangle$ *for* $\theta = k_B T\,(C_S+C)\,/e^2 = 0.01$ *(solid line),* 0.1 *(dashed line) and* 10 *(dotted line), as a function of the polarization charge* $\tilde{Q} = C_S U$.

4.2. THE SET TRANSISTOR

4.2.1. Device description

The SET transistor consists of two tunnel junctions in series and of a gate capacitor connected to the island between them. The two junctions are voltage biased by a source V (see Fig. 4.4a); a voltage source U_0 couples through a capacitance C_0 to the island betweeen the junctions. It can be seen as a single electron box with separate "in" and "out" lines. The behaviour of this device can be analyzed using the numbers n_L and n_R of extra electrons on the island that would minimize the energy if the other one was considered as a pure capacitor: n_L (n_R) corresponds to tunneling being allowed through junction L (R) only. $n_L(U_0)$ and $n_R(U_0)$are identical staircase functions but shifted by V. They are plotted in Fig. 4.4b for $V < e/C_i$.

Let us consider first that U_0 is such that $C_0U_0 \approx (n + 1/2)e$. Then $n_1(U_0) = 0$ and $n_2(U_0) = 1$. Suppose now that the initial island configuration is $n = 1$. This state is stable with respect to tunneling through junction R; but it is unstable with respect to tunneling through junction R: the tunneling of one electron through junction R will lead to a state of lower energy. Therefore the system will switch to the configuration $n = 0$. This state is stable with respect to tunneling through junction L, but it is unstable with respect to tunneling through junction R, which would lead to a new state $n = 1$ (this new state differs from the initial one, because in the complete sequence leading from one to another one electron went through the device). The system will then switch to this new $n = 1$ state. After one cycle $1 \rightarrow 0 \rightarrow 1'$, one electron has gone through the device and the cycle can start again. This cascade process continues indefinitely, the charge on the intermediate island being alternatively 0 and 1, and a current flows then through the device (Fig. 4.4c).

If on the contrary U_0 is such that $C_0U_0 \approx ne$, the two functions $n_L(U_0)$ and $n_R(U_0)$ coincide and will be, as follows from the analysis of the single electron box, anchored to the value n. Thermal fluctuations are too small to induce charge fluctuations for these values of U_0 and V : no current can flow through the device.

Since the functions $n_L(U_0)$ and $n_R(U_0)$ are e/C_0 periodic, the current through the

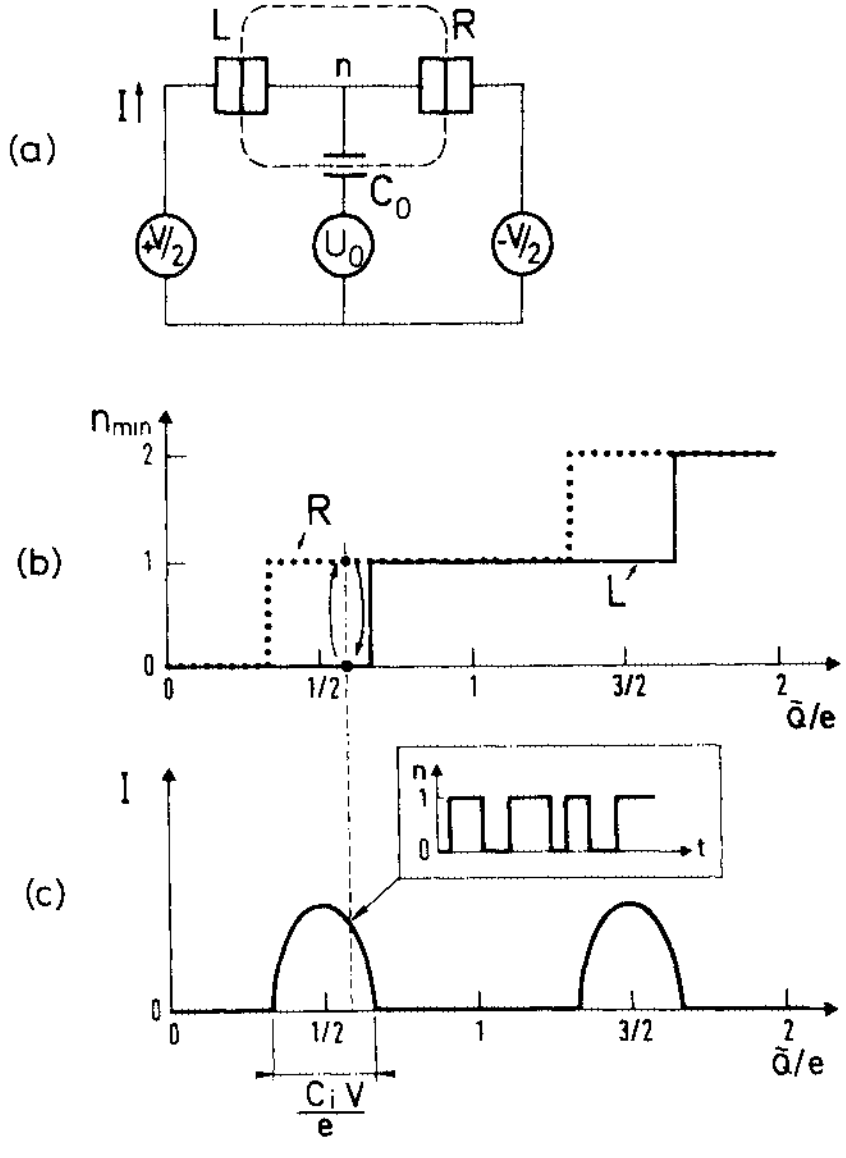

Fig. 4.4 (a) *SET transistor biased by a voltage source* V *and coupled to a gate voltage* U_0 *through a capacitor* C_0. *The island is delimited by a dashed line.* (b) *Numbers of extra electrons* n_L *and* n_R *on the island minimizing the energy with respect to tunneling through junction* L *only (full line) and through junction* R *only (dotted line).* (c) *Current through the SET transistor as a function of the gate voltage. The current is non zero only when* $n_L \neq n_R$; *the island charge oscillates then between* n_L *and* n_R.

junctions is modulated by U_0 with a period e/C_0 (Fig. 4.4c). A small modulation of the charge C_0U_0, even smaller than the electron charge e modulates the current by a noticeable fraction of its maximum value. The SET transistor can therefore be used as an electrometer.

4.2.2. Experimental determination of the parameters of the the SET transistor and performances as an electrometer

The current-voltage characteristics of the electrometer we fabricated (Fig. 4.5) correspond qualitatively to the results obtained with our SETCAD simulation program. For $C_0U_0 = 0$ modulo e, the $I-V$ characteristic shows a clear gap structure corresponding to the Coulomb blockade of the SET transistor. When $C_0U_0 = e/2$ modulo e, the characteristic is gapless. The modulation of I with U_0 at a given bias voltage (Fig. 4.6) is periodic, as expected from the $\langle Q \rangle$ versus $\tilde{Q}$ function for the electron box (Fig. 4.3); assuming that the period is e/C_0 we found $C_0 = 73 \pm 1$ aF. This value is in reasonable agreement with the estimation $C_0 = 50$ aF calculated with the C2D program.

The amplitude of the modulation of the current with U is maximal when the electrometer is biased at the Coulomb gap. Using a lock-in amplifier, we estimated the gate capacitor charge sensitivity to be at least 10^{-4} e/$\sqrt{\text{Hz}}$ at 1 kHz.

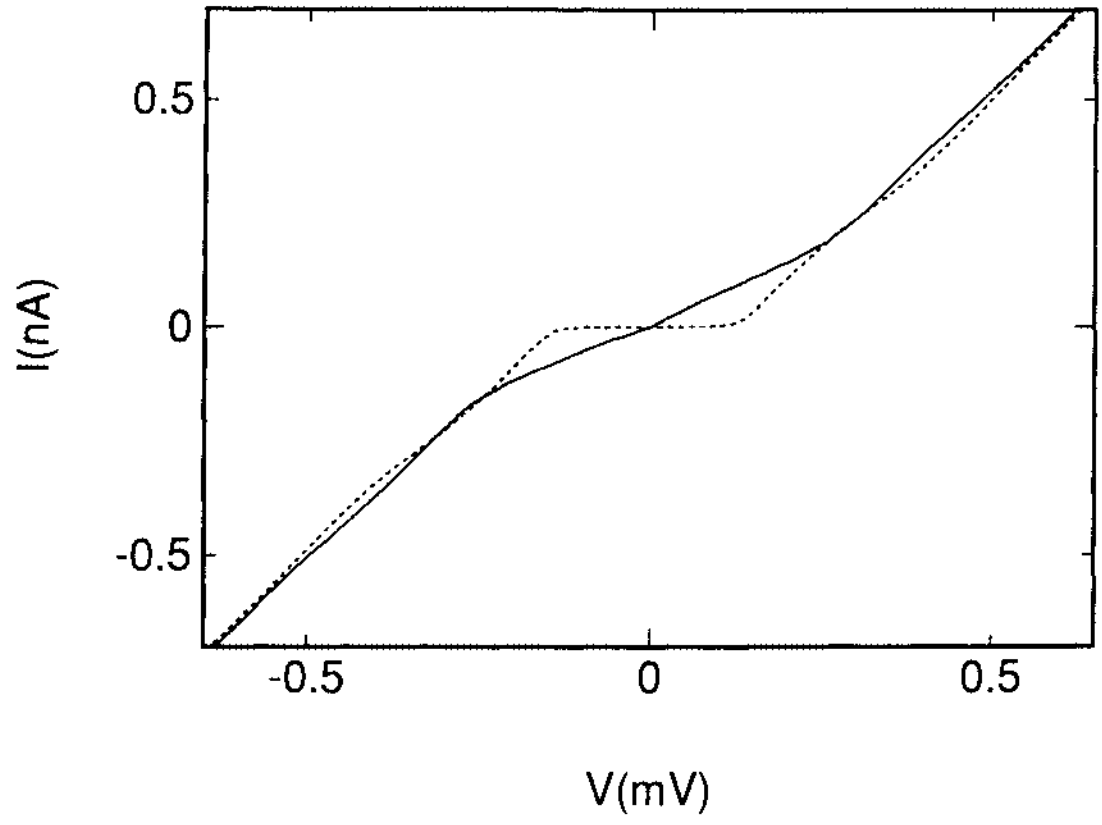

Fig. 4.5 *Electrometer* I – V *characteristic at* 20 mK. *Solid line: minimum Coulomb gap; dotted line: maximum Coulomb gap.*

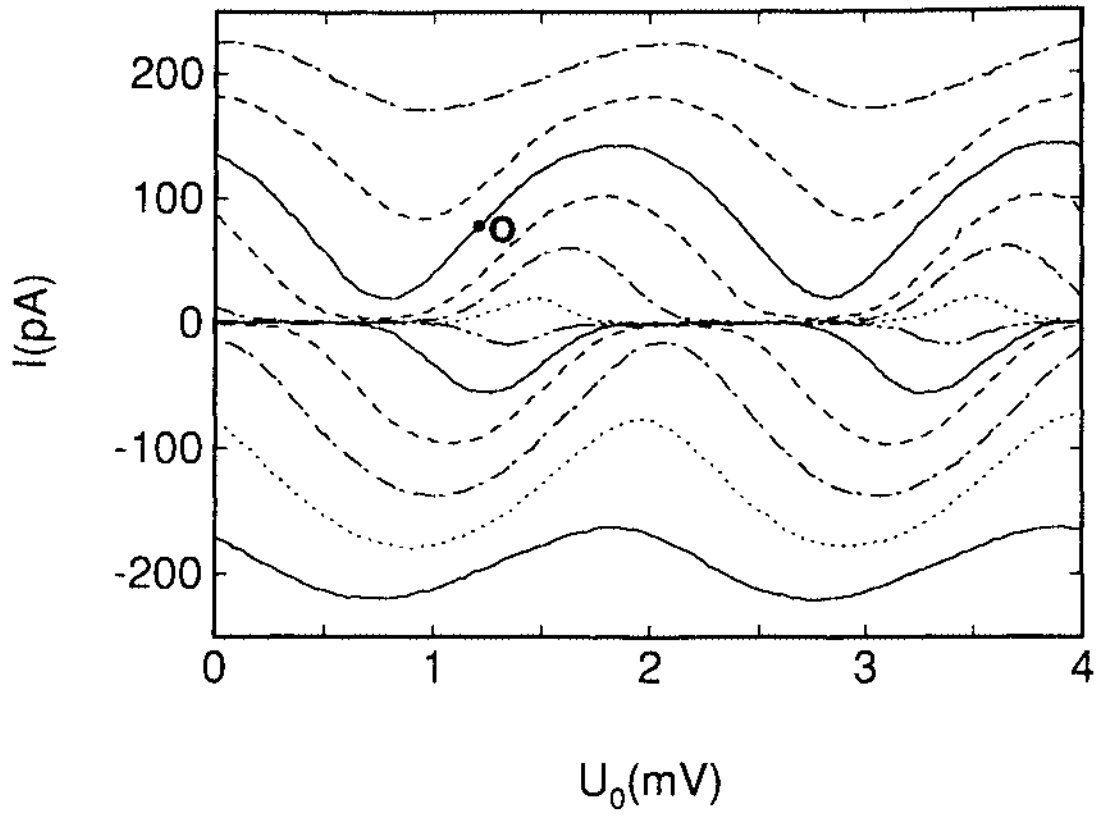

Fig. 4.6 *Electrometer current* I *versus electrometer gate voltage* U_0 *for a set of values of bias voltage* V *separated by* 25 μV. *The temperature is* 20 mK.

4.3. DETAILED OBSERVATION AND CONTROL OF THE COULOMB BLOCKADE OF TUNNELING IN THE ELECTRON BOX

We have measured the variations of $\langle Q \rangle$ versus $\tilde{Q}$ in the electron box using the SET electrometer described in the previous section. The experimental setup (shown schematically in Fig. 4.7a) consists of a 2-junction-in-parallel version of the electron box of Fig. 1.3, with the island b connected by a coupling capacitor C_c to island m of the electrometer. Nominally $C_s = C_c = C_0 = C/10$. When the average charge in the electron box is $\langle Q \rangle$, the charge on C_c is simply $(C_c/C)\langle Q \rangle$. As a consequence, the change in the electrometer current I due to a variation $\Delta\langle Q \rangle$ of $\langle Q \rangle$ is

$$\Delta I = \frac{C_c}{C}\left(\frac{dI}{C_0 dU_0}\right)\Delta\langle Q \rangle$$

were the slope of the $I - U_0$ characteristic is measured at the polarisation point U_0.

The circuit pattern is shown in Fig. 4.7b, where the numbers and letters labeling the aluminium electrodes refer to the corresponding nodes of the circuit shown in Fig. 4.7a. A SEM photograph of the effective circuit is shown is Fig. 4.8. The large-scale shape of the electrodes and their guards were designed to minimize cross-talk capacitances. Before a run, the junctions were checked by measuring the resistance between pads 1 and 3 and between pads 4 and 6. Because all four junctions have nominally the same area $50\times 50\text{nm}^2$, these two resistances should have the same value. This checking procedure is why the box measurement was carried on a parallel combination of two junctions instead of one: immediately after the junction resistance check, pads 1 and 3 were connected together using a strip of silver paint. At room temperature, the resistance of the SET transistor was found to be 460 kΩ and that of the electrometer 450 kΩ. At 4 K the total resistance of the electrometer was 620 kΩ.

The variations of I with U (see Fig. 4.9) are a superposition of a small-amplitude short-period sawtooth modulation and a large-amplitude large-period modulation. We attribute the slower modulation to a small cross-talk capacitance between pads 2 and m: assuming that the period of this modulation was e/C_{2m}, we deduced $C_{2m} \simeq 9$ aF, in good agreement with our estime from a C2D calculation, which was 8 aF. A small correcting

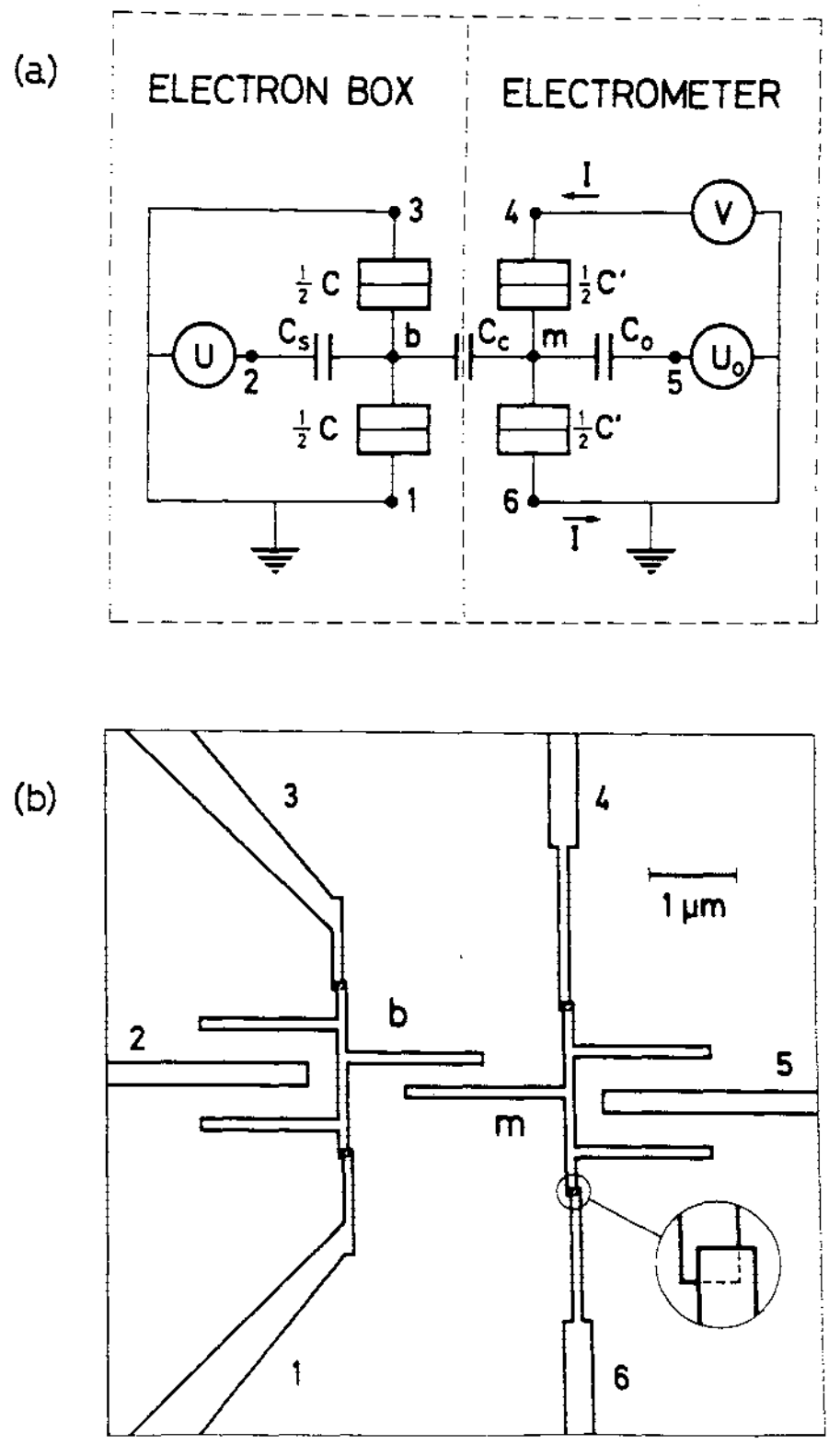

Fig. 4.7 (a) *Schematic representation of the experimental set up. An electron box with two junctions in parallel is coupled to the SET transistor used as an electrometer.* (b) *Electron beam lithography implementation of the circuit shown in* (a). *Superfluous electrodes (see* Fig. 4.8*) resulting from the use of the shadow evaporation technique have been omitted for clarity.*

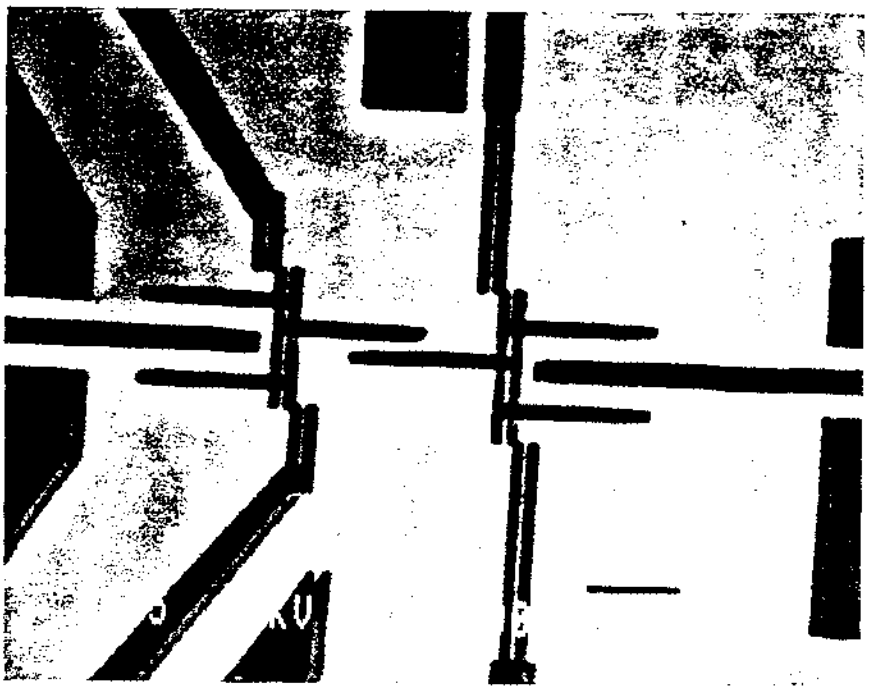

Fig. 4.8 *SEM photograph of the single electron box coupled to the SET transistor. The black bar corresponds to* 1 μm. *Superfluous electrodes, which are artifacts of the shadow mask evaporation technique, are visible. The different contrasts correspond to different metal thicknesses.*

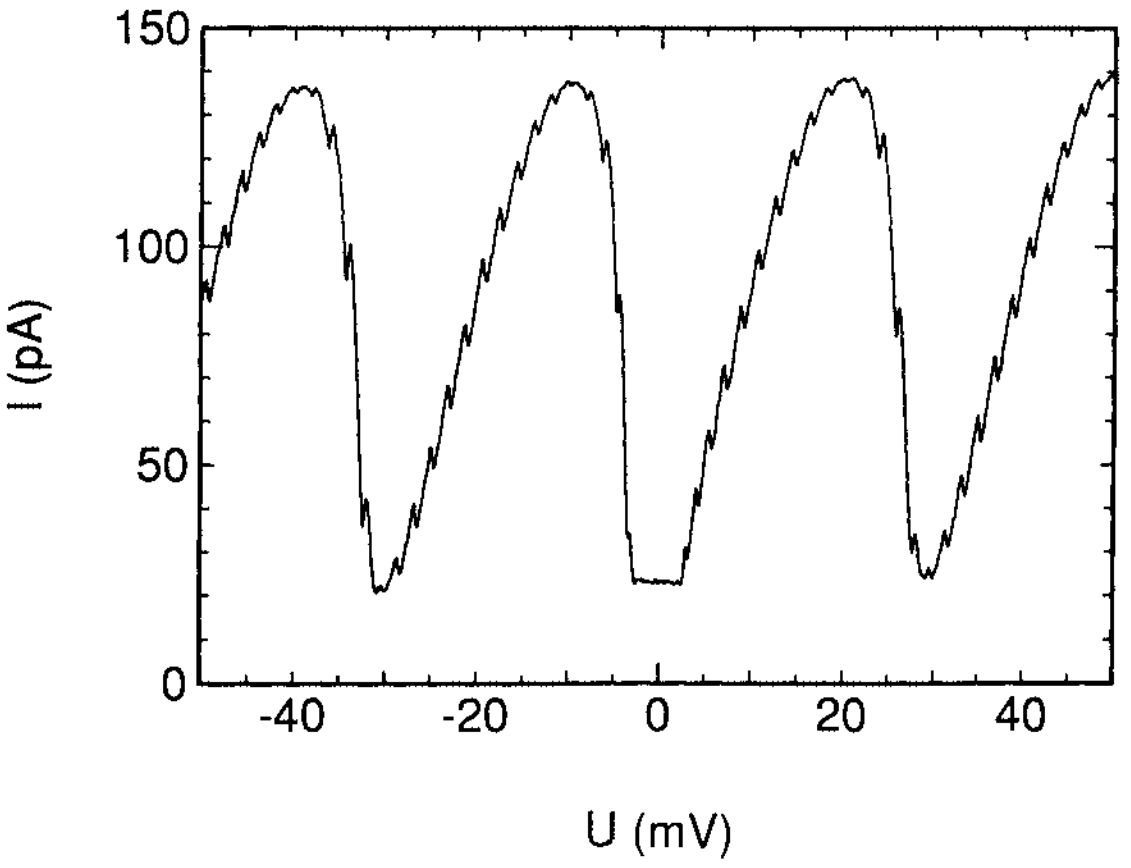

Fig. 4.9 *Electrometer current* I *versus electron box voltage* U *at* 20 mK. *The curve is clipped near* U = 0 *because one attenuator in the* U *line filtering system became superconducting at the lowest temperature when too little current flowed through it.*

voltage equal to $(C_{2m}/C_0)U$ was superimposed on U_0 to compensate for the modulation of I due to this cross-talk. By polarizing the electrometer with U_0 at a point of maximal slope (dI/dU_0) (see Fig. 4.6), we obtained the largest electrometer gain. Furthermore, in order to get rid of low frequency noise, we then used a lock-in amplifier with a 1 KHz, 40 μV modulation on the U input (corresponding to a $e/50$ modulation of the polarization charge $\tilde{Q}$) and recorded the variations of dI/dU as a function of U. Very sharp peaks appear that correspond each to an increase of the charge of the island b by one electron. The resulting curve at 20 mK is shown in Fig. 4.10. After integration, we finally arrived at the genuine variations of $\langle Q \rangle$ versus $\tilde{Q}$ (Fig. 4.11). The calibration of the horizontal axis involves the value of C_s while the calibration of the vertical axis involves both the values of the ratio C_c/C and a prior calibration of the electrometer using the voltage U_0 and the capacitance C_0. Assuming that the periodicity of the sawtooth variations is e, we found $C_s = 85 \pm 1$aF, $C_c = 74 \pm 1$aF, which are close to the expected values. Since the scan took 50 s per oscillations, the SET current through the junctions was 3 10^{-21}A.

Given the signal to noise ratio of the charge variations, this indicates that the leakage current from island b and its offset charge drift was at least one order of magnitude less than this value. Note that the downward variations of $\langle Q \rangle$, which should be relatively sharp at 20 mK, look rounded when compared with the theoretical prediction of Eq. (4.1.1) and (4.1.3) (dashed line in Fig. 4.11). In order to investigate this rounding we performed measurements at various temperatures. The results at different temperatures are shown in Fig. 4.12 (solid lines) where we also show for comparison the predictions of Eq. (4.1.1) and (1.3.2) (dashed lines). Since the electrometer gain is temperature dependent, a calibration was performed at every temperature. Although the experimental results are in agreement with the theoretical predictions above 100 mK, there is a discrepancy at lower temperatures between the thermometer temperature and the temperature that would fit the data. At 20 mK this discrepancy is 40 mK. 25 % of this discrepancy can be explained as due to the back action noise induced by electrometer on the box island, which we have calculated at finite temperature using numerical simulations. Parasitic rf signals on the U_0 and U lines could induce a broadening of the charge variations, although checks were performed to ensure that the direct influence of the background noise in the laboratory had no effect.

A further contribution could come from quantum fluctuations of the electron number n. It has been assumed so far that n is a classical variable, since the junctions tunnel resistance is much greater than the resistance quantum R_K. The quantum calculation of the average junction charge $\langle Q \rangle$ calculated with second order perturbations (i.e. taking into account the fluctuations $n \rightarrow n+1$ and $n \rightarrow n-1$) gives

$$\langle Q \rangle = \frac{C}{C+C_S}\left(\tilde{Q} + e\frac{R_K}{4\pi^2 R_T}\ln\left(\frac{\frac{e}{2}-\tilde{Q}}{\frac{e}{2}+\tilde{Q}}\right)\right)$$

Quantitatively, this correction does not explain the rounding observed in the experiment, but the expression diverges logarithmically when $\tilde{Q} = e/2$ where one expects $\langle Q \rangle = 0$ by symmetry: a non-perturbative calculation is clearly needed.

We also performed experiments in the superconducting case, by suppressing the magnetic field which was applied to bring the sample in the normal case. In the superconducting case, the optimum electrometer gain is located at the superconducting gap. The result of the measurement of $\langle Q \rangle$ versus $\tilde{Q}$ are plotted in Fig. 4.11 (solid curve labeled "S"); the improved signal-to-noise ratio in the superconducting case originates from the larger electrometer gain. The sawtooth variations of $\langle Q \rangle$ with $\tilde{Q}$ correspond as in the normal case to charges of value e tunneling through the junctions. The small value of the current ($3\ 10^{-21}$ A) through the junctions of the box implies that the $e-$periodicity of the variations of $\langle Q \rangle$ could be due to the presence of only <u>one</u> quasiparticle in the island.

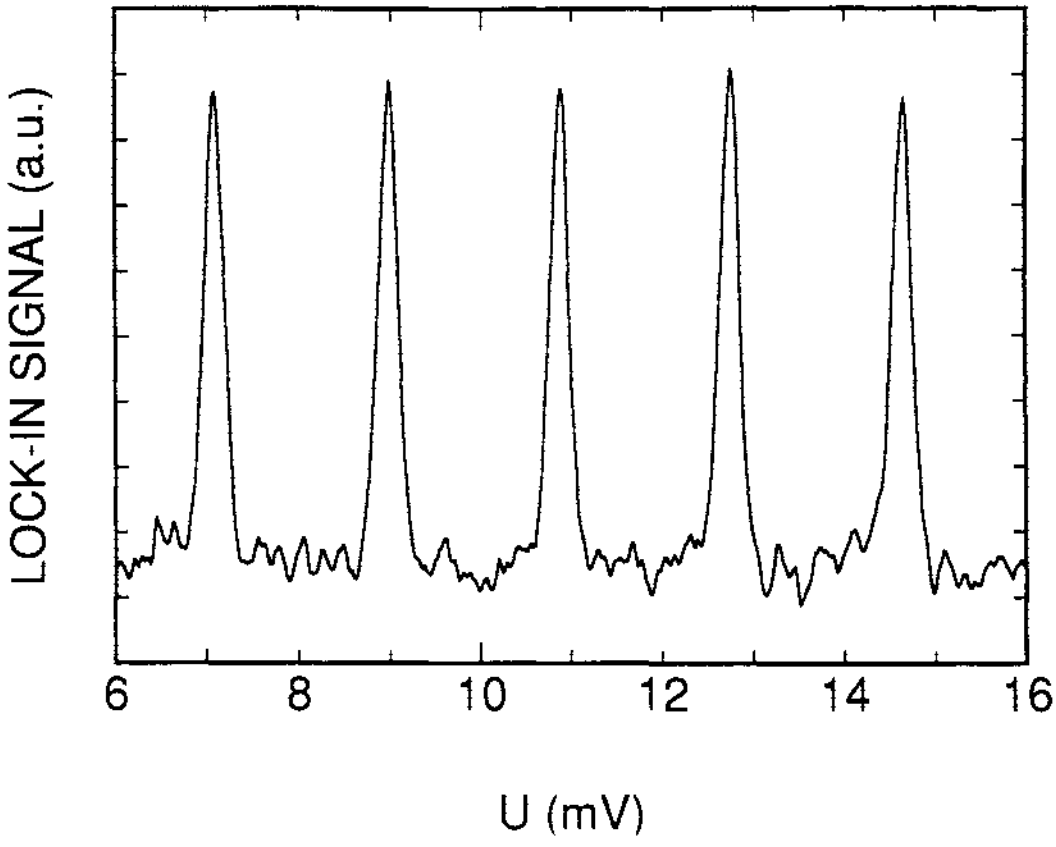

Fig. 4.10 *Lock-in signal as a function of electron box voltage* U, *in the presence of a correcting signal superimposed on the dc value of* U_0. *The temperature is* 20 mK. *Each peak is associated with the charge of the island* b *(see Fig. 4.5) increasing by one electron.*

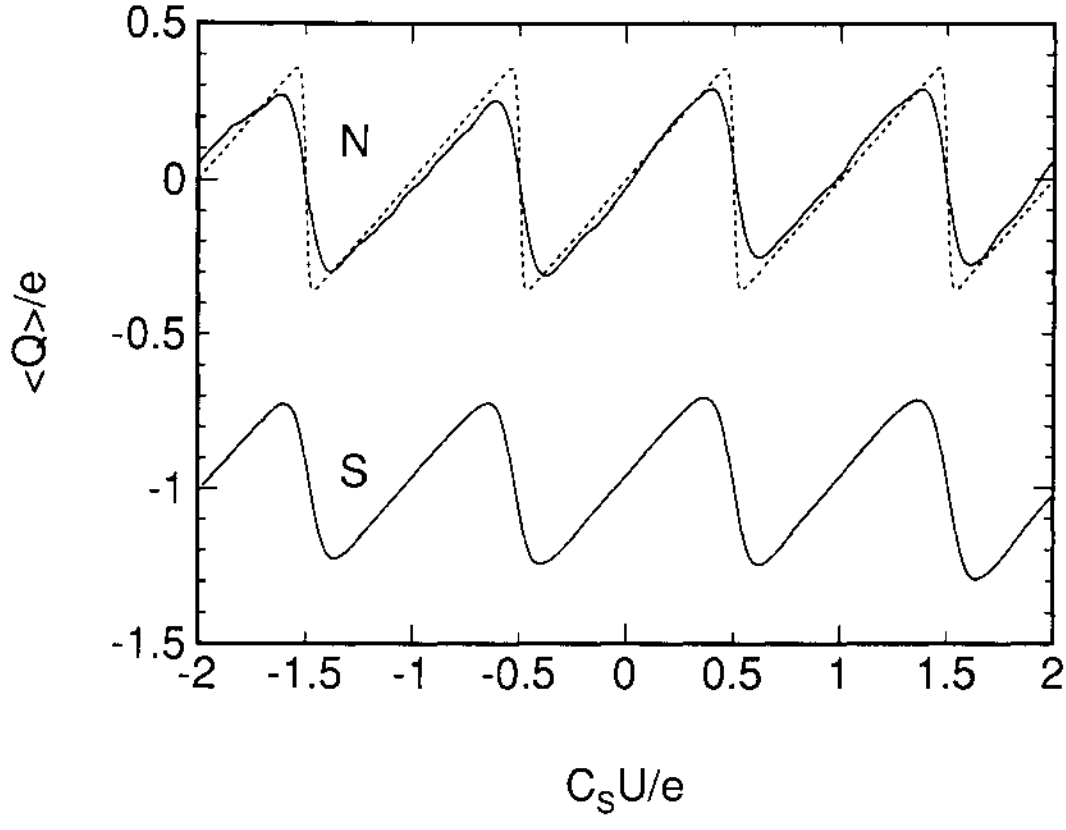

Fig. 4.11 *Charge variations on the junction in the normal state* (N) *and in the superconducting state* (S) *at* 20 mK. *For clarity, the curve labeled* S *has been shifted vertically.*

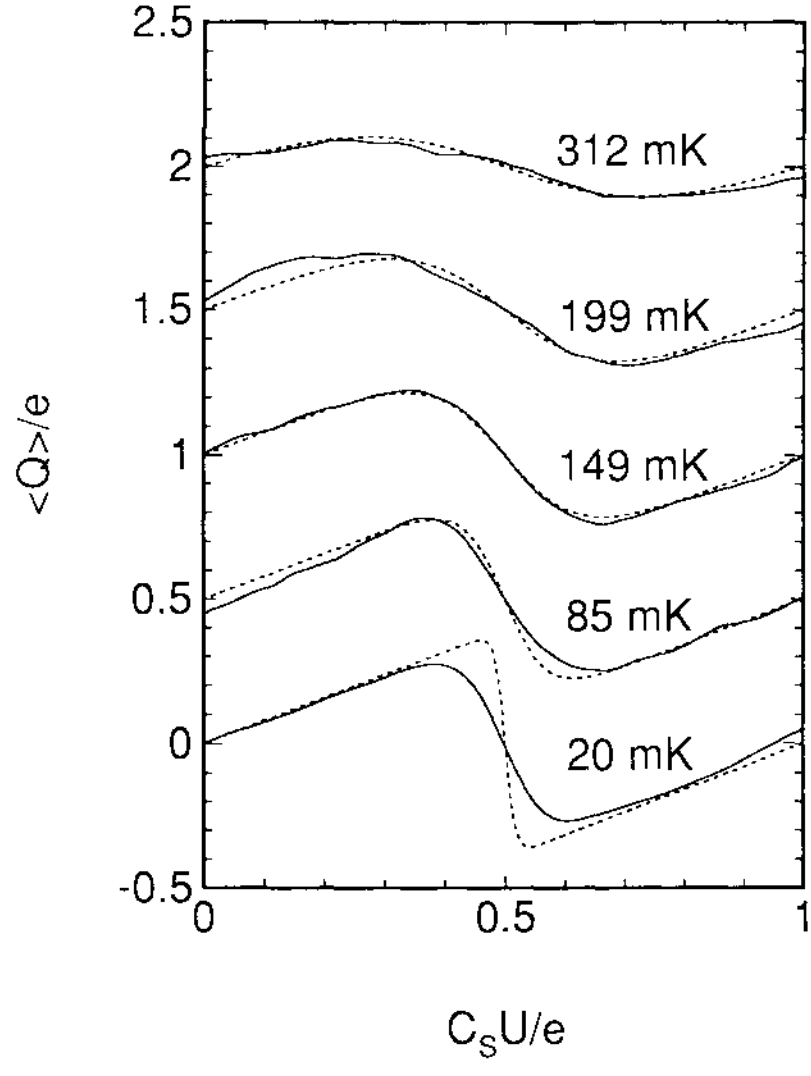

Fig. 4.12 *Solid lines: variations of the junction average charge* ⟨Q⟩ *at different temperatures, plotted in units of* e; *dashed lines: theoretical predictions of* Eq. 4.1.1.

A possible extension of this experiment would be to measure single tunnel events of electrons in the normal case or Cooper pairs in the superconducting case using two or more junctions in series instead of one. Indeed, the present experiment measures only the thermodynamic expectation $\langle Q \rangle$ of Q, as explained in section 4.1, and single elctron tunneling events are not resolved: the tunneling from one state to one next was very fast compared to the frequency of the U sweep. By "closing" the electron box with more junctions, the transitions would be radically slowed down because at the threshold $U = e/2C_0$ an electron charge can enter the box only by a co-tunneling through all the junctions (see appendix 3). This process is of higher order in the perturbation theory than the tunneling through one junction, and its rate is be much lower. We estimate that a box locked by four junctions would let the electron out at a rate close to 1 Hz, which is slow enough for individual events to be resolved.

5. CONTROLLED TRANSFER OF SINGLE CHARGES

In the electron box, single charges are moved in and out of the island in a controlled way. However, in order to transfer single charges through a device, the "in" and "out" ports must be different. In the SET transistor, a gate controls the current through two voltage biased junctions. At low bias voltages and low temperatures, we have shown that the number of extra electrons in the island between the junctions was either constant or oscillating between two successive integers, depending on the value of the gate voltage U_0 : a tunnel event through one junction is always followed by a tunnel event through the other one, resulting in a dc current. Thus, in a certain sense, electrons flow through the electrometer one by one, but the control provided by the gate is only a control of the rates, not of the time at which the transfer of each electron occurs through the device. In order to control this time, the electron must be trapped and then released in a controlled fashion.

To understand how this can be done, we have to generalize the concept of the Coulomb blockade that we developed in chapter 1 for the electron box to the more general case of a linear array of junctions. In a linear array of N junctions of capacitance C, such as those of Fig. 5.1a and Fig. 5.10a, an integer number of extra electrons will sit on each metallic island between two junctions. We call these numbers $\{n_i\} = (n_1, n_2, ..., n_{N-1})$ the electrostatic "configuration" of the device (Urbina *et al.*, 1991). Two configurations are called neighbours if one can be reached from the other by a single tunnel event on one junction of the array. For a given set of gate voltages, with a V across the array set to zero, particular configurations $\{n_i^s\}$ exist for which the energy of all its neighbours is higher by an amount of the order of $e^2/2C$. If the junctions are small enough, this energy is much higher than the characteristic energy of thermal fluctuations. Tunneling is then blocked in all of the junctions, and the circuit is trapped in a configuration $\{n_i^s\}$, hereafter referred to as a "stable configuration". When the gate voltages are now changed, the configuration will remain stable until the charge of one of the junctions reaches its critical value. Then the circuit may move to a new stable configuration by undergoing one or

more tunnel events. Charges can thus be transferred in a controlled way by modulating the gate voltages along a trajectory of configuration space so as to follow a sequence of stable configurations.

We have designed and operated two types of circuits, which we called "turnstiles" and "pumps", for which there exist a sequence of stable configurations.

In the turnstile (Fig. 5.1), a gate is connected to the central island of a linear array biased below the Coulomb gap. The charge of each junction is therefore below its critical charge. By then decreasing the gate voltage, the charge on the junctions on the left arm of the gate is increased to their critical charge. A cascade of tunnel events in the left arm transfers then a charge $+e$ to the central island. When the gate voltage is then increased, the charge $+e$ escapes from the island through the right arm. In the turnstile, the electron transfer is irreversible because the electrons are transferred in the direction imposed by the bias voltage: it is impossible to force the electrons against the bias voltage with only a single gate.

The pump (Fig. 5.10), as opposed to the turnstile, is however a reversible device. It can be operated with zero bias voltage. A charge e is taken from the leftmost electrode to the left island by decreasing the left gate voltage; the electron is then transferred from the left island to the right island by increasing the first gate voltage while decreasing the second one; finally it is transferred from the right island to the rightmost electrode by increasing the second gate voltage. The circuit being driven from one stable configuration to a neighbouring stable configuration, the transport is adiabatic. The modulation of the gates in the opposite sequence transfers the charge in the opposite direction. In practice two phase-shifted sinusoidal signals are used, and one electron is "pumped" per cycle through the device.

In both the turnstile and the pump, the current generated by the repetition of the transfer sequence at a frequency f is equal to ef, where $e \simeq 1.6022\ 10^{-19}$ C $\simeq$ 0.16022 fA/MHz.

In the following we describe the detailed operation of the turnstile and of the pump, so as to demonstrate their "generic" nature (generic in the sense that they transfer electrons

one by one, irrespectively of the precise value of the capacitances and tunnel resistances of the junctions, as well as the precise values of the driving voltages) and why they are "minimal" (no simpler devices could achieve the same type of control of individual charge carriers).

5.1. THE TURNSTILE

5.1.1. Operation principle

The turnstile (Fig. 5.1a) is a two-arm, one gate device like the SET transistor, but in which the electrons enter and leave the center at two different values of the gate voltage U. This separation of the entrance and the exit voltages is obtained by placing at least two junctions in each arm the device. In the same way as a SET transistor can be viewed as a single electron box with separate "in" and "out" lines, a turnstile can be viewed as a "single electron trap" with separate "in" and "out" lines.

The single electron trap

The single electron trap (Fig. 5.2) consists of two tunnel junctions of capacitance C biased by a voltage source U through a capacitor C_s. This circuit cannot accommodate any extra electrons on the island between the two junctions (one junction charge would be larger than $e/2$ which is always larger than the critical charge). Thus, a stable configuration has no extra electron in the island between the junctions and n extra electrons on the island connected to the capacitor C_s. For $\tilde{Q} = C_s U = 0$, $n = 0$ is the stable configuration. When $\tilde{Q}$ is increased from zero, $n = 0$ becomes unstable at the point wherethe charges of each junction $Q = (C/(2C + C_s))\tilde{Q}$ reaches the critical charge $Q_c = (e/2)(1 - C_s/(2C_s + C))$, i.e. when $\tilde{Q}/e = 1/2 + C_s/2C$. The trap switches then to the configuration $n = 1$ by undergoing two tunnel events. If $\tilde{Q}$ is then decreased, the configuration $n = 1$ becomes unstable when $Q = (C/(2C_s + C))(\tilde{Q} + e)$, which is less than or equal to zero, reaches $-Q_c$, i.e. when $\tilde{Q}/e = 1/2 - C_s/2C$. The electron trap is therefore bistable for $\tilde{Q}/e \in [1/2 - C_s/2C, 1/2 + C_s/2C]$. This bistability is due to the energy barrier between stable configurations due to the charging energy of the intermediate island. In consequence of

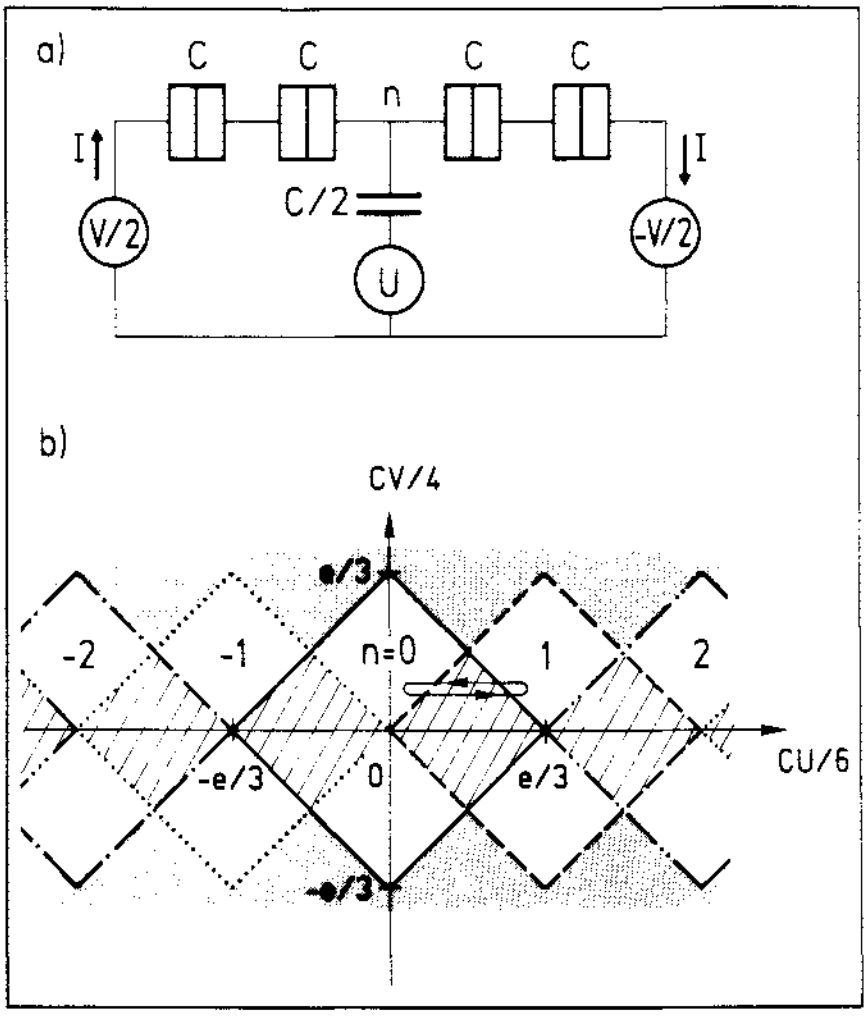

Fig. 5.1 (a) *Single electron turnstile schematic. The device consists of four tunnel junctions and one gate. The number of extra electrons in the central island is denoted by* n. (b) *Turnstile stability diagram in the* (U, V) *plane for the particular capacitance ratio in* (a). *For example* $n = 1$ *is locally stable when the voltages parameters are inside the dashed line square. One cycle along the trajectory shown transfers one electron across the device in the direction imposed by* V.

(a)

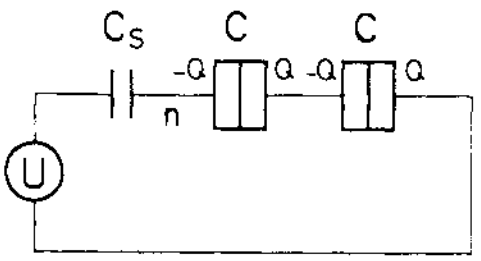

(b)

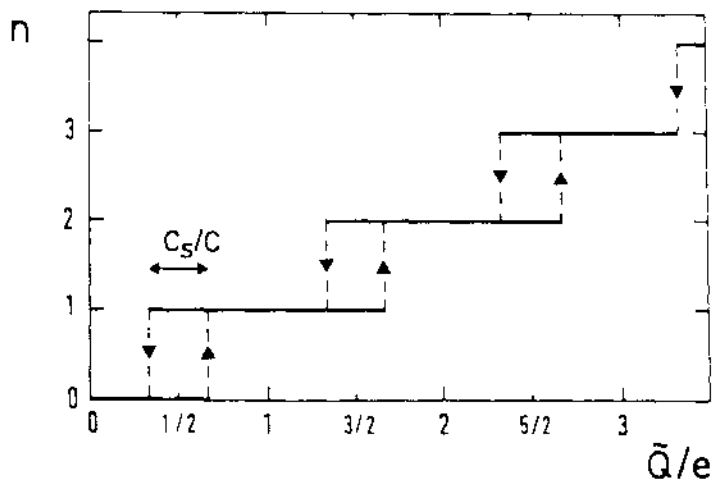

Fig. 5.2 (a) *Single electron trap. Two junctions in series are biased through a true capacitance. No electrons can be stored in the island between the two junctions. The stable configurations are described by the number* n *of extra electrons on the leftmost island.* (b) *Stable configurations of the trap as a function of* $\tilde{Q} = C_s U$. *For certain ranges of* $\tilde{Q}$ *there exists two locally stable configurations.*

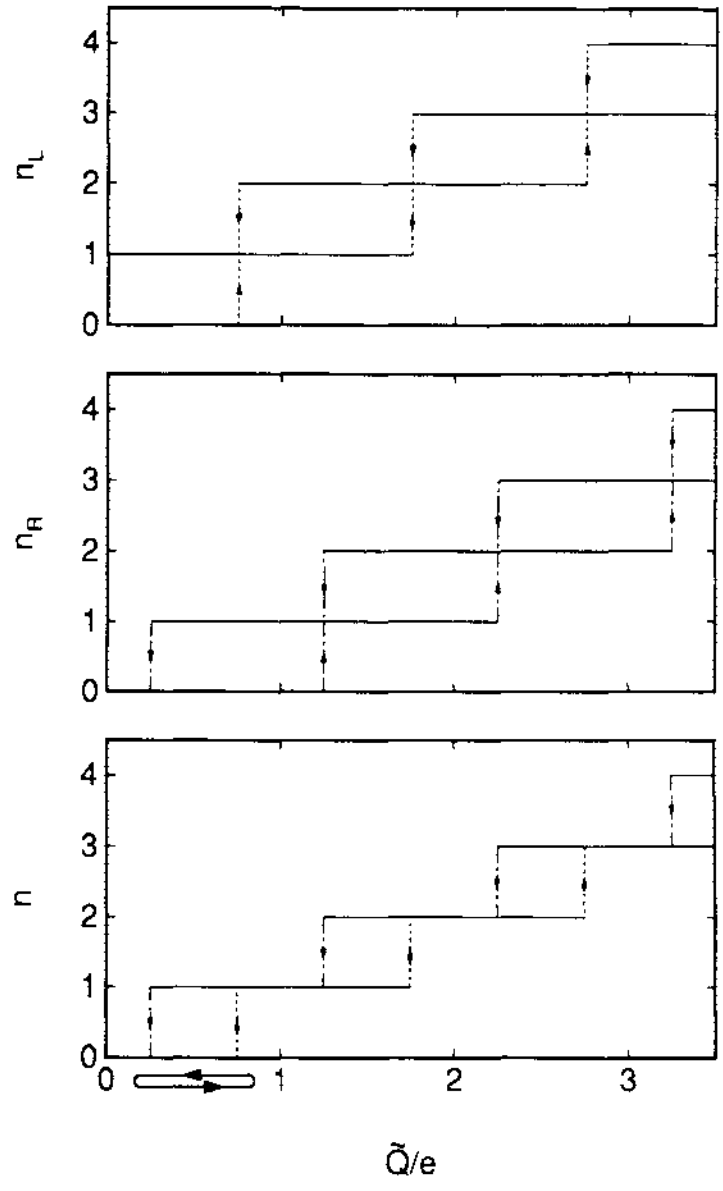

Fig. 5.3 *Locally stable configurations of the turnstile with gate capacitance* C/2 *(cf.* Fig. 5.1*) with respect to tunneling through the left arm only (top pannel), through the right arm only (middle pannel) and both (bottom pannel). The shift between the two upper curves corresponds to a bias voltage* V = e/3C. *One cycle along the trajectory shown transfers one electron across the device.*

this bistability, the turnstile is hysteretic, irreversible and dissipative.

Stability of the configurations of the turnstile

We now analyze the behaviour of the turnstile of Fig. 5.1a with the numbers n_L and n_R of extra electrons on the central island that would minimize the electrostatic energy if tunneling was allowed only through the left arm (the right junction), the right one (the left one) behaving like a true capacitor. If we assume that tunneling occur through one arm, the turnstile can be viewed as a trap, voltage biased by $U/2 \pm V/4$ through $C_s = C$. We define $\tilde{Q} = CU/2$. The numbers $n_L(\tilde{Q})$ and $n_R(\tilde{Q})$ are therefore identical bivalued functions of $\tilde{Q}$, shifted from one another by $CV/2$ (Fig. 5.3). If $\tilde{Q}$ is increased from zero, the configuration $n = 0$ becomes first unstable to transfer across the left arm: one electron enters the island through the left arm, and $n = 1$ is the new stable configuration. If $\tilde{Q}$ is then decreased, $n = 1$ becomes unstable relative to tunneling through the right arm: the electron leaves the island through the right arm and $n = 0$ is the new configuration. This state differs from the initial one: overall one electron went through the turnstile from left to right. In short, one electron is transferred through the device, by sweeping $\tilde{Q}$ over one hysteresis region. In the same way, N electrons are transferred when $\tilde{Q}$ is modulated back and forth over N hysteresis regions: the island first stores N electrons coming through the left arm and then empties itself through the right arm. Note that if $\tilde{Q}$ is modulated with an amplitude Ne, the number of hysteresis regions encircled is N or $N-1$, depending on the central value of the modulation.

Direct description of the turnstile with its stability diagram

The hysteresis of the turnstile can also be deduced from the stability diagram of its configurations (Fig. 5.1b). Different stability domains overlap in the (U, V) plane, which means that the turnstile is hysteretic. A cut of the stability diagram at a given bias voltage corresponds to the preceding description (Fig. 5.3). Therefore a modulation of U like the one depicted in Fig. 5.1b is the same as the one depicted in Fig. 5.3: it transfers one electron per cycle.

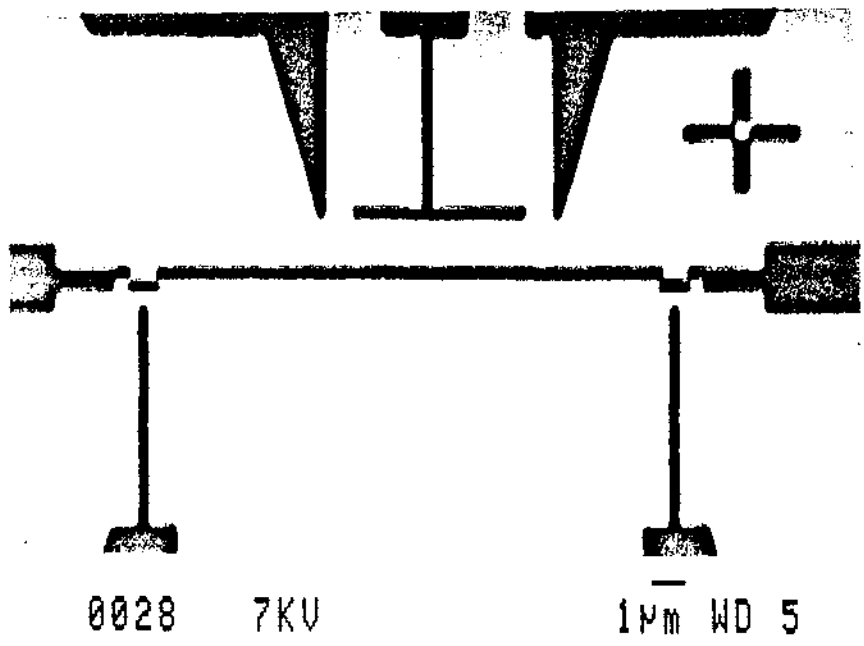

Fig. 5.4 *SEM photograph of a 2+2 junction turnstile. The central island is larger than the islands of the arms in order to have a large gate capacitance. The cross in the upper right corner of the picture was used for alignment between two magnifications. This device was fabricated before we developped a good understanding of two dimensional electrostatics (see section 3.2.1): no interdigitated capacitors were used, and the guarding scheme was far from being optimal.*

5.1.2. Controlled transfer of single electrons one by one in 2+2 junction turnstiles

We performed experiments with turnstiles consisting of two or three tunnel junctions in each arm. Paper 2 reports the operation of a $2+2$ turnstile fabricated in Delft. We report here results on another $2+2$ turnstile fabricated in Saclay.

A SEM photograph of the $2+2$ turnstile fabricated in Saclay is shown in Fig. 5.4. The gate line is coupled to the central island with a large capacitance. Two other gate lines couple weakly to the islands in the arms. They are meant to correct the offset charges (Likharev, 1988) appearing on those islands when the sample is cooled down. Offset charges reduce the charging energy of the intermediate state, which diminishes the width of the hysteretic regions. Only dc voltages are applied to these correcting gates.

The parameters of the turnstile

The four junctions of the turnstile were identical. We call R_T and C the tunnel resistance and the capacitance of one junction. We deduced R_T and C from the $I-V$ characteristic at medium scale: the slope of the asymptotes gave roughly the total tunnel resistance of the device: $4R_T \simeq 2.16$ MΩ, so $R_T \simeq 540$ kΩ. The offset of 980 μV between the two linear sections of the $I-V$ characteristic at positive and negative voltage should be equal to $3 \times e/C$, which gives $C = 0.54$ fF.

We measured the dependance of the current on the gate voltage when the turnstile is polarized over the Coulomb gap. From the period e/C_s of this modulation we deduced $C_S = 0.14$ fF.

The transfer of electrons

We measured the current through the device as a function of the dc value U of the gate voltage, and also while superposing to U an alternating vtage of frequency $f = 3$ MHz, and amplitude near e/C_s. These measurements are the two lowest curve of Fig. 5.5. With rf, the current oscillates between zero and ef. A current of ef is obtained for the values of

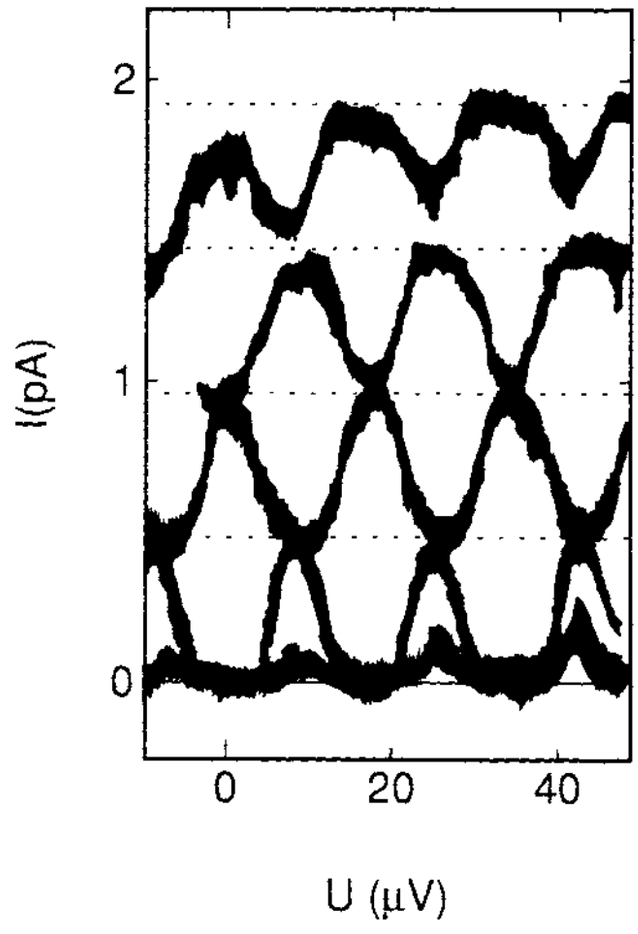

Fig. 5.5 *Current* I *through the turnstile as a function of the gate voltage* U. *The bias voltage* $V = 100\ \mu V$ *is below the Coulomb gap. The current of the lowest curve is due to co-tunneling through all the junctions of the turnstile. The other curves were obtained by superimposing on the dc value of* U *a rf voltage at* $f = 3$ MHz *with peak-to-peak amplitudes that were multiples of* $2e/C$. *The dashed lines indicate the current at multiples of* $ef \approx 0.48$ pA. *This figure was obtained from a photograph of the screen of a storage oscilloscope.*

U for which the alternating voltage sweeps over a complete hysteresis region. For example with a peak to peak amplitude of $2e/C_S$, a trajectory centered at $U = e/2C_s$ encircles one hysteresis region, and the current is ef whereas a trajectory centered at $U = e/C_s$ encircles two hysteresis regions, and the current is $2ef$ (see Fig. 5.3).

We repeated this measurement with peak to peak amplitudes of the alternative voltage proportional to e/C_S (Fig. 5.5). As the dc gate voltage is swept, the current oscillates between two values. These two values are well given by two successive multiples of ef. They correspond to the number of hysteresis regions encircled by a trajectory of constant amplitude.

We measured the current voltage characteristics with the dc gate voltage set near $e/2C_S$ according to the interpretation of the current versus gate voltage measurement, and a rf voltage of amplitude around e/C_S peak to peak at frequencies between 1 and 10 MHz. The characteristics exhibit plateaus of constant current whose height depend on the frequency (see Fig. 5.6). In Fig. 5.7, we plot the current measured at the inflexion points as a function of frequency. The current obeys the relation $I = ef$ within the experimental accuracy, which was around one percent.

5.1.3. Deviations from the ideal I = ef behaviour

Whereas one would expect from the description of section 5.1.1 to find perfectly flat plateaus at $I = ef$, the experimental plateaus are not. The rounding of the plateaus is attributed to various "error" mechanisms that either cause missed cycles or parasitic tunneling events. Some of these errors can be explained within the "global rules" : parasitics events occur due to a non-zero bath temperature; some events are lost because the operation frequency is not negligible compared to the characteristic frequency of tunneling $(R_T C)^{-1}$. Other error sources are due to more complex processes: electrons get hotter than the phonons due to the weak electron-phonon coupling, and co-tunneling makes it possible for electrons to take paths other thann the desired ones. Another error source is the cross-talk between the central gate and the lateral islands that slightly modulates the energy barrier for tunneling across the two arms.

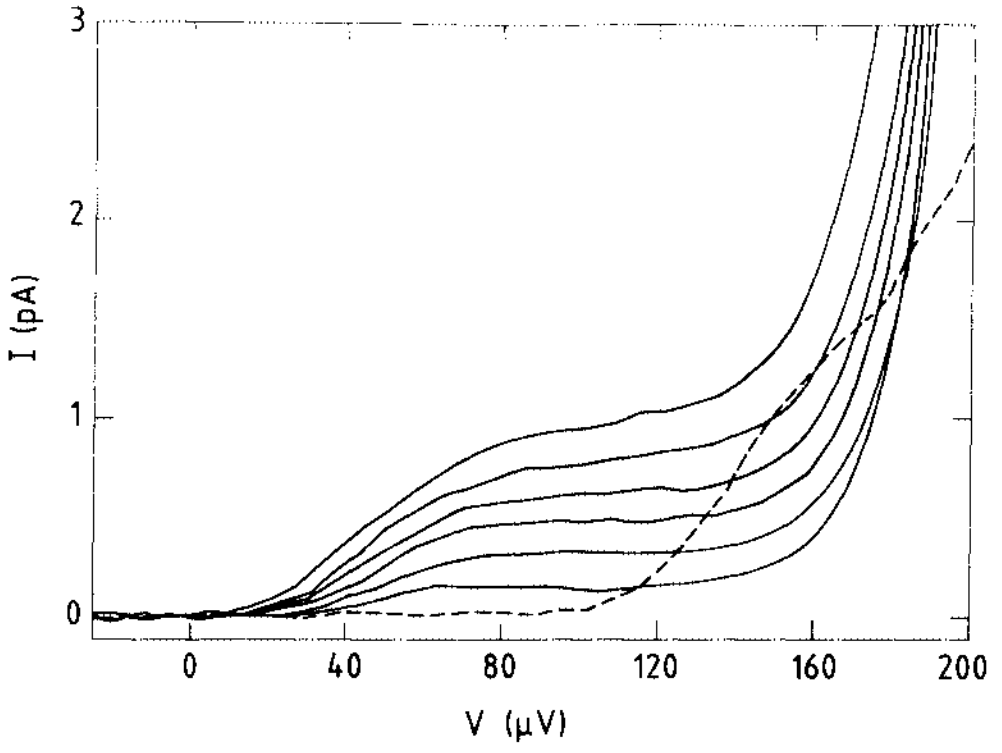

Fig. 5.6 I – V *characteristic of the turnstile without rf on the gate (dashed line) and with rf at* f = 1, 2, 3, 4, 5, 6 MHz *(solid lines, from bottom to top). Equally spaced plateaus can be observed. Their rounding is more pronounced at higher frequencies.*

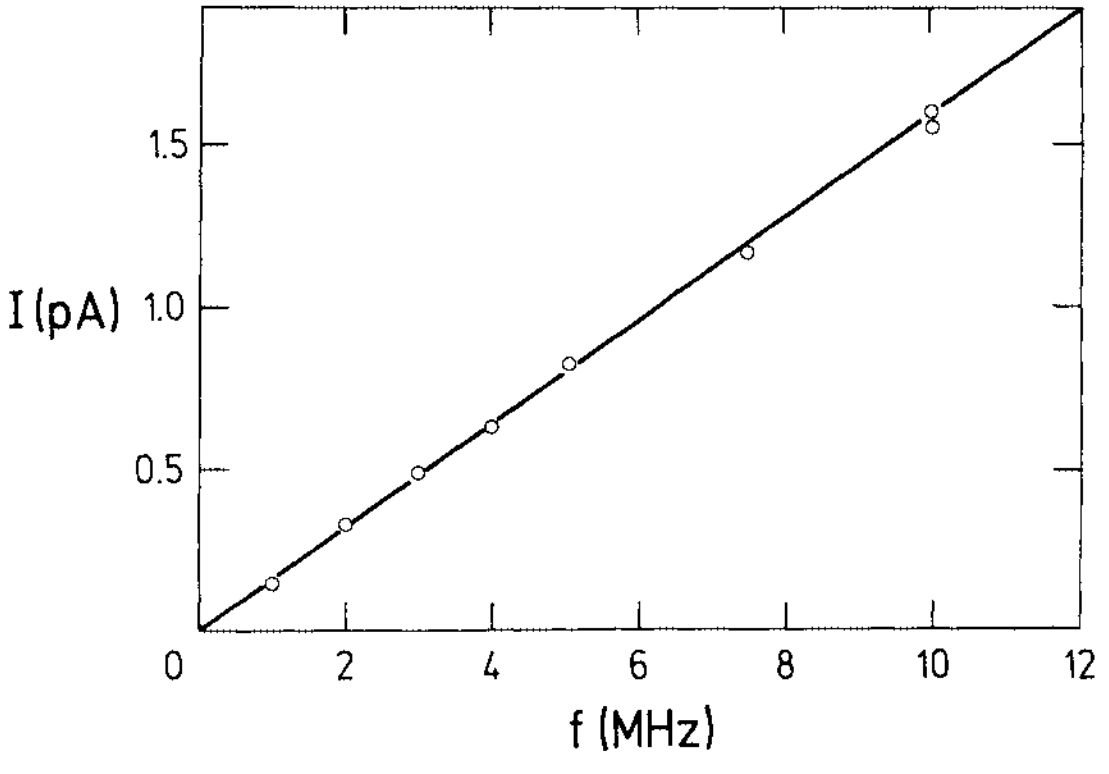

Fig. 5.7 *Current at the inflexion point of the plateau of the* I – V *characteristic as a function of the rf frequency* f *(open dots). The solid line indicates* I = ef.

5.1.3.1. Effect of the temperature

According to the global rules (Eq. 2.3.4), at zero temperature the tunneling rate through a junction is zero when its charge Q is below its critical charge Q_c. This is not the case at finite temperature. In particular, if $k_BT << |\Delta E|$, where $\Delta E = (e/C)(Q - Q_c)$,

$$\Gamma \simeq \frac{1}{e^2 R_T} \Delta E \left(1 + \exp\left(\frac{-\Delta E}{k_B T}\right)\right) \text{ if } \Delta E \geq 0$$

$$\Gamma \simeq \frac{1}{e^2 R_T} |\Delta E| \exp\left(\frac{-|\Delta E|}{k_B T}\right) \text{ if } \Delta E \leq 0$$

It results in an imperfect blockade of tunneling. The consequences for the operation of the turnstile operation are i) a finite current flows below the Coulomb gap ; ii) there is a non-zero probability for one electron to enter the central island through the "wrong" arm. We measured the temperature dependence of the current-voltage characteristic of a turnstile (see Fig. 5.8), which clearly demonstrated the rounding of the plateau induced by an increase of the temperature.

5.1.3.2. Effect of the operation frequency

The characteristic frequency scale for tunnel events is $(R_T C)^{-1}$. If the operation frequency is not small compared to this characteristic frequency, some tunnel events will not have enough time to occur.

More precisely, in the turnstile operation, the charge of each junction varies in a periodic fashion with a typical amplitude Q_c, and the tunneling rates are of the order of $(R_T C)^{-1}(Q_c/e)$. If the operation frequency is not low enough compared to the frequency $(R_T C)^{-1}(Q_c/e)$, some tunnel events will be missed during the cycle because of the stochastic nature of the tunnel process. Consider for simplicity a square modulation of the gate voltage with mean value $U = e/C$, with a peak to peak amplitude of e/C, at the bias voltage $V = e/3C$. Then when $n = 0$ and $U = e/C$, the charge on a junction of the right arm is $Q = 5e/12$. Since $Q_c = e/3$, an electron is expected to tunnel through this arm inside the island. The probability for this event not to occur during a half-cycle of U is:

$$P_{01} = \exp\left(-\int_0^{1/2f} \Gamma(t)\, dt\right) = \exp\left(-\frac{1}{24 f R_T C}\right)$$

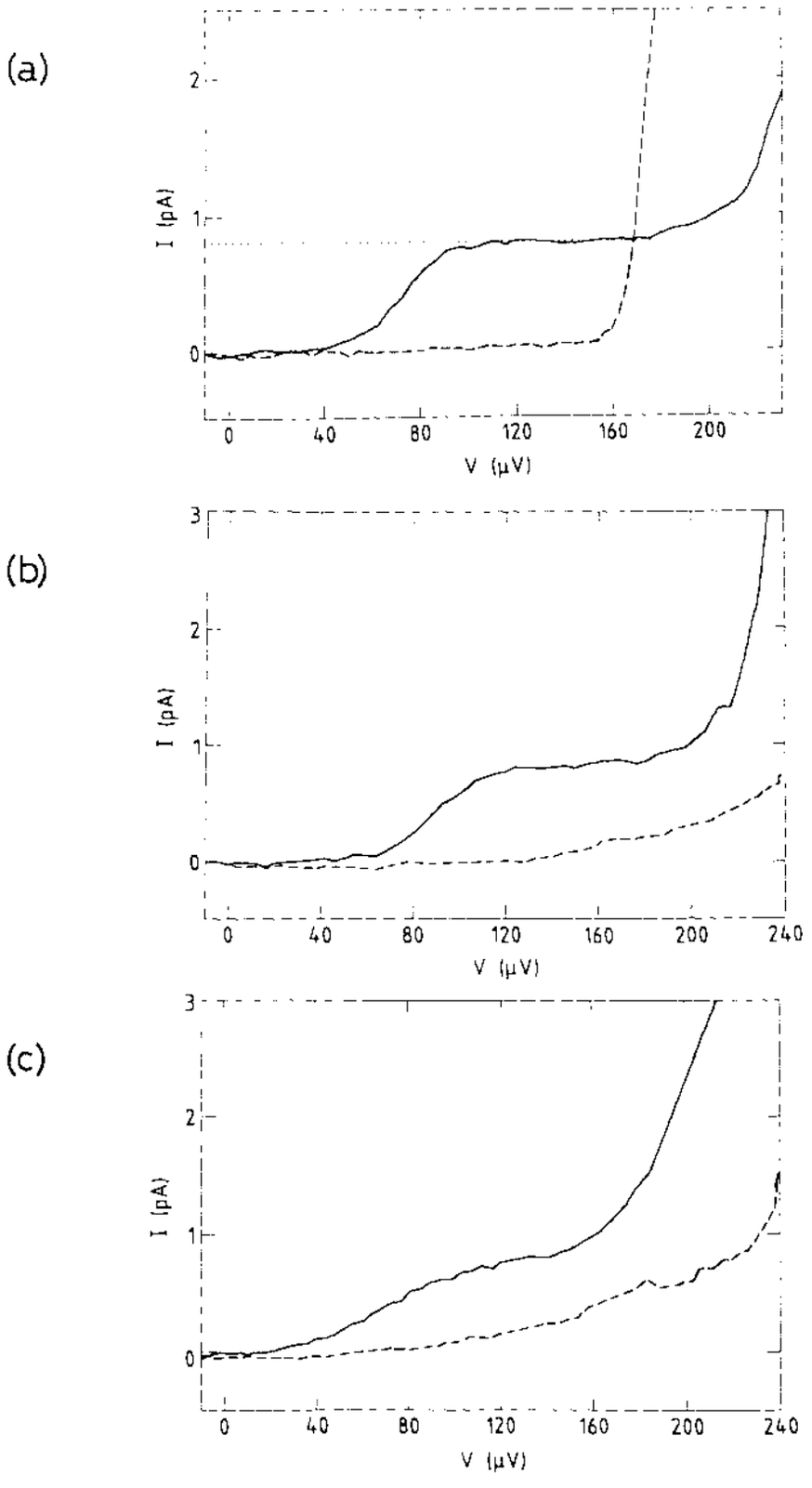

Fig. 5.8 *Temperature dependence of the* $I-V$ *characteristic of the turnstile without rf (dashed line) and with rf (solid line) at* $f = 5.05$ MHz; *dotted line corresponds to* $I = ef \simeq 0.81$ pA : (a) $T = 20$ mK; (b) $T = 36$ mK; (c) $T = 103$ mK.

Hence, the probability of missing a cycle is 10^{-2} for $fR_TC = 10^{-2}$ and 10^{-18} for $fR_TC = 10^{-3}$. This effect is much more sensitive when using a sinusoidal modulation of U, since for most of the cycle the tunneling rate is lower than with a square-wave modulation.

We measured the $I - Vs$ at different frequencies between 1 and 10MHz. Figure 5.6 shows examples between 1 and 6 MHz. These characteristics clearly illustrate the rounding of the plateau with increasing frequency.

5.1.3.3. Hot electron effects

The turnstile operation is based on the existence of metastable configurations. When a tunnel event occurs, the difference of electrostatic energy is converted in kinetic energy of the tunneling electron. A change of stable configuration of the turnstile is obtained by the tunneling of an electron through one arm, i.e. at least two junctions. Even if the first tunnel event occurs at the threshold Q_c, the second tunnel event will occur well above the threshold and the energy at least equal to $\Delta E = e^2/3C$ will be transformed into kinetic energy. The energy e^2/C corresponds in our experiment to a temperature of 1.1 K. The hot electron is scattered both by the other electrons and by the phonons, and it thermalises through these two channels (Fig. 5.9). The coupling of the electron gas to the phonon gas can be very small at low temperatures, as demonstrated by Roukes *et al.* (1985) and Wellstood (1988), so the temperature of the electrons can be different to the phonon temperature when heated by hot electrons.In the following we evaluate quantitatively the effect of the heating of the electron gas by the tunneling electrons. The input power provided by the tunneling electrons at frequency f in the operation of the turnstile heats the electron gas. In order to estimate the equilibrium electron gas temperature T_e, we follow Wellstood and write:

$$P = \Sigma\Omega(T_e^5 - T_{ph}^5)$$

where:

i) Ω is the volume of metal

ii) Σ is a coupling constant given by $\Sigma \simeq 0.524\alpha^*\gamma$ where we call α^* the thermally averaged electron-phonon scattering constant and γ the ratio of the electronic heat capacity per unit

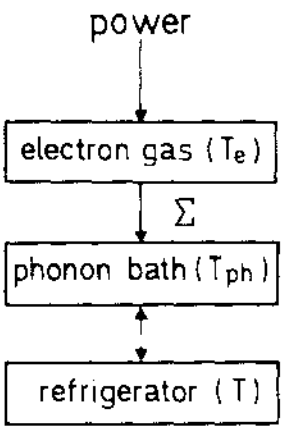

Fig. 5.9 *Heating of the electron gas during the turnstile operation. The energy of the tunneling electrons is redistributed within the electron gas. The finite power flow between the electron gas and the phonon gas, characterized by the parameter* Σ, *causes the two temperatures* T_e *and* T_{ph} *to differ.*

volume and the electron gas temperature: $\gamma = C_{el}/T_e$. α^* is itself given by

$$\alpha^* \simeq \frac{6\xi(3)M_0^2 k_B^3}{\pi\hbar^5 s^3 V_F}$$

with $\xi(3) \simeq 1.202$; s is the velocity of sound is the metal; $M_0^2 = (\hbar/2\mu s)(2\epsilon_F/3)^2$; μ is its mass density; ϵ_F is its Fermi energy. Using the parameters for aluminium (Kittel, 1963): $\epsilon_F = 11.63$ eV; $\mu = 2.7\ 10^3$ kg/m^3; $s = 3040$ m/s; $\gamma_{Mole} = 9.12\ 10^{-4}$J/(mol.K^2) we found finally $\Sigma_{Al} \simeq 3.8.10^9$ W/(K^5.m^3). Similar evaluations for copper, silver and gold-copper lead to values of Σ roughly half those obtained in experiments (Wellstood, 1988).

The total volume of all the metallic islands in our device is $\Omega \simeq 10^{-19}$ m^3. The power dissipated per cycle in all the islands is roughly $P \simeq 2(e^2/3C)f$ (the factor of 2 accounts for the two tunnel events occuring during one cycle: the first one when the electron enters the island, the second one when it leaves it). Assuming that the phonon bath temperature is 20 mK, the electron gas temperature is therefore given by

$$T_e \simeq \left(\frac{\frac{2e^2}{3C} f}{3.8\ 10^{-10}} + \left(20.10^{-3}\right)^5 \right)^{1/5}$$

With $C = 0.5$ fF we find:

$$T_{e[\mathrm{mK}]} \simeq 20\left(1 + 30 f_{[\mathrm{MHz}]}\right)^{1/5}$$

At $f = 1$ MHz this leads to $T_e \simeq 40$ mK, and at $f = 10$ MHz to $T_e \simeq 60$ mK. This values corresponds to the temperature we had to introduce in the simulations of the current-voltage characteristics to account for the experimental results of paper 2.

5.1.3.4. Effect of co-tunneling

As the operation of the turnstile is based on the use of metastable states, co-tunneling events may degrade the regularity. Two types of effects result from co-tunneling: some give an increase in the current, others a decrease. First, the entrance of an electron onto the island can occur by co-tunneling through the wrong arm: this decreases the net current. Second, when the electron has entered the island, it can leave it by co-tunneling for certain

combinations of V and U while another one replaces it: two electrons will have been transferred during the cycle. Similar errors can occur in the second part of the cycle.

However, the tunnel resistance of the devices we used were high enough so that the largest errors were due to thermal fluctuations. Nevertheless, for the design of a turnstile for metrological applications, those processes should be taken into account when estimating the precision.

5.2. THE PUMP

The pump consists of three junctions with capacitances C, C' and C'', and two gates whose capacitances C_1 and C_2 are much smaller than the junction capacitances (see Fig. 5.10a). By modulating both gate voltages, an electron can be driven from island to island in a reversible way.

5.2.1. Controlled transfer of electrons one by one in a 3-junction pump

The bias voltage and the two voltages applied to the gate capacitors are denoted by V, U_1 and U_2. The configuration of the circuit is given by the island integer charges (n_1, n_2).

Figure 5.10b shows, for $V = 0$ and $C = C' = C''$, the stability domains of the different couples (n_1, n_2) in the $C_1U_1 \otimes C_2U_2$ plane. These domains are elongated hexagons and tile the plane to form a lattice with quadratic symmetry, the periods being e along both axes. Neighbouring domains in parameter space correspond to nearest neighbours in configuration space. The boundaries of three mutual neighbouring domains share a triple point: for example, point P of Fig. 5.10b is shared by domains (0,0), (1,0) and (0,1). The pumping of electron is based on this topological property, and does not depend on the precise values of the capacitances. Note that there are two triple points per unit cell of the quadratic lattice [see points P and Q in Fig. 5.10b]. Every neighbour of a "P type" triple point is a "Q type" triple point and vice versa. At finite bias voltage V, the honeycomb pattern of Fig. 5.10b is distorted: the triple points are replaced by triangle-shaped regions, inside which no stable configurations can exist and where conduction thus takes place (Fig. 5.11). The size of these regions increases linearly with the bias voltage.

The pump is operated by first applying dc voltages to the gates so as to place the circuit in the vicinity of a triple point. The bias voltage is kept well below the Coulomb gap voltage $e/3C$. Two periodic signals with the same frequency f but dephased by $\Phi \sim \pi/2$ are then superimposed on the gate voltages. The circuit thus follows a closed trajectory like the circle shown around point P in Fig 5.10b. The frequency is chosen low enough $[f \ll (RC)^{-1}]$ to let the system adiabatically follow its ground state, which changes along

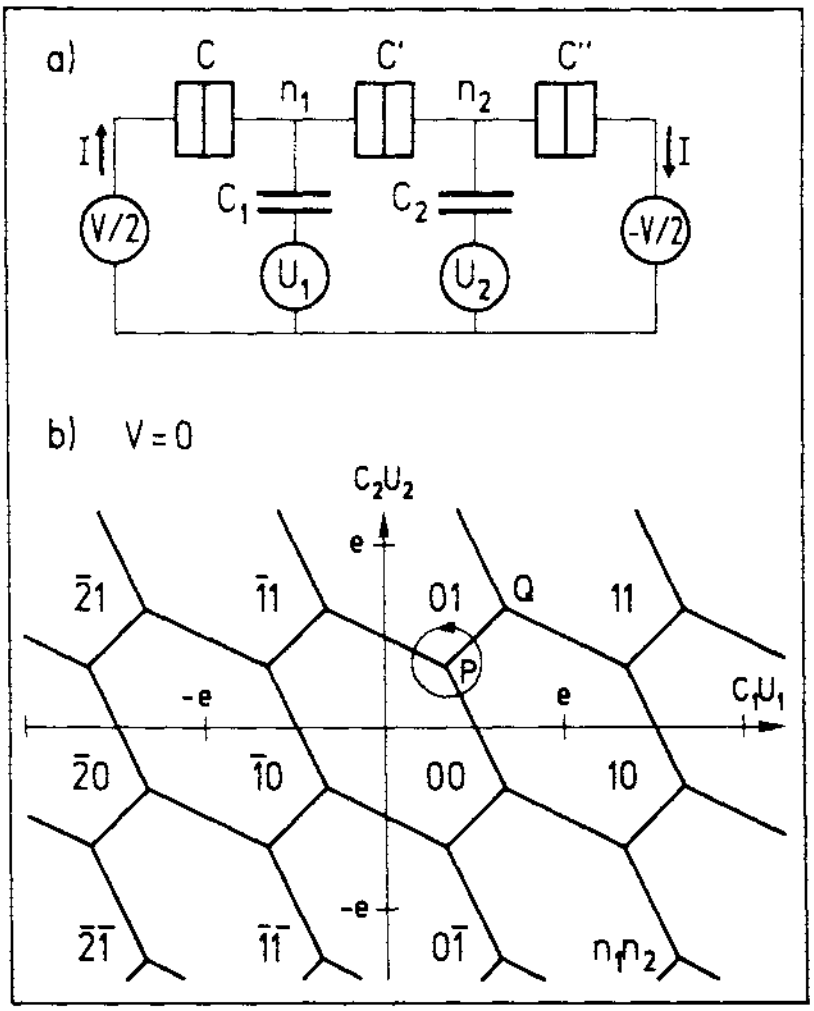

Fig. 5.10 (a) *Electron pump. The stable configurations are given by the numbers* n_1 *and* n_2 *of extra electrons on the two islands. Since the gate capacitances* C_1 *and* C_2 *are much smaller than the capacitance* C *of the junctions, the gates provide a quasi charge bias of the islands.* I *denotes the current through the pump. A bias voltage* V *can be applied, but is not necessary for the pumping of electrons.* (b) *Stability diagram of the configurations* n_1, n_2 *of the pump at zero bias voltage as a function of the bias charges* C_1U_1 *and* C_2U_2. *A closed trajectory around point* P, *such as the one shown, transfers one electron per cycle through the pump (see Fig. 5.12). The direction of the transfer depends only on the direction of the rotation.*

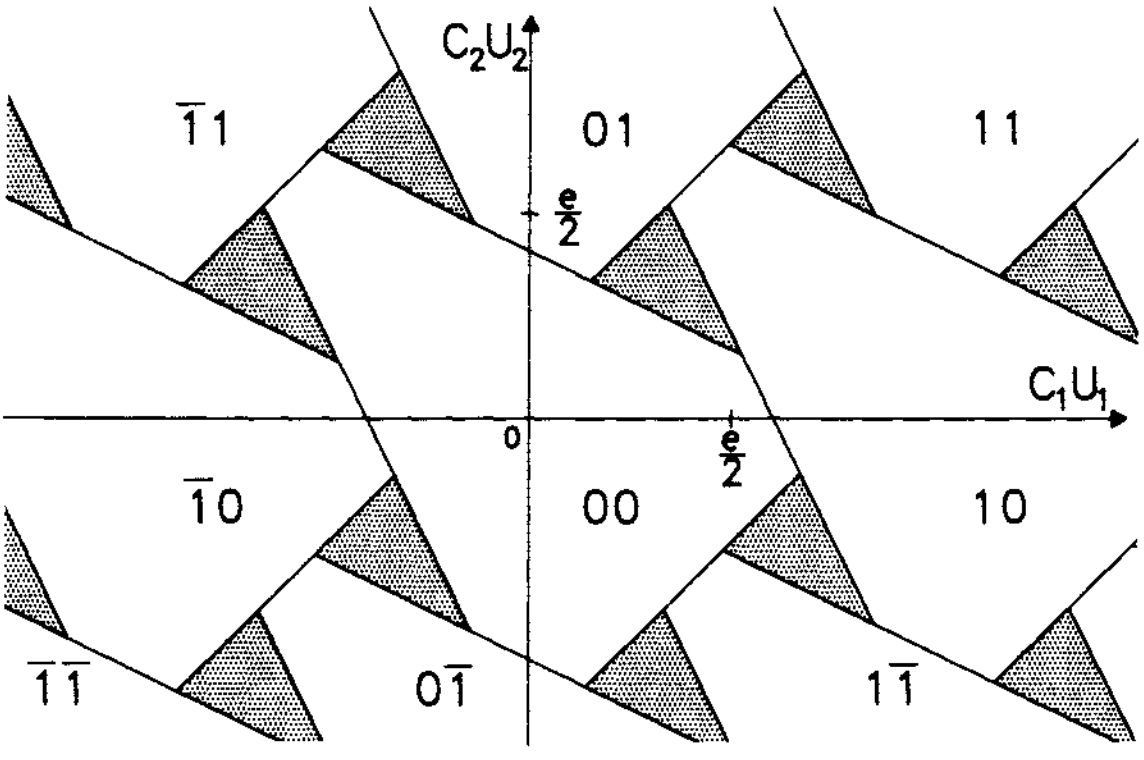

Fig. 5.11 *Stability diagram of the configurations* n_1, n_2 *of the pump at finite (positive) bias voltage* V. *The pump conducts in the grey triangular regions, where no configuration is stable.*

the trajectory. In Fig. 5.12 we shown both the trajectory in configuration space and the corresponding sequence of states in the real space. Suppose that the initial island configuration is $(0,0)$ and that the trajectory is followed counterclockwise. The circuit goes first from $(0,0)$ to $(1,0)$ by letting one electron tunnel through the leftmost junction. Then the island configuration changes to $(0,1)$ when one electron goes through the central junction. Finally, the system returns to its initial island configuration $(0,0)$ by letting one electron out through the rightmost junction. In a complete cycle one electron is transferred from left to right. If the sense of rotation in parameter space is reversed, in practice by adding π to the phase shift Φ, the electron transfer will take place in the opposite direction. Note also that the same original positive rotation around a "Q type" triple point produces a transfer from right to left. In summary, these geometrical considerations show that for zero bias voltage V, two rf gate voltages induce a current $I = ef$ to flow through the circuit, provided the dc gate voltages are set in the vicinity of a triple point. The direction of current is solely determined by the phase shift and the type of triple point.

As the voltage V is increased, electrons can still be pumped provided that the trajectory followed in parameter space encloses the conduction regions. Note that this can occur even if V and I have opposit signs. Numerical simulations have shown that regular electron transfers can persist up to one-fifth of the Coulomb gap voltage for an optimal rf amplitude. Coherent simultaneous tunnel events (co-tunneling) on two junctions, which provide the mechanism for transitions between next nearest neighbour configurations, are expected to slightly degrade the pump regularity. The same type of operation should in principle lead to the pumping of Cooper pairs, with a current $I = 2ef$, provided the device is in an ideal superconducting state with no quasi-particles present. By contrast, the principle of the turnstile cannot directly be generalized to Cooper pairs since it involves dissipative tunnel events. Finally, let us mention for completeness that a pump for normal electrons based on an heterojunction structure and operating on a totally different principle has been considered by Niu (Niu, 1990).

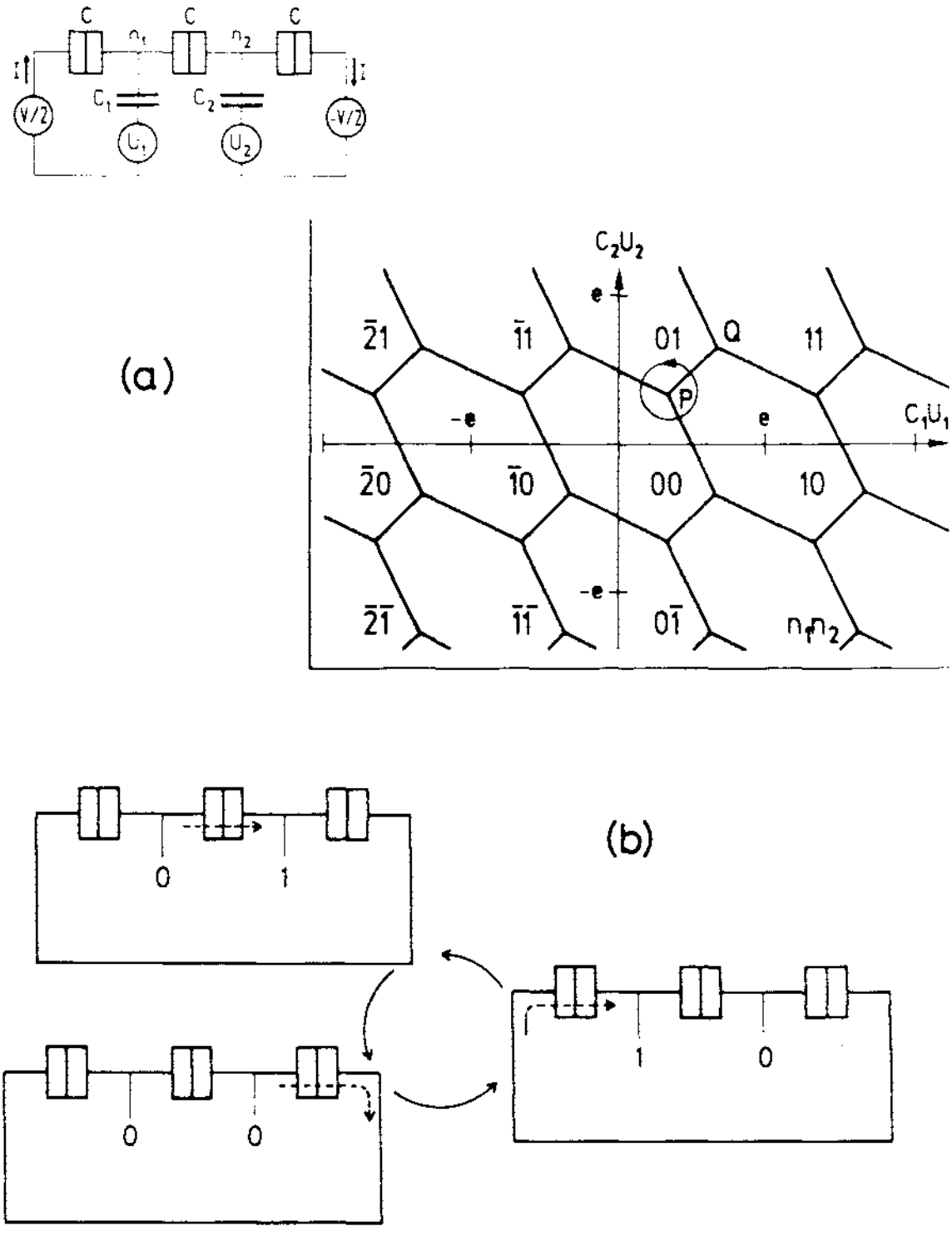

Fig. 5.12: *Principle of the operation of the pump in both gate voltages space* (a) *and in real space (b). The circle trajectory in (a) is obtained by adding two phase shifted rf voltages on top of the dc value* $e/3C_1$ *(resp.* $e/3C_2$*) of gate voltage* U_1 *(resp.* U_2*). Each time the trajectory in gate voltage space crosses a border between the stability regions of two configurations* (a)*, the configuration of the pump changes due to a tunnel event through one junction* (b)*. Therefore a complete cycle around point* P *results in the transfer of one charge* e *through the entire pump. A rotation in the same direction around point* Q *would transfer one electron per cycle in the opposite direction.*

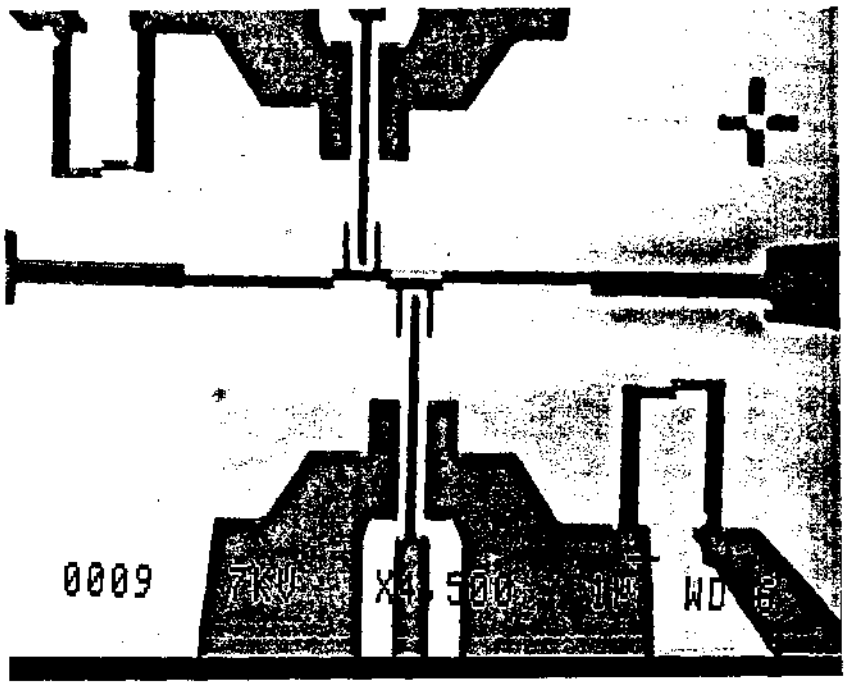

Fig. 5.13 *SEM photograph of a pump. The two guarded gate lines couple to the pump islands with interdigitated lines. The junctions of the pump are located at the overlap between the shifted films near the center of the picture. Two test junctions are visible in the upper left and lower right corners of the image.*

Preliminary results on a pump in which the geometry of the gates was not optimized to diminish the cross-talk were published (Pothier *et al.*, 1991a). We report here measurements on an optimized pump with a total normal resistance of 380 kΩ. A SEM photograph of the device is shown in Fig. 5.13. The average junction capacitance was estimated from the Coulomb gap (Fig. 5.14) to be about 0.4 fF. In Fig. 5.15 we show the results of an experiment in which the current through the array was recorded as the dc gate voltages U_1^{dc} and U_2^{dc} were scanned. The bias voltage V was set to zero and two 0.3 mV amplitude rf signals in quadrature at frequency f = 4 *MHz* were superimposed on the dc gate voltages. In the top panel of Fig. 5.15 we show the result of a scan of U_1^{dc}, U_2^{dc} being kept constant. This panel represents a cut though a current surface which is represented in the bottom panel, the position of the cut being indicated by a dotted line. For clarity, we have represented the current "hills" and "valleys" using the following convention: A white dot means a positive current of between $+0.8ef$ and $+1.05ef$ (upper pair of dashed lines in top panel), a black dot means a negative current of between $-0.8ef$ and $-1.05ef$ (lower pair of dashed lines) and the absence of dots means a current between $-0.8ef$ and $+0.8ef$. Apart from a slight global deformation and an overall translation, the pattern of hills and valleys reproduces the honeycomb pattern of Fig. 5.10b, a hill (valley) corresponding to a P-type (Q-type) triple point. We attribute the slight deformation of this experimental honeycomb pattern to the cross-capacitance C_x between islands and gates. We have calculated the ground state diagram for arbitrary C_1, C_2, C_x, $(C+C'')/C'$ and $(C-C'')/C'$. The best fit to the data is shown in the bottom panel of Fig. 5.15 and corresponds to $C_1 = 74 \pm 2$ aF, $C_2 = 61 \pm 2$ aF, $C_x = 7 \pm 1$ aF, $(C+C'')/C' = 2.1 \pm .5$ and $(C-C'')/C' = -0.3 \pm 0.06$. In the fitting, we have of course allowed an overall translation of the diagram corresponding to arbitrary offset charges (Likharev, 1988) on the gate capacitors. Although these offset charges were found constant on a time scale of a few hours, abrupt shifts of the pattern on longer time intervals were often observed. The capacitances that we obtain from the fit agree with the values estimated from the geometry of the nanolithographic mask. Fig. 5.16 shows the bias voltage dependence of the current at a "P type" triple point with $f = 4$ MHz and for two phase shifts separated by π; a plateau is observed near the center of the I-V curve. The sign of the height of the plateau reverses abruptly as the phase shift between

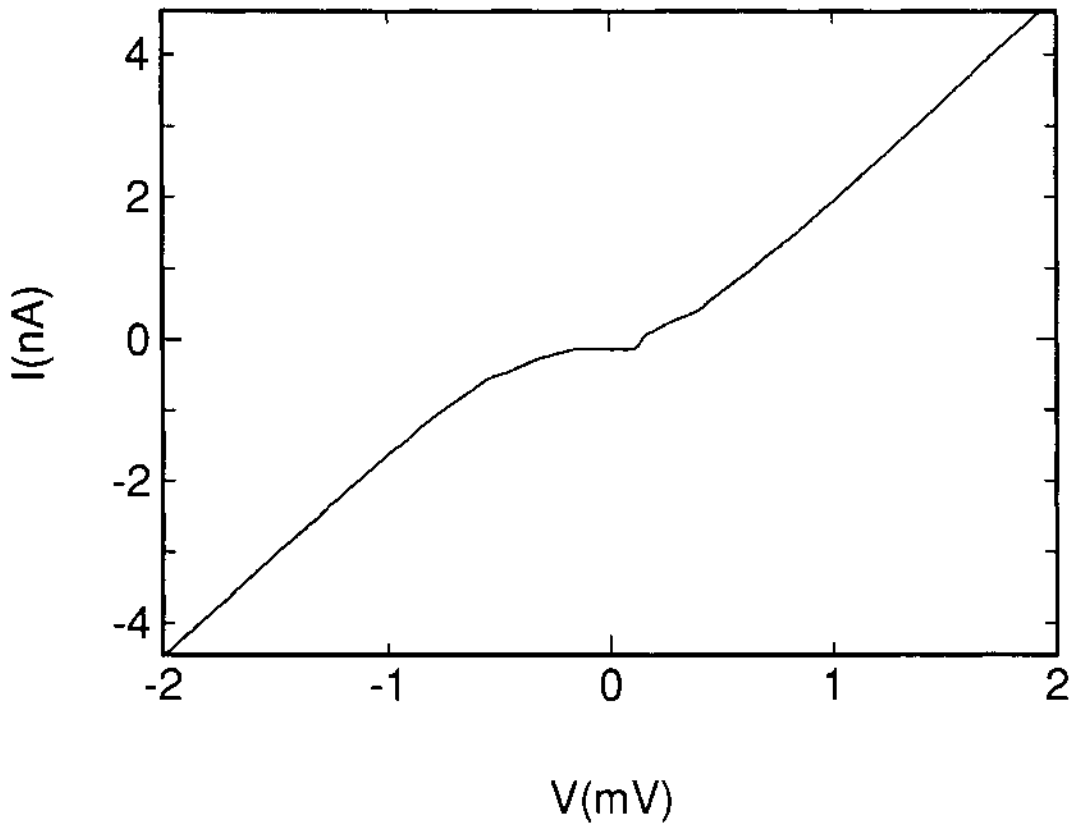

Fig. 5.14 I – V *characteristic of the pump. The characteristic is not symetrical because the two gate voltages were not zero.*

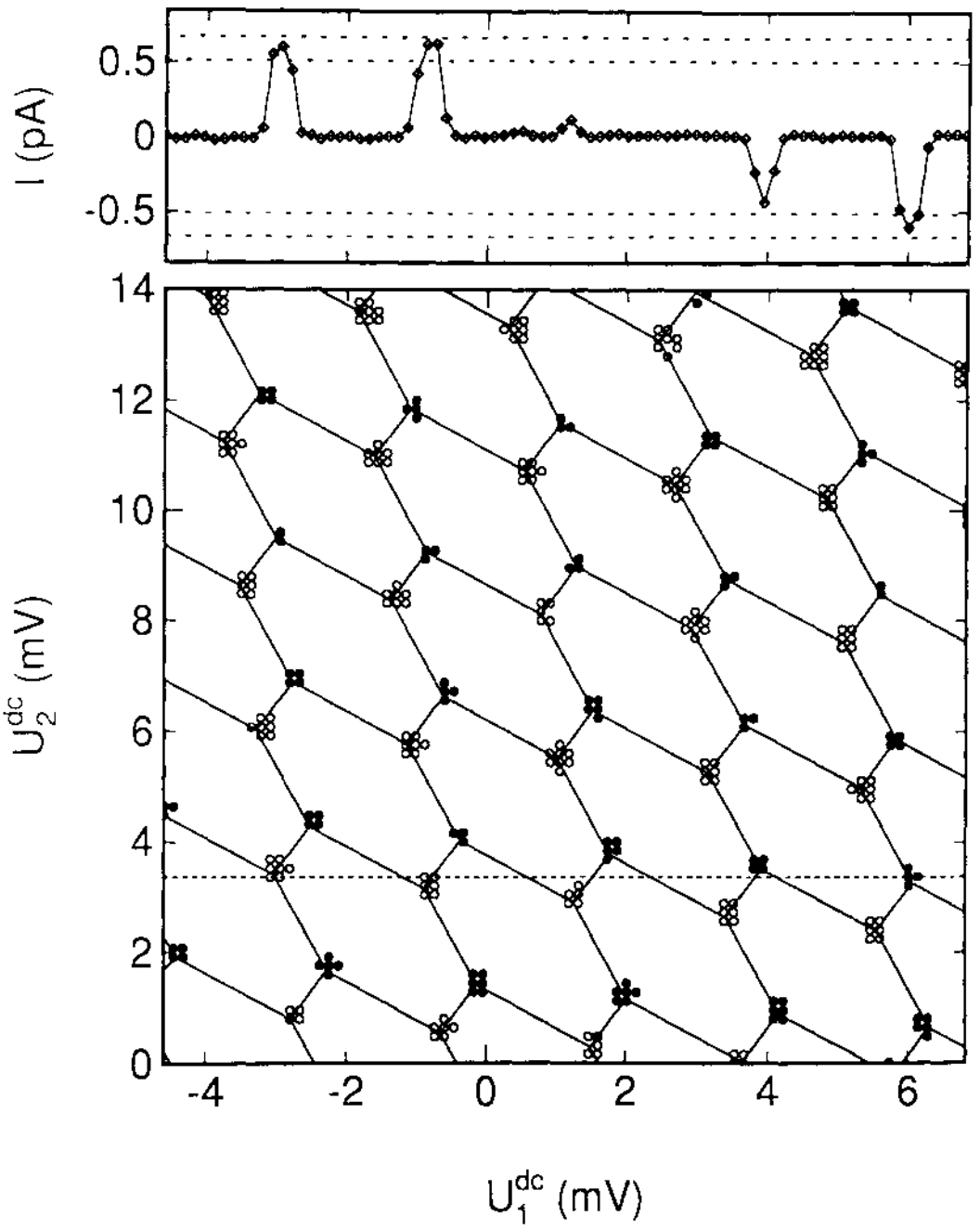

Fig. 5.15 *Current through the device at zero bias voltage* (V = 0) *as a function of the dc gate voltages. Two in quadrature rf signals have been superposed on the dc gate voltages. Amplitude and frequency of this rf gate modulation were* 0.3 mV *and* 4 MHz. *In bottom panel, white (black) dots denote current of between* 0.8ef *and* 1.05ef *(*-1.05ef *and* -0.8ef). *A typical measurement, taken along the dashed line of the bottom panel, is shown in the top panel, together with the lines* $I = \pm 0.8$ef *and at* $I = \pm 1.05$ef. *Full lines represent the calculated ground state diagram that best fits experimental data.*

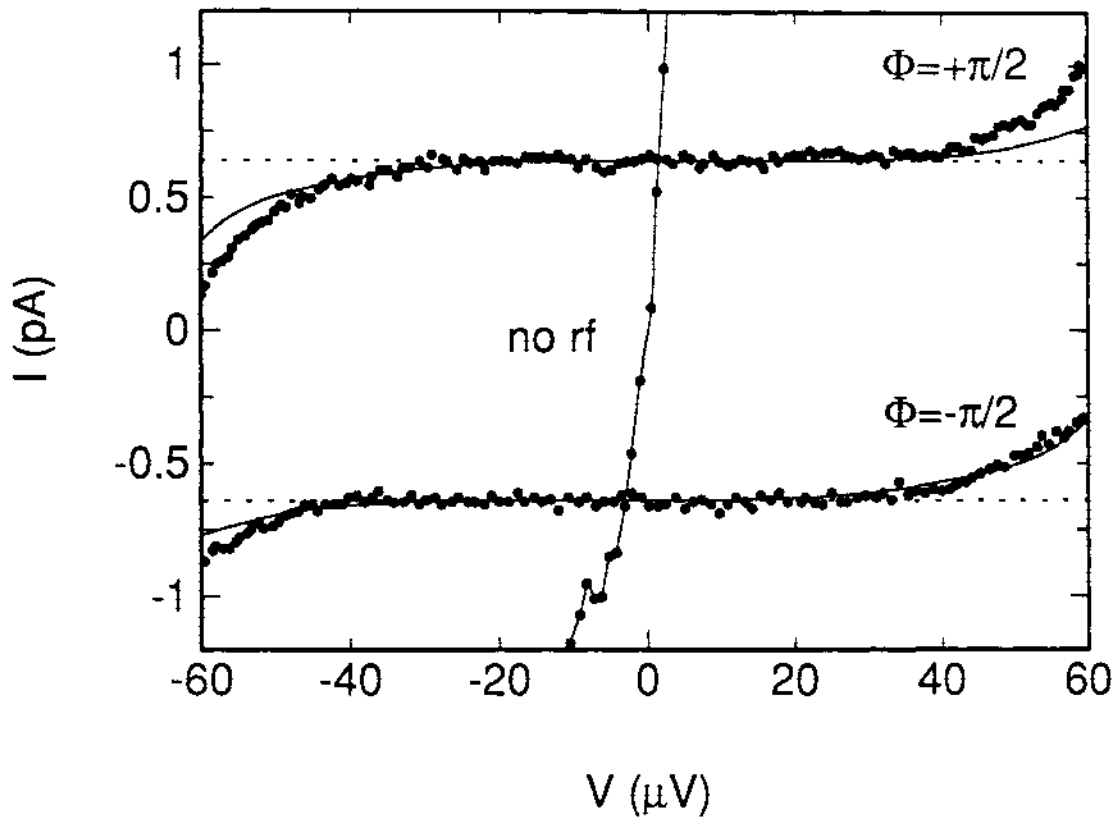

Fig. 5.16 I – V *characteristic with and without* f = 4 MHz *gate voltage modulation around a "P-type" point (white point in* Fig. 5.15). *The* U_1 *and* U_2 *rf amplitudes were respectively* 1 mV *and* 0.6 mV. *Dashed lines mark* $I = \pm ef$. *Full lines are fits calculated with the SETCAD program by taking co-tunneling into account.*

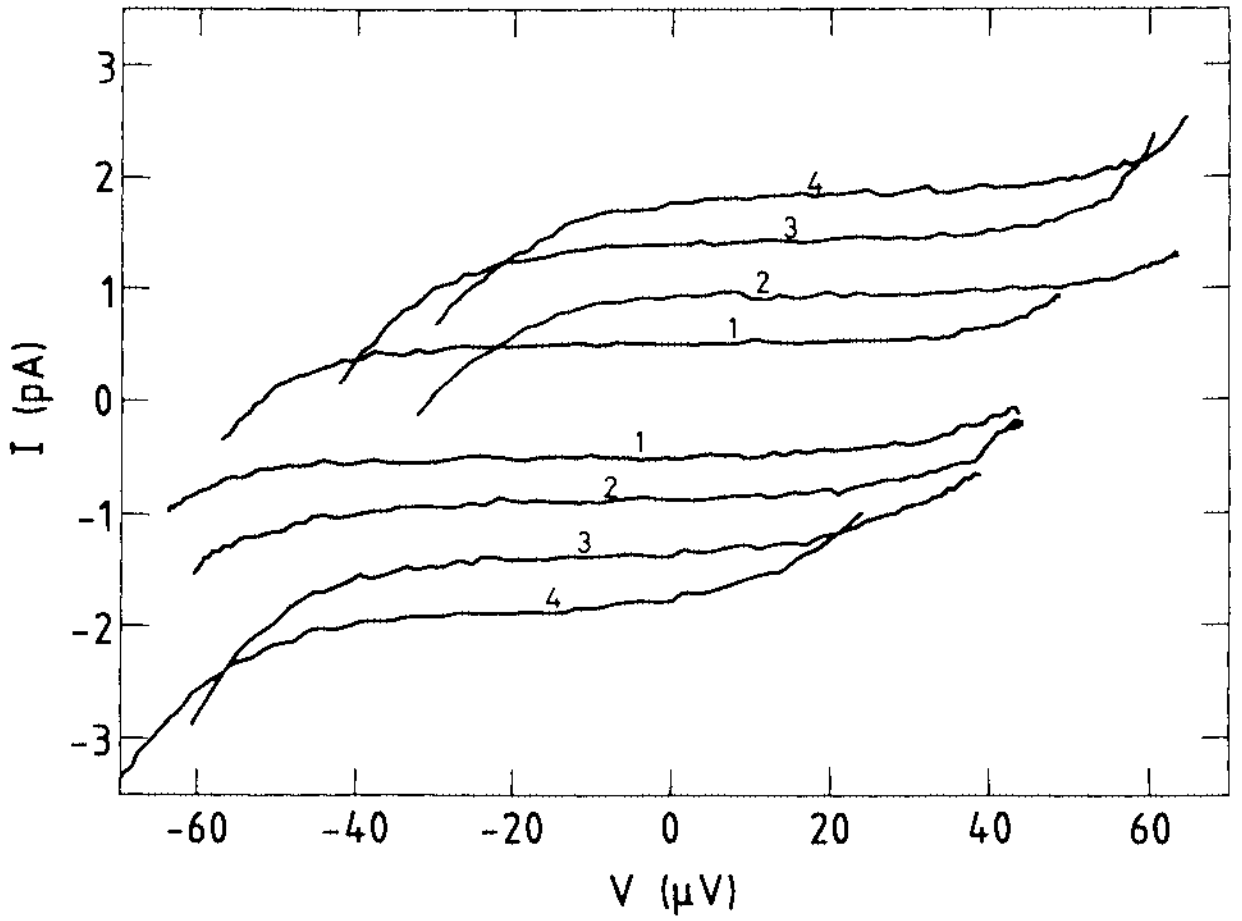

Fig. 5.17 I – V *characteristic of the pump operated at* f = 3 MHz *(curves labeled* 1), 6 MHz *(curves labeled* 2), 9 MHz *(curves labeled* 3) *and* 12 MHz *(curves labeled* 4). *The two curves at each frequency correspond to phase shifts between gates differing by* π.

the rf voltages is varied continuously from $+\pi/2$ to $-\pi/2$. We also show for comparison the I-V curve with no rf.

We have measured the $I-V$ characteristics for various frequencies (see typical characteristics in Fig. 5.17) and measured the current at the inflexion point for various frequencies between 2 and 20 MHz. As shown in Fig. 5.18, we find that this current satisfies the expected relation $I = ef$ within the experimental uncertainty $\Delta I = 0.05$ pA.

The precision of the transfer in our 3-junction pump is not better than 1% . However, we will see that the error sources are well understood, and that a better accuracy can be obtained with a pump containing more junctions: the $N-$pump. The error sources of the 3-pump are going to be evaluated directly in the N-pump.

5.2.2. Operation principle of the N-pump

The N-pump consists of N junctions in series and N-1 gates attached to the islands between them (Fig. 5.19). We call $\tilde{Q}_i$ the charge induced by the i-th gate voltage on the i-th island. The configuration of the circuit is given by the numbers $(n_1, n_2, ...n_{N-1})$ of extra electrons on the islands. Like the pump with 3 junctions, the N-pump operation is based on a topological property of its configuration stability diagram: the $N-1$ configurations with one electron on one island have the same energy that the configuration with empty islands when $\tilde{Q}_i = e/N$ on all the gates. This point is called the multiple point.

The principle of the transfer

A trajectory in the vicinity of the multiple point crossing all the borders between different stability regions once drives one electron successively across all the islands. One electron charge is in the end transferred through the entire array. The direction of the transfer is determined solely by the direction of the trajectory.

In practice, a simple way to transfer a single charge through the N-pump, is to apply shifted triangle shaped pulses to the gates so that a potential well containing one electron is propagated from one end of the array to the other (see Fig. 5.20).

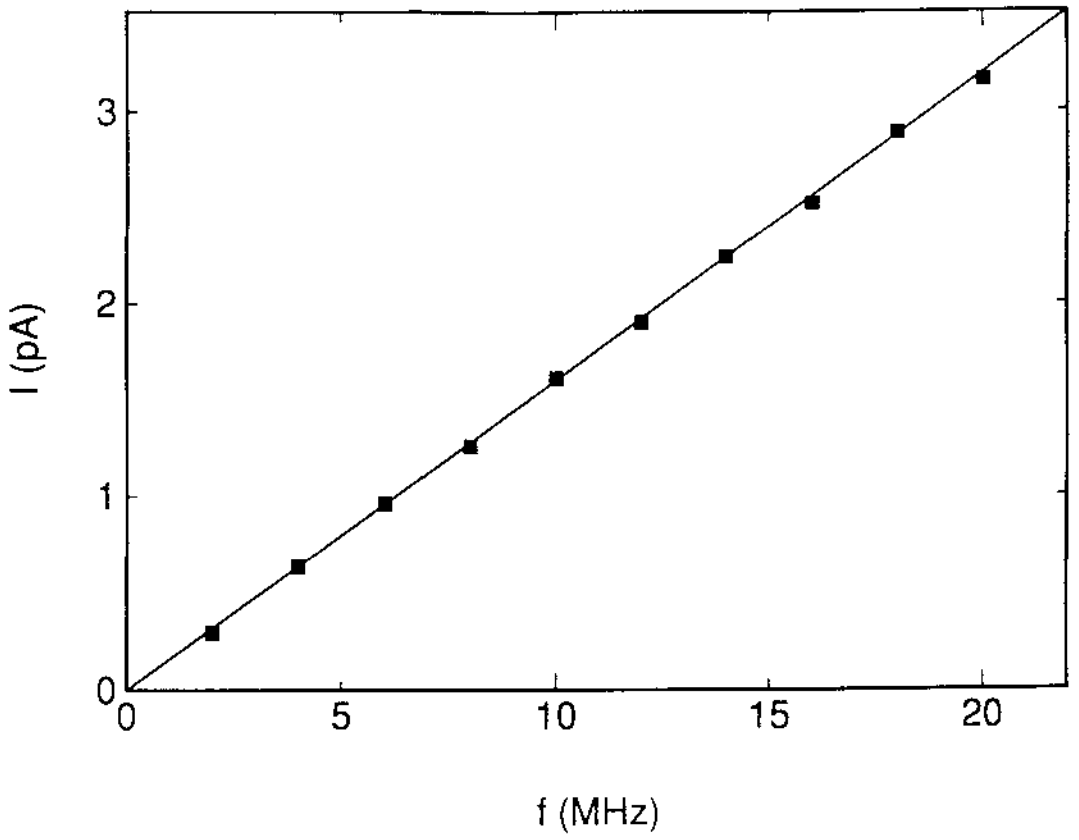

Fig. 5.18 *Current at the inflexion points of the plateaus of the* $I-V$ *characteristics of the pump as a function of the rf frequency. The full line represents* $I = ef$.

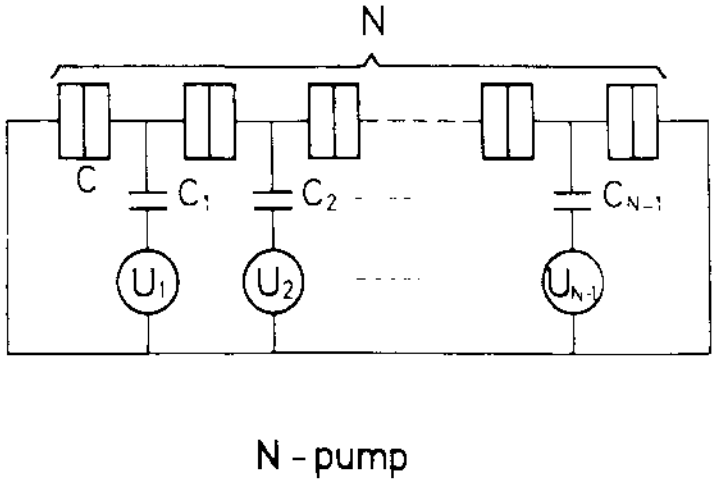

Fig. 5.19 *N-pump. A gate couples to each one of the* $N-1$ *islands of the linear array of* N *junctions.*

5.2.3. Deviations from a regular transfer of single charges in a pump

5.2.3.1. Co-tunneling effects in the 3-junction pump

In Fig. 5.16 we show the detailed shape of the rf induced plateau (dots) compared with the result of a finite temperature numerical simulation which takes into account coherent simultaneous tunnel events on two junctions (full line). All parameters entering in this calculation were chosen within the accuracy range of previous measurements, except the value of the phase shift whose precise value was fitted since it had only been estimated by rf measurements at room temperature. The extension of the plateau on either side of the inflexion point is well explained by the double tunnel events. At the precision level of the simulation which was 1 part in 10^3, the tangent to the calculated curve at the inflexion point is the $I = ef$ line. We attribute the deviation between experiment and theory at larger voltages as mostly due to higher order tunnel processes not taken into account by the simulation, although it is possible that hot electron effects could also play a role.

5.2.3.2. Frequency dependence of the current at zero bias voltage

We now consider for a 3-junction pump the triangle-shaped trajectory in the (U, V) plane shown in Fig. 5.21, which corresponds to the general gate modulation scheme for a N pump for $N = 3$. We calculate the probability for one transition not to occur due to the stochastic nature of tunneling.

Consider the transition $(0,0) \rightarrow (0,1)$. The tunneling rate through junction 1 is given at zero temperature by:

$$\Gamma_1 = \frac{Q_1 - Q_C}{eR_TC}$$

when $Q_1 > Q_c$, $\Gamma_1 = 0$ otherwise. We call $x = \left(2\tilde{Q}_1 - e\right)/e$. Then $Q_1 = (x+1)e/3$ and $\Gamma_1 = x/(3R_TC)$ when $x > 0$, 0 otherwise. The probability to miss the tunnel event is then

$$\mathcal{P} = \exp\left(-\int \Gamma_1(t)dt\right) = \exp\left(-\int_0^1 \frac{dx}{\dot{x}}\frac{x}{3R_TC}\right) = \exp\left(-\frac{1}{6R_TC\dot{x}}\right)$$

Using now $\dot{x} = 6f$, we get $\mathcal{P} = \exp\left(-1/(36R_TCf)\right)$.

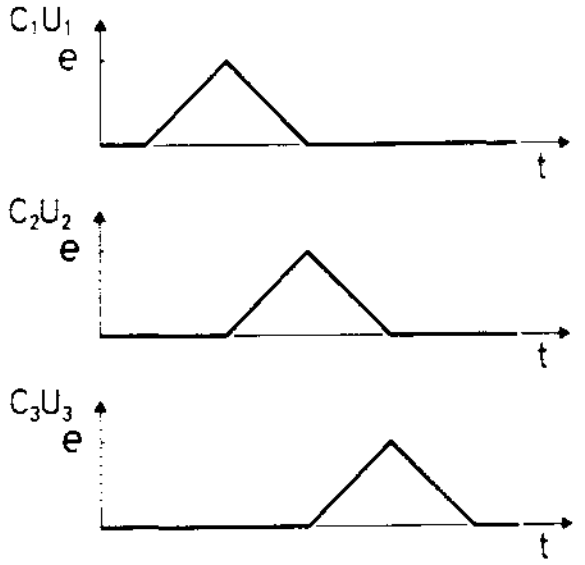

Fig. 5.20 *Signals on the three gate voltages* U_1, U_2, U_3 *of a 4-junction pump which lead to the transfer of one electron. The electron follows the potential well created by the gate voltages.*

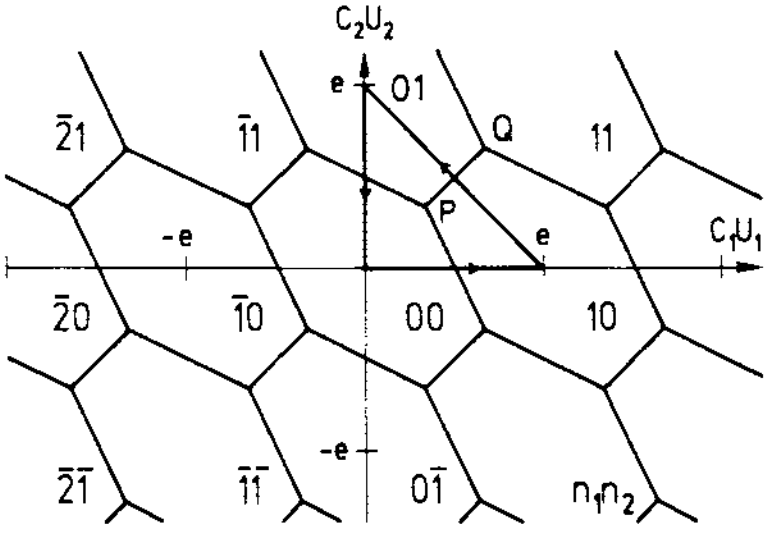

Fig. 5.21 *Trajectory in the* (U_1, U_2) *plane which corresponds to triangular signals like in* Fig. 5.20 *applied to the gates of the 3-junction pump.*

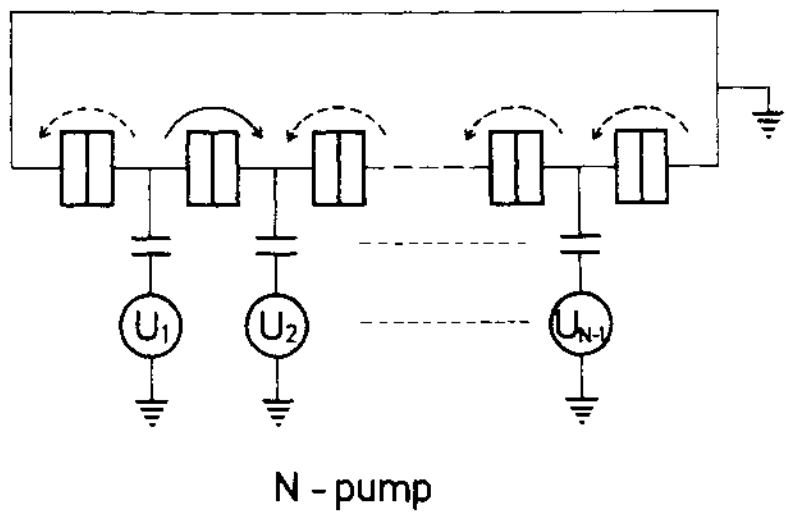

Fig. 5.22 *Co-tunneling process leading to an error in the operation of the* N*−pump: instead of one tunnel event through one junction (full line arrow),* $N-1$ *tunnel events occur coherently through all the other junction (dashed line arrows). The net effect of this co-tunneling process is to transfer a charge from right to left.*

This result can be readily generalized to the case of the N-junction pump, where $Q_1 = (x+1)Q_e$ and $x = 2Nft$. We then get

$$\mathcal{P} = \exp\left(-(N-1)/(8N^2 R_T C f)\right),$$

With the parameters of the 3-junction-pump presented in section 5.2.1, the probability to miss a transition during the whole cycle is

$$\mathcal{P}_{tot} = 3\,\exp\left(-550/f\,[\mathrm{MHz}]\right).$$

Therefore, the frequency limitation for a precision of 10^{-8} in the electron transfer at zero bias voltage is 30 MHz. This is clearly not a dominant source of error in our pump. But for a 5-junction pump that would have the same parameters,

$$\mathcal{P}_{tot} = 5\,\exp\left(-395/f\,[\mathrm{MHz}]\right)$$

and a lower bound for the frequency limitation for a precision of 10^{-8} in the electron transfer at zero bias voltage would be with the same parameters of junctions than in our 3-junction pump 20 MHz. However, this is a severe estimation because we considered only the part of the cycle when the potential hill was in the neighbouring island.

5.2.3.3. Hot electron effects in the N-junction pump

The pump was designed as a device which could reversibly transfer single electrons. When the pump is operated at very low frequency, each electron tunnels at the threshold point, without energy dissipation, as opposed to the turnstile where the entrance of one electron in the central island is obtained by at least one tunnel event well above the threshold, even at zero frequency. However, when operated at higher frequency, the pump is also dissipative: the transitions do not occur at the threshold where the rate is zero, but at a slightly higher charge. We then expect the electron gas to be heated as in the turnstile. We calculate this heating effect in this section.

We estimate the average power delivered to the electron gas $\mathcal{P}$ by "hot" electrons by calculating at first the average junction charge at which the tunnel events occur:

$$P = \frac{ef}{C}\left\langle Q - Q_e \right\rangle$$

With the notations of the last section, $\langle Q - Q_c \rangle = \langle x \rangle Q_c$ and

$$\begin{aligned}\langle x \rangle &= \int_0^1 \frac{dx}{\dot{x}} x\Gamma_1(x) \exp\left(-\int_0^x \frac{dx'}{\dot{x}}\Gamma_1(x')\right) \\ &= \frac{4N}{\sqrt{(N-1)}}\sqrt{2fR_TC}\int_0^1 u^2 \exp\left(-u^2\right) du\end{aligned}$$

and hence

$$\langle Q - Q_c \rangle \simeq 0.54e\sqrt{(N-1)fR_TC}$$

Note how close to the threshold the tunnel event occurs: for the parameters of the 3-junction pump presented here, $R_TC \simeq (20\text{ GHz})^{-1}$ so at $f = 10$ MHz $\langle Q - Q_C \rangle \simeq 2\,10^{-2}e$. Finally, one obtains

$$P \simeq 0.54\frac{e^2}{C}\sqrt{(N-1)R_TC}\; f^{3/2}$$

T_e is determined using $P = \Sigma\Omega\left(T_e^5 - T_{ph}^5\right)$ (Wellstood, 1988):

$$\frac{T_e}{T_{ph}} \simeq \left(1 + \frac{0.54\frac{e^2}{C}\sqrt{(N-1)R_TC}}{\Sigma_{Al}T_{ph}^5\Omega} f^{3/2}\right)^{1/5}$$

Numerically, for $T_{ph} = 20$ mK and $C = 0.4$ fF, it gives

$$\frac{T_e}{T_{ph}} \simeq \left(1 + 2\sqrt{N-1}f^{3/2}\right)^{1/5}$$

where f is in MHz. For $N = 3$ and $T_{ph} = 20$ mK, it gives: at $f = 1$ MHz, $T_e \simeq 26$ mK; at $f = 10$ MHz, $T_e \simeq 50$ mK. At the same frequencies, T_e would be only 2 mK higher in a 5-junction pump.

Therefore, electron overheating is reduced in the pump compared to the turnstile.

5.2.3.4. Co-tunneling rates in the N-pump operation

The simulations of section 5.2.3.1. for the 3-junction pump indicate that co-tunneling is the major cause for the rounding of the plateaus. Is it possible to decrease the probability of co-tunneling events? As in the turnstile, the solution is to increase the number of junctions. How many junctions are needed so as not to be limited by co-tunneling errors?

This section attempts to answer this question by calculating an upper bound of the error rate in a N-junction pump.

In the N-pump operation there are only two types of co-tunneling processes that affect the ideal precision of the device. The first type is co-tunneling through the whole array. It can be reduced quite radically by increasing the number of junctions of the device (see Appendix 3). The second type is co-tunneling events through N-1 junctions, occuring at the same time as a single normal pump tunnel event (Fig. 5.22): when the bias charges of two neighbouring islands are sweept so as to let one electron tunnel from one island to the next one, the most probable tunnel event is through the junction between the two islands. But another possible process is that N-1 tunnel events in the opposite direction happen coherently on all the other junctions. If all the succeeding transitions occur as desired, the whole transfer cycle will not have transferred any electrons.

Calculation of the co-tunneling rate

The co-tunneling process considered here is the co-tunneling through N-1 junctions as shown in Fig. 5.22. We begin in the situation where one electron is on the k-th island and has to be transferred to the (k+1)-th island under the influence of the bias charges $\tilde{Q}_k$ and $\tilde{Q}_{k+1}$. We calculate the co-tunneling rate at zero bias voltage and zero temperature along the lines of appendix 3.

Before any tunnel events, the charge Q_0 is the same on all the junctions (except the k-th one), as $\tilde{Q}_{k+1} = e - \tilde{Q}_k$ and one electron charges the k-th island:

$$Q_0 = \frac{1}{N}\tilde{Q}_{k+1}$$

Therefore the probability amplitude for each path (corresponding to one sequence of tunnel events: see appendix 2) is equal. As in appendix 2, we call ΔQ the increase of charge of all the other tunnel junctions when an electron tunnels through one of them. We use the global rules to calculate the change of electrostatic energy of the circuit associated with the i-th virtual tunnel event,

$$E_i - E_{i-1} = \frac{-e}{C}\left(Q_{i-1} - Q_c\right),$$

and substitute $Q_c = (e - \Delta Q)/2$ to get the electrostatic energy of the circuit after i virtual tunnel events:

$$E_i = \frac{e}{2C} i \left(e - 2Q^0 - i\Delta Q \right).$$

The direct transition and the co-tunneling transitions become possible at the same value of $\tilde{Q}_{k+1}$ when $V = 0 : \tilde{Q}_{k+1} = e/2$. We calculate the co-tunneling rate for $q_{k+1} \in [0.5e, e]$. We call $x = (2\tilde{Q}_{k+1} - e)/e$. Then

$$E_i \geq \frac{e^2}{2NC} i(N - 2 - i),$$

and

$$\prod_{i=1}^{N-3} E_i \geq \left(\frac{e^2}{2NC} \right)^{N-3} (N-3)!^2$$

Since

$$E_{N-2} = \frac{e^2}{NC}(N-2)(1-x)$$

and since the final energy reads

$$E_{N-1} = \frac{e^2}{2NC}(N-1)x,$$

we calculate an upper bound for the co-tunneling rate:

$$\Gamma < \frac{2\pi}{\hbar} \frac{e^2}{2C} (t^2)^{N-1} \frac{(N-1)^{2N-1}}{N(2N-3)!(N-3)!^2} \frac{x^{2N-3}}{(1-x)^2}$$

This expression is surprisingly independant on the tunneling resistance of the junctions. This is discussed at the end of the present section.

An artificial divergence occurs at $x = 1$ because the energy of the last intermediary state is the same as that of the initial state. The rate is of course finite at this point where the last virtual tunnel event becomes allowed in the first order perturbation theory in t^2. We get rid of this artificial divergence by limiting the range of x to $0.9e$ in the integrals.

Calculation of the error rate

The dominant decay process of the state with the electron on the k-th island is single tunneling to the state with the electron on the (k+1)-th island. The rate for this tunneling

process is given by the global rules: since the energy difference between the initial and the final state is E_{N-1} (at zero bias voltage, the final energy is the same whatever the direction along with the electron was transferred), it reads:

$$\Gamma_1 = \frac{2\pi}{\hbar}\frac{e^2}{2C}t^2\frac{N-1}{N}x$$

The probability for this transition not to have occured at a certain value of x is:

$$\exp\left(-\int_0^x \Gamma_1(x')\frac{dx'}{\dot{x}}\right).$$

The probability for the co-tunneling event to occur is therefore:

$$P_{c-t} = \int_0^{.9}\frac{dx}{\dot{x}}\Gamma_{N-1}(x)\exp\left(-\int_0^x \Gamma_1(x')\frac{dx'}{\dot{x}}\right)$$

We call

$$\alpha = \frac{1}{\dot{x}}\frac{2\pi}{\hbar}\frac{e^2}{2C}t^2\frac{N-1}{N}$$

and

$$\beta = \frac{1}{\dot{x}}\frac{2\pi}{\hbar}\frac{e^2}{2C}\left(t^2\right)^{N-1}\frac{(N-1)^{2N-1}}{N(2N-3)!(N-3)!^2}$$

The co-tunneling probability is then

$$P_{c-t} = \beta\int_0^{0.9}\frac{x^{2N-3}}{(1-x)^2}\exp\left(-\frac{\alpha}{2}x^2\right)dx$$

In order to give a lower bound to the precision of the devices, we calculate a very rough upper bound of the co-tunneling probability using $(1-x)^{-2} \leq 100$ and $\int_0^{0.9}(...)dx < \int_0^1 x^{2N-3}e^{-x^2}dx = I_N$. We then get

$$P_{c-t} \leq \left(\frac{\hbar}{2\pi}\frac{2C}{e^2}\dot{x}\right)^{N-2}\frac{100(N-1)^N N^{N-2}}{(2N-3)!(N-3)!^2}I_N$$

The integrals I_N are given by the recurrence relation

$$I_N = \frac{-1}{2e} + (N-2)I_{N-1}$$

and by $I_2 = (1-1/e)/2$. If we call f the operation frequency of the turnstile, $\dot{x} = 2Nf$. Finally:

$$P_{c-t} < \left(\frac{R_K C f}{\pi^2}\right)^{N-2}\frac{100(N-1)^N N^{2(N-2)}}{(2N-3)!(N-3)!^2}I_N$$

As noted before, this result does not depend on the tunneling resistance of the junction: there is an exact compensation between the dependance of Γ_1 and of Γ_{N-1} in R_T. Nevertheless, R_t was supposed to be much larger than R_K, because we neglected higher orders in the perturbation theory. Assuming $R_t \gg R_K$, the only relevant parameters are then the capacitance of the junction, the operation frequency and, of course, the number of junctions in the device.

Numerically, $P_{c-t} < f(N) \left(R_K C f/\pi^2\right)^{N-2}$, where approximate values of $f(N)$ are given for some values of N in the following table:

N	3	4	5	6
$f(N) \simeq$	150	1500	5000	9000

The error rate is given by NP_{c-t}. Co-tunneling causes tunneling events to happen in the wrong direction: the error rate corresponds to a decrease of the current. At $f = 1$ MHz, with $C = 1$ fF, $\left(R_K C f/\pi^2\right) \simeq 2.5\ 10^{-6}$ so the co-tunneling rate per transition is smaller than 10^{-8} with $N = 4$. With $N = 5$, the error rate for the whole cycle is smaller than 10^{-8} at all frequencies below 30 MHz.

In conclusion, we have calculated an upper limit of the error due to co-tunneling in the N-pump operation at zero temperature and zero voltage. We find that this error is very strongly reduced when the number of junctions is increased, and that a 5-junction pump could meet the requirements of metrological applications discussed in next section.

5.3. SINGLE ELECTRON DEVICES AND METROLOGY

The turnstile and the pump operated until now are accurate with only a one percent precision accuracy. Nevertheless, the realisation of a current standard has seriously been considered by metrological laboratories of several countries (France, Germany, Holland, USA). A second possible metrological application was pointed out by Williams and Martinis: the precise measurement of the fine structure constant α. In this section, we discuss the reasons of interest for these metrological applications. We then compare the expected accuracy of turnstiles and pumps and discuss some possible new experiments using the present state of the art of junction fabrication.

5.3.1. Transferring electrons one by one: what for?

The present definition of the ampere is defined by the Laplace force between two infinite wires. This definition is not convenient to realize in practise, and metrologists have adopted a representation of the ampere given by the combination of the quantum Hall effect (von Klitzing, 1986) and the Josephson effect (Josephson, 1969): the volt is represented by the voltage inducing an oscillation frequency of 483597.9 GHz in the ac Josephson effect, and the ohm as one part in 25812.807 of the "von Klitzing" resistance R_{K-90} (defined as the ratio of the Hall voltage and the current corresponding to the plateau $i = 1$ in the quantum Hall effect). The question arises as to the consistency of such a representation of the ampere. One way to check it is to close the "metrological triangle" (Fig. 5.23) by comparing two currents: one obtained through the combination of the Josephson effect and of the quantum Hall effect; the second directly obtained from a single charge transferring device. Such a device could provide the missing link in the triangle.

The second metrological application proposed by Williams and Martinis is a new measurement of the fine structure constant α. This would allow an accurate comparison between the predictions of Quantum Electrodynamic (QED) and the measurements for the electron anomalous magnetic moment $(g-2)$. It would be achieved by measuring, with a voltmeter calibrated with the ac Josephson effect, the voltage across a capacitor charged

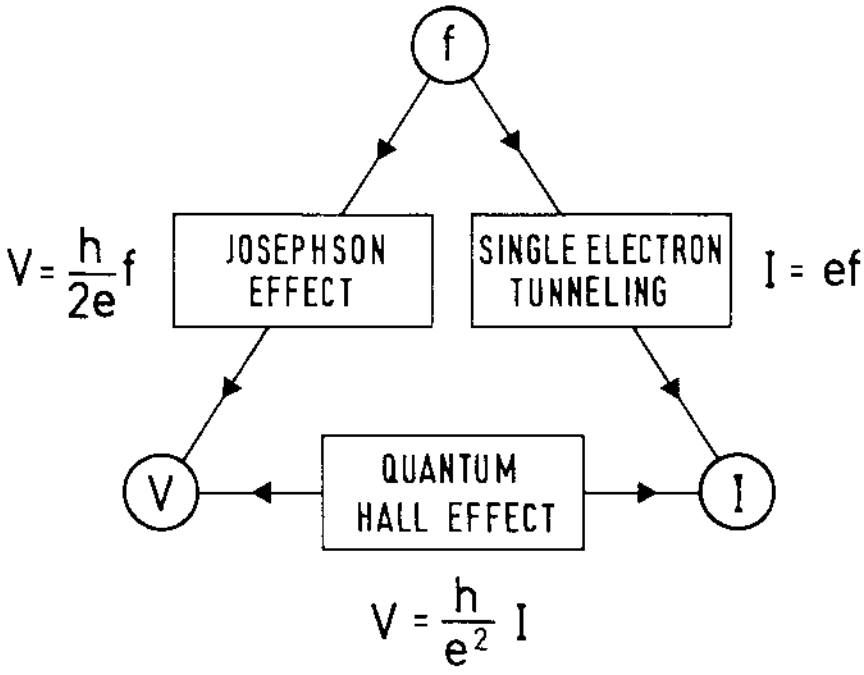

Fig. 5.23 *The triangle of quantum metrology showing the relation between single electron tunneling effects and the two other macroscopic quantum effects: the ac Josephson effect and the quantum Hall effect.*

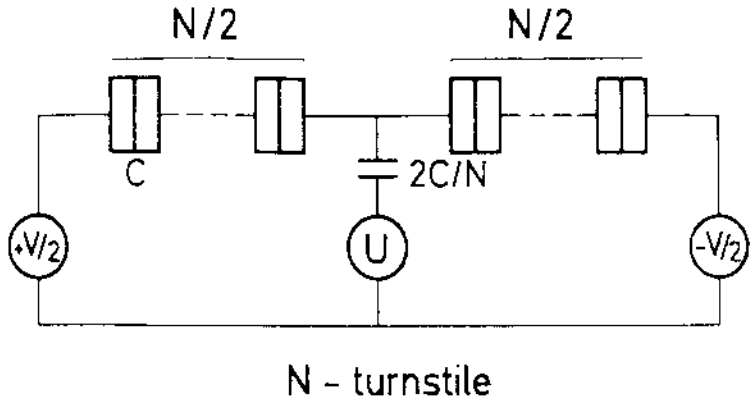

Fig. 5.24 *N-turnstile. One gate couples to the central island of a linear array of* N *junctions of capacitance* C. *The gate capacitance is* 2C/N. *The principle of the operation is the same as a 2+2 turnstile. The larger the number of junctions in each arm, the lower the co-tunneling rates.*

with a known number of electrons; the value of the capacitance would be compared to that of a calculable capacitor (Shields *et al.*, 1989) which is related to the vacuum impedance Z_{vac}. This measurement would be, with a known numerical factor, the ratio of (e/Φ_0) and $(1/Z_{vac})$, which is 4α.

5.3.2. Is metrological accuracy achievable?

We accounted in sections 5.1.3 and 5.2.3 for the inaccuracy of turnstiles and pumps due to finite electron temperature and to co-tunneling effects. In both cases, errors in the transfer involve intermediate configurations of higher energy than the initial and final configurations. Clearly, the more intermediate states and the higher their energies, the fewer the errors. Since the energy barrier for the passage of a single charge across p junctions is approximatly $(p/4)(e^2/2C)$ (see appendix 3), the number of errors due to the finite temperature will decrease as $\exp\left(-Ne^2/16Ck_BT\right)$. The exponential factor for thermal activation is also the reason why the combination of co-tunneling and thermal activation is always negligible compared to co-tunneling alone. Therefore, the co-tunneling constitutes the main limitation to the accuracy of our devices. As we saw in sections 5.1.3.4 and 5.2.3.4, N-turnstiles and N-pumps are quite different as far as co-tunneling is concerned.

The N-turnstile:

The N-turnstile (Fig. 5.24) operates only at a finite bias voltage, of the order of half the Coulomb gap voltage. Therefore, even at zero frequency, a current flows through the whole device due to co-tunneling through the whole turnstile (see Appendix 3). This current is given by $e\Gamma_N$. At $V = e/4C$, a current below 10^{-8} pA is achievable with $N = 8$ junctions.

The co-tunneling error sources during the transfer are of many different orders, depending on the bias voltage and the amplitude of the modulation. They have not yet been calculated until now.

The N-pump (Fig. 5.19):

We calculated in section 5.2.3.4 that the error in the transfer of single charges in a five-junction pump could be made smaller than 10^{-8}. Moreover, the lower the operation frequency is, the more precise the transfer becomes.

What experiments for metrology?

The realisation of a current standard faces many difficulties because of the smallness of the currents (a few pA) obtained with our devices. The design of a current comparator (Gutmann and Niemeyer, private communication) at this level would itself be a major technological problem. Much hope has been put into the parallelization of our devices: this approach is dual to the series combination of Josephson junctions forthe standard of the volt. However, the problem of offset charges needs to be solved to make parallelization achievable. Recent results by Delsing in the direction of offset charge suppression (Delsing *et al.*, 1991) are encouraging. A more direct way to obtain higher currents would be to decrease the junction capacitances so as to speed up the operation. This is not only a challenging technological problem, but raises also the problem of knowing how close to the atomic dimensions the notion of capacitance will still be valid.

The measurement of the fine structure constant α by a new method seems more feasible. The 5-pump seems to be precise enough for this measurement since an operation frequency of 1 MHz would be enough to built up a voltage of 10 V on a 1 pF capacitance within one minute. The pump would have the advantage that electrons can be pumped in, then pumped out; the measurement of a zero voltage across the capacitor after a cycle would ensure the absence of errors during the operation.

5.3.3. Conclusion

We demonstrated that given our state of knowledge on multi-junction devices, a precise transfer of charge carriers should be achievable. This in turn, should allow to test the consistency of an electrical system of units based only on macroscopic quantum effects and

allow a new measurement of the fine structure constant α.

6. CONCLUDING SUMMARY

Single electron effects were originally predicted to occur in current-biased small-capacitance tunnel junctions because of the large change of the electrostatic energy of the junction when a single electron tunnels. In chapter 2, we showed that these effects were very difficult to observe because, in practice, the biasing circuit induces zero point charge fluctuations much larger than e on the junction capacitor. We evaluated quantitatively this effect by calculating the electron tunneling rate through a small-capacitance junction in a low-pass environment, i.e. in series with a dc conducting impedance and a voltage source. Only if this impedance is larger than the quantum of resistance $R_K = h/e^2$ are the charge fluctuations on the junction smaller than e. Then electrons can tunnel inelastically, by exciting the environmental modes. The energy of the dominant inelastic channels are around $e^2/2C$; the tunneling rate is therefore reduced at voltages below the "Coulomb gap" $e/2C$. This situation changes radically when a true capacitor or other junctions are in series with the junction considered ("high-pass" environment): the circuit contains an island connected to the rest of the circuit only through capacitors and tunnel junctions. The charge of this island is quantized because it can change only when electrons tunnel through the junction. Its charge fluctuations are therefore quenched, and the Coulomb blockade of tunneling occurs without any high resistor in series.

The simplest circuit containing an island consists of one junction in series with a true capacitor and a voltage source. We have called this circuit the "single electron box" because it allows to control at the single electron level the charge of the island by changing the value of the voltage. We have fabricated a single electron box in which the dimensions of the junction were of the order of 0.1 μm. We have used a SET transistor, composed of two tunnel junctions in series and a gate, as an ultra sensitive electrometer in order to measure the charge of the junction, which was always below the electron charge e. The variations of the junction charge as a function of the bias voltage were in good agreement with the theory of the Coulomb blockade.

The single electron box is the building block for more complex devices with which we have controlled the current one electron at a time. The first of these devices, nicknamed

"turnstile", is based on an hysteretic version of the box, called the "trap", that contains at least two junctions in series. The turnstile consists of a single gate coupled to the central island of a linear array of $2N$ junctions ($N \geq 2$). The direction of the transfer is determined by the sign of the bias voltage. We have operated two 4-junction turnstiles at frequencies between 1 MHz and 20 MHz and observed plateaus on the $I-V$ characteristics at $I = ef$ with a 1% accuracy. The rounding of the plateaus was attributed to the heating of the electron gas by the tunneling electrons and to co-tunneling. The second device transferring electrons one by one is the "pump". It consists of a linear array of tunnel junctions with a gate attached to each island. The electron is moved along the array by shifting a potential well induced by the modulation of the gate voltages. The direction of the transfer of electrons is only determined by the direction of the shift of this well. No bias voltage is needed to transfer the charges. We operated a 3-junction pump where the relation $I = ef$ between the current I through the pump and the frequency f of the modulation of the gates was also obeyed at the 1% precision level. The error sources of the 3-junction pump are quantitatively explained, the main one being co-tunneling. The same error sources should nevertheless allow a precision better than one part in 10^8 in a 5-junction pump. Metrological applications have already been considered: the realization of a current standard with a pump or a turnstile faces the difficulty of the small value of the currents, but a precise measurement of the fine structure constant α in an experiment combining a pump and a calculable capacitor seems possible.

The devices we presented here were mainly operated with normal metal junctions. Experiments in the superconducting state were also performed in order to manipulate single Cooper pairs. We showed in chapter 4 that in the superconducting electron box the period and the amplitude of the sawtooth modulation of the junction charge were the same than in the normal case, whereas they should have been twice as large. In fact, the presence of only one quasi-particle in the electrodes of the Josephson junction could explain that the results were the same than in the normal state. Similar experiments with a "trap" instead of a box are more promising because it could be possible to have a lower co-tunneling rate for quasiparticles than for Cooper pairs. The realization of this project is in progress. We

have also tried to transfer Cooper pairs one by one in a superconducting version of the pump, and we saw plateaus close to $I = 2ef$ (Geerligs *et al.*, 1991). However, many details of this experiment are not well understood at the moment. In fact the superconducting case in many experiments is poorly understood (Geerligs *et al.*, 1990b; Fulton *et al.*, 1989). Only the measurement of the influence of the environment on the tunneling of Cooper pairs seem to agree with the theoretical predictions that are given in appendix 1 (Haviland *et al.*, 1991).

The experimental study of the influence of the environment on the tunneling rate through a single junction focused much effort, both in the normal (Cleland *et al.*, 1990) and in the superconducting case (Haviland *et al.*, 1991); the effort was put on junctions in high impedance environments, which is technologically difficult to achieve because of the low value of the vacuum impedance $Z_{vac} = 377\ \Omega$. In chapter 2, we showed that even a low impedance environment manifests itself, in the way the $I - V$ characteristic approaches its asymptote at large voltages.

Another extension of this work could be the study, both theoretical and experimental, of the charging effects when the junction tunnel resistance is of the order or smaller than the resistance quantum R_K. A non-perturbative approach is needed when the expansion parameter of the perturbation theory $R_K/(4\pi^2 R_T)$ is not much smaller than one. In particular, a very important question concerns the co-tunneling current at the Coulomb gap of a SET transistor: how much does it increase when R_T is lowered? The understanding of this problem determines the ultimate sensitivity of the SET transistor used as an electrometer. It could be investigated experimentally in semiconductor devices, where tunnel barriers can be modulated (Glattli *et al.*, 1991; Kouwenhoven *et al.*, 1991). Moreover, semiconductor systems could make it also possible to investigate the interplay between charging effects and other quantum effects, such as the Aharonov-Bohm effect (Beenakker *et al.*, 1991) or ballistic transport (Averin and Nazarov, 1990).

APPENDIX 1.

THE INCOHERENT COOPER PAIR TUNNELING RATE

The calculation of the quasi-particle tunneling rate in the normal state (2.2.28) can be transposed to the case of incoherent Cooper pair tunneling in the superconducting case (Averin *et al.*, 1990; Falci *et al.*, 1991). First, the tunnel hamiltonian H_T is replaced by the Josephson hamiltonian

$$H_J = -E_J cos(\delta) = (-E_J/2)e^{i\delta} + h.c.$$

(where E_J is the Josephson energy and δ the superconducting phase difference between the electrodes of the junction). This expression is similar to that of H_T in (2.2.9") where $t \rightarrow -E_J/2$ and $e\Phi/\hbar \rightarrow \delta$. As δ is conjugate to a number of Cooper pairs this last transformation is equivalent to $e \rightarrow 2e$. If the temperature is well below the superconducting transition temperature and if the bias voltage V is such that $eV < 2\Delta$ (where Δ is the superconducting energy gap), the initial and final states are free from quasi-particles. Therefore, we substitute in (2.2.15) $E' = 2eV$ and $E'' = 0$ and obtain for the tunneling rate of for Cooper pairs:

$$\Gamma_{CP} = \frac{\pi}{2}\frac{E_J^2}{\hbar}P_S(2eV)$$

where $P_S(E)$ is the function $P(E)$ calculated with the quantum of charge $2e$ instead of e. It follows from relations (2.2.17), (2.2.18) and (2.2.21) that $P_S(E)$ has the same expression than the function $P(E)$ but for an impedance $Z_t(\omega)$ four times larger. In other words,

$$\tilde{P}(t) = \exp(J(t)) \ ; \ \tilde{P}_S(t) = \exp(4J(t))$$

The superconducting current at zero temperature is given by $I_S = 2e\Gamma_{CP}$.

We therefore predict a simple relation between the second derivative of the current voltage characteristic in the normal state and the current voltage characteristic in the superconducting state below the superconducting gap (at zero temperature) since:

$$R_T \left.\frac{d^2 I_N}{dV^2}\right|_{V=2V_0} = eP(2eV_0)$$

and

$$\frac{\hbar I_S(V_0)}{\pi E_J^2} = eP_S(2eV_0)$$

where I_N and I_S are the normal and superconducting currents. In particular, a sharp Coulomb gap in the normal state should correspond to a current peak at twice the voltage in the supercoducting case.

Very recently, the details of the $I-V$ characteristic of small Josephson junctions in a low pass high impedance environment were compared with the predictions of this theory and a good agreement was found (Haviland *et al.*, 1991).

APPENDIX 2:
PUMP PATTERN FILE FOR THE SEM

We describe in this section a typical file used for the e-beam lithography with the Scanning Electron Microscope. This file was used by the $HP-1000$ computer to generate the scan of the e-beam on a chip. It defines the pattern of a pump at the highest scale (magnification $\times 5000$). The corresponding final device is shown in Fig. 5.13.

The file (Fig. A2.1) starts with the standard charge dose st expressed in pC/μm^2. For the resist we use, the appropriate dose is around 2 pC/μm^2. The third and fourth line define the magnification g and the SEM current i, expressed in pA. The setting of those parameters is done on the microscope prior to each exposition step. The rest of the file is the definition of the pattern itself. All the coordinates are given in μm. The origin of the coordinates system is the center of the field. The pattern is composed of quadrilaterals, either rectangles, scanned horizontally (*box*) or vertically (*boy*) and defined by the coordinates of their lower left corner and of their higher right corner, or trapezoidals whose parallel sides are horizontal (*trx*) or vertical (*try*), and defined by the Y (resp. X) coordinates of their parallel sides and by the X (resp. Y) coordinates of all the corners. The definition of each type of quadrilateral is followed by a remark between stars (e.g. $***$*ile gauche* $***$ means *left island*). The next line contains the coordinates of the quadrilateral considered: for the first one (a *box*), (−1.615 .07 .065 .17) means that the coordinates of the lower left corner are $(-1.615, 0.07)$ in μm, and those of the higher right corner are $(0.065, 0.17)$). The last data of this line is the relative dose d for this quadrilateral. The next line contains the steps dX, dY and the number of scans n (see section 3.1.2). The first quadrilateral is the small left island of the pump: its dose needs to be $d = 2.3$ higher than the standard dose $st = 2$ pA/μm^2. Such a dose can be obtained with $dX = 2$, $dY = 1$, $n = 1$. The optimal values for the relative doses were obtained with test lines at different doses (like at the end of this pattern file, boxes after $***$*croix alignement* $***$).

```
st   ***pompe avec petites iles et capa interdigitees***
 2.
0.1
 5000 15.
box ***ile gauche***
-1.615 .07 .065 .17 2.3
2 1 1
box ***ile droite***
 .065 -.07 1.615 -.07 2.3
2 1 1
boy ***doigt ile gauche***
-1.3 .17 -1.2 1.57 2.3
2 1 1
boy ***doigt ile gauche***
-.4 .17 -.3 1.57 2.3
2 1 1
boy ***doigt ile droite***
.3 -1.57 .4 -.17 2.3
2 1 1
boy ***doigt ile droite***
1.2 -1.57 1.7 -.17 2.3
2 1 1
box ***electroue gauche***
-6.2 -.17 -1.585 -.07 2.3
2 1 1
box ***electroue droite***
1.585 .07 6.2 .17 2.3
2 1 1
box ***entree fonctions gauche***
-11.9 -.27  6 .27 1.5
2 2 1
box ***entree fonctions droite***
6 -.27 11.9 .27 1.5
2 2 1
boy ***piste gate gauche***
-.9 .47 -.7 5.3 2.
2 2 1
boy ***piste gate droite***
.7 -8.5 .9 -.47 2.
2 2 1
box ***jonction test gauche***
-8.515 3.07 -7 3.17 2.3
2 1 1
box ***jonction test gauche***
-10 2.83 -8.485 2.93 2.3
2 1 1
box ***jonction test droite***
7 -3.17 8.565  3.07 2.3
2 1 1
box ***jonction test droite***
8.435 -2.93 10 -2.83 2.3
2 1 1
boy ***contact test gauche***
-10 2.8 -9.5 8 1.5
2 2 1
boy ***contact test droite***
9.5 -8 10 -2.8 1.5
2 2 1
boy ***contact test gauche***
-7.5 2 -7 8 1.5
2 2 1
boy ***contact test droite***
7 -8 7.5 -3 1.5
2 2 1
trx ***garde piste gate gauche***
-5 -2 6.2 -5.5 -2.4 7.5 1.5
2 2 1
trx ***garde piste gate gauche***
.4 3.4 6.8 .0 3.9 7.5 1.5
2 2 1
boy ***garde piste gate gauche***
-2.1 3.5 -1.2 6.8 1.5
2 2 1
boy ***garde piste gate gauche***
 .4 5.5 .5 6.8 1.5
2 2 1
trx ***garde piste gate gauche***
-5.8 -3.1 5  5  2.1 6.8 1.5
2 2 1
trx ***garde piste gate gauche***
.5 2.2 5 .5 3.4 6.8 1.5
2 2 1
trx ***garde piste gate droite***
2.4 5.5 -7.5 2 5 -6.8 1.5
2 2 1
trx ***garde piste gate droite***
-3.9 -.8 -7.5  3.4 -.4 -6.8 1.5
2 2 1
boy ***garde piste gate droite***
1.2 -6.8 2.1 -3.5 1.5
2 2 1
boy ***garde piste gate droite***
-.5 -6.6 .4 -3.5 1.5
2 2 1
trx ***garde piste gate droite***
2.1 5 -6.8 2.1 3.8 -5 1.5
2 2 1
trx ***garde piste gate droite***
-3.4 -.5 -6.8 -2.2 -.5 -5 1.5
2 2 1
boy ***croix alignement***
10.5 5 11 6 1.5
2 2 1
boy ***croix alignement***
10.5 3.5 11 4.5 1.5
2 2 1
box ***ligne 100 A***
-11 -3 -9 -2.99 2
2 1 1
box ***ligne 100 A***
-11 -3.5 -9 -3.49 2.8
2 1 1
box ***ligne 200 A***
-11 -4 -8.5 -3.98 2.8
2 1 1
box ***ligne 200 A***
-11 -4.5 -8.5 -4.48 2.5
2 1 1
box ***ligne 300 A***
-11  5 -8 -4.97 2.5
2 1 1
box ***ligne 300 A***
-11 -5.5 -8 -5.47 2.3
2 1 1
box ***ligne 400 A***
-11 -6 -7.5 -5.96 2.3
2 1 1
box ***ligne 400 A***
-11 -6.5 -7.5 -6.46 2
2 1 1
box ***ligne 500 A***
-11 -7 -7 -6.95 2.3
2 1 1
box ***ligne 500 A***
-11 -7.5 -7 -7.45 2
2 1 1
end
```

Fig. A2.1 *Listing of the pattern file which defines the design of a pump at magnification* $\times 5000$.

APPENDIX 3.
CO-TUNNELING

"Electrons like freedom."
(Yu. Nazarov, Les Houches, 1991)

The tunnel hamiltonian $H_T = t \sum_{L,R} a^\dagger_{k_R} a_{k_L} \exp(ie\Phi/\hbar) + \text{h.c.}$ treated by second order perturbation theory only couples states deduced one from another by the tunneling of one quasi-particle through one junction. Higher order processes have to be taken into account when $R_K/4\pi^2 R_T$ is not much smaller than unity. They correspond to concomitant tunnel events through several junctions and are called "co-tunneling". In the simplest situation of two identical junctions of capacitance C in series biased with voltage V below the Coulomb gap $e/2C$, tunneling through any of the two junction is forbidden at low temperature because it would increase the charging energy of the island between the junctions. In fourth order in perturbation theory, tunneling is no longer forbidden: if two quasi-particle tunnel simultaneously through the two junctions, the charge of the island remains unchanged. This results in a finite current through the two junctions for $V < e/2C$ even at zero temperature. This current was calculated by Averin and Odintsov (Averin and Odintsov, 1989) using perturbation theory, and a good agreement was found with their results in experiments by Geerligs (Geerligs *et al.*, 1990c). The same authors calculated in the same article the co-tunneling rate through a series of N junctions at low voltage. These calculations being of major importance for the precision of single electron devices, we rederive them in the case of finite temperature. We also calculate the rate of transfer of a single charge between two neighbouring islands by a co-tunneling event through all the junctions in the array but the one between the neighbouring islands (see Fig. 5.2.2); this rate is needed to analyze the N-pump.

A3.1. CO-TUNNELING RATE THROUGH TWO JUNCTION IN SERIES

We consider here a SET transistor with junctions of capacitances C_1 and C_2 (Fig. A3.1) biased below the Coulomb gap $e/(C_1 + C_2 + C_0)$. Co-tunneling is the coherent

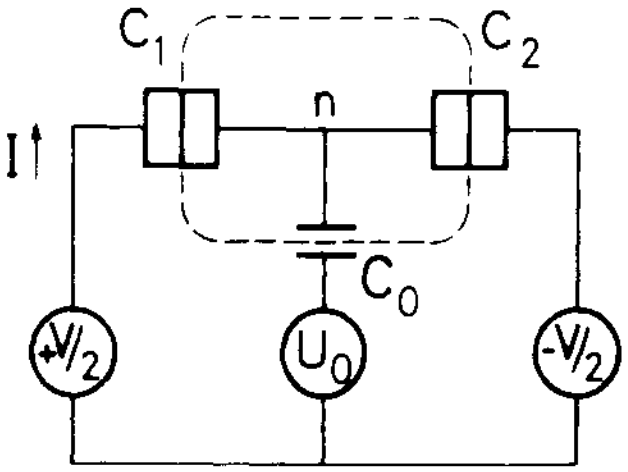

Fig. A3.1 *SET transistor with junction capacitances* C_1 *and* C_2*, gate capacitance* C_0*.* n *denotes the number of extra electrons on the island.*

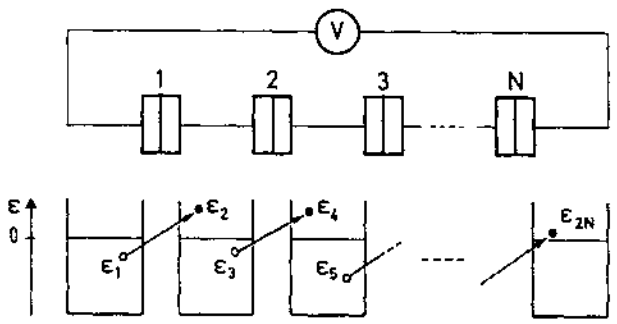

Fig. A3.2 *Co-tunneling through the* N *junctions of a linear array: when the bias voltage* V *is below* e/2C*, current through the array is due to coherent tunnel event through the* N *junctions.* ϵ_1, ϵ_3, ..., ϵ_{2N-1} *are the energies of the holes created and* ϵ_2, ϵ_4, ..., ϵ_{2N} *are the energies of the electrons created in the* N *tunnel events.*

tunneling of two electrons through the two junctions. After this coherent tunneling, one electron has left the leftmost electrode and one has appeared in the rightmost one; the island contains an electron and a hole. The charge of these particles cancel each other on a time scale given by the plasma frequency. As we have done for the tunnel proces itself, we take this cancellation to occur instantaneously, and use an electrostatic expression for the intermediate energies. Hence, in a virtual intermediate state, the island is charged by $\pm e$ (depending on the junction through which the first tunnel event takes place) and the energies of the two possible intermediary states are:

$$E_1 + (\epsilon_1 + \epsilon_2) = \frac{(Q_0 + e)^2}{2C_i} - \frac{C_2}{C_1 + C_2} eV + (\epsilon_2 + \epsilon_1)$$
$$E_2 + (\epsilon_4 + \epsilon_3) = \frac{(Q_0 - e)^2}{2C_i} - \frac{C_1}{C_1 + C_2} eV + (\epsilon_4 + \epsilon_3)$$

where $C_i = C_0 + C_1 + C_2$ is the total capacitance of the island, ϵ_1 and ϵ_3 are the kinetic energies of the quasi-holes left in the leftmost and middle electrodes, ϵ_2 and ϵ_4 the kinetic energies of the quasi-electrons created in the middle and rightmost electrodes (Fig. A3.2). The final energy after the two tunnel events is :

$$E_f + \sum_{i=1}^{2N} \epsilon_i = \frac{Q_0^2}{2C_i} + \sum_{i=1}^{2N} \epsilon_i$$

The co-tunneling rate is given by the Fermi Golden rule (Schiff, 1955):

$$\Gamma = \frac{2\pi}{\hbar} \sum_{\epsilon_1, \epsilon_2, \epsilon_3, \epsilon_4} M^2_{\epsilon_1, \epsilon_2, \epsilon_3, \epsilon_4} \rho_F^2 \delta(E_f - E_i)$$

where the effective matrix element for the transition is given by second order pertubation theory (Roman, 1965):

$$M_{\epsilon_1, \epsilon_2, \epsilon_3, \epsilon_4} = t^2 \left(\frac{1}{E_1 + (\epsilon_2 + \epsilon_1) - E_i} + \frac{1}{E_2 + (\epsilon_4 + \epsilon_3) - E_i} \right)$$

and where ρ_F is the density of states at the Fermi energy. Note that the paths for the transition with different quasi-particles final states are discernables, hence they do not interfere. However, given the quasi-particle final energies, two paths are possible, depending on the order in which the tunnel events take place: these two paths do interfere constructively (see the "+" sign between the two fractions in the preceding equation).

At zero temperature, the kinetic energies ϵ_i are positive. A straightforward integration gives then:

$$\Gamma = \frac{2\pi}{\hbar}\left(\frac{R_K}{4\pi^2 R_T}\right)^2 \left\{\left[eV + \frac{2E_1E_2}{eV+E_1+E_2}\right]\left[\sum_{i=1}^{2}\ln\left(1+\frac{eV}{E_i}\right)\right] - 2eV\right\} \qquad (A1.1)$$

yielding the current $I = e\Gamma$. At low voltage, it is found that the current is proportional to V^3.

A3.2. CO-TUNNELING RATE THROUGH A LINEAR ARRAY

Consider a linear array of N identical tunnel junctions of capacitance C. We make the assumption that the initial charge on each island is zero. The Coulomb gap voltage is $(N-1)e/2C$ according to the global rules. Below the Coulomb gap, the current is by definition zero in first order in $R_K/(4\pi^2 R_T)$. The co-tunneling current is given by higher order perturbation theory: at low bias voltage, in a sense given in the following, it corresponds to the coherent tunneling of N electrons through the N junctions (Fig. A3.2).

The co-tunneling rate results therefore from the sum of the rates corresponding to all the processes with the allowed final quasi-particle energies. Each of these processes is constructed from the interference of the $N!$ different paths defined by all the sequences of tunnel events through the N junctions. The Fermi Golden rule reads then:

$$\Gamma = \frac{2\pi}{\hbar}\sum_{\epsilon_1,\epsilon_2,\ldots\epsilon_{2N}} \rho_F^{2N} M^2_{\epsilon_1,\epsilon_2,\ldots\epsilon_{2N}}\,\delta\left(\sum_{i=1}^{2N}\epsilon_i - eV\right)$$

where

$$M_{\epsilon_1,\epsilon_2,\ldots\epsilon_{2N}} = \sum_{paths}\frac{t^N}{\prod_{i=1}^{N-1}E_i}$$

is the effective matrix element for the N-th order transition (Roman, 1965) and E_i is the energy of the system after the i-th tunnel event. This energy is the sum of an electrostatic energy, of the order of the charging energy $e^2/2C$, and of the quasi-particles energies. Since the sum of those quasi-particle energies is, after the N tunnel events, equal to eV, we neglect them in the low bias voltage limit for the evaluation of the effective matrix element. The sum over the quasi-particle energies only gives then a factor $g_N(eV, k_BT)$.

Calculation of the factor g_N due to quasi-particles

$$g_N(eV, k_BT) = \int_{-\infty}^{+\infty} d\epsilon_1 d\epsilon_2 ... d\epsilon_{2N} f(\epsilon_1) f(\epsilon_2) ... f(\epsilon_{2N}) \delta \left(\sum_{i=1}^{2N} \epsilon_i - eV \right)$$

where $f(\epsilon) = 1/(1 + \exp(-\epsilon/k_BT))$ denotes the Fermi function. This integral is evaluated by noticing that it is a convolution product and calculating it in the Fourier space (Averin, private communication). Using the residu theorem we get that $g_N(eV, k_BT)$ is the residu at $\lambda = 0$ of the function:

$$h(\lambda) = \sum_{p=0}^{+\infty} C_{2N}^p \sum_{q=0}^{+\infty} \frac{(ieV)^q}{q!} \lambda^{2(p-N)+q} \times \left(\sum_{r=0}^{+\infty} 2(-1)^r \frac{\lambda^{2r}}{\beta^{2(1+r)}} \frac{(1 - 2^{1+2r})\pi^{2(1+r)}}{[2(1+r)]!} \left| B_{2(1+r)} \right| \right)^p$$

where

$$C_{2N}^p = \frac{(2N)!}{p!(2N-p)!}$$

and where B_k denotes the Bernouilli numbers. We also used the notation $\beta = (k_BT)^{-1}$.

We have calculated explicitly $g_N(eV, k_BT)$ for low values of N :

$$g_2 = \frac{1}{3!}(eV)^3 + \frac{4}{6}(eV)(\pi k_BT)^2$$

$$g_3 = \frac{1}{5!}(eV)^5 + \frac{1}{6}(eV)^3(\pi k_BT)^2 + \frac{8}{15}(eV)(\pi k_BT)^4$$

$$g_4 = \frac{1}{7!}(eV)^7 + \frac{1}{90}(eV)^5(\pi k_BT)^2 + \frac{7}{45}(eV)^3(\pi k_BT)^4 + \frac{16}{35}(eV)(\pi k_BT)^6$$

$$g_5 = \frac{1}{9!}(eV)^9 + \frac{1}{3024}(eV)^7(\pi k_BT)^2 + \frac{13}{1080}(eV)^5(\pi k_BT)^4 + \frac{82}{567}(eV)^3(\pi k_BT)^6 + \frac{128}{315}(eV)(\pi k_BT)^8$$

At zero temperature, $g_N = (eV)^{2N-1}/(2N-1)!$ (Averin and Odintsov, 1989).

Calculation of the matrix element M:

We approximate the intermediate energy E_i with the electrostatic energy alone, and neglect quasiparticle energies. A shortcut in the evaluation of E_i is to use the global rules: suppose that the i-th tunnel event happens through the k-th junction. The change

in electrostatic energy of the total circuit when one electron tunnels through the k-th junction is related to the difference between the charge Q_k of this junction before the tunnel event and the critical charge Q_c (which is the same for all the junctions in the present case):

$$E_i - E_{i-1} = \frac{e}{C}(Q_k - Q_c)$$

We evaluate Q_k by calculating in two different ways the change of the charge of a junction through which a electron tunnels from the right to the left: when an electron tunnels through a junction of the chain, the charge of this junction decreases by $2Q_c$ (if its charge was equal to the critical charge Q_c, tunneling would not change the energy of the circuit by definition of Q_c; so the reverse tunnel event would have the same property after the first one has occured: the charge after the tunnel event is $-Q_c$). The charge of all the other junctions increases by the same amount ΔQ, which is also the charge transferred through the source. In order to calculate ΔQ, we relate it to the change of charge of the junction through which the electron tunneled: since the charge of the neighbouring junctions increased by ΔQ and as the charge of the island where one hole left decreased by e, the charge of the junction increased by $\Delta Q - e$. Finally we get $2Q_c = e - \Delta Q$ and hence $\Delta Q = e - 2Q_c$.

On the other hand, after $i-1$ tunnel event, the charge of the junction k through which no tunnel event happened before is $CV/N + (i-1)\Delta Q$, where CV/N is the charge induced by the voltage source, and:

$$E_i - E_{i-1} = \frac{e}{C}((i-1)\Delta Q - Q_c) - \frac{eV}{N}$$

We finally deduce the electrostatic energy after i tunnel events:

$$E_i = \frac{-e}{C}\left(\frac{i(i-1)}{2}\Delta Q - iQ_c\right) = \frac{i}{N}\left((N-i)\frac{e^2}{2C} - eV\right)$$

We now deduce the validity range of this N-th order perturbation theory: all the intermediate energies must be positive, otherwise the dominant process for the current would be a combination of co-tunneling and "real" tunnel events. The energy of the system after N-1 tunnel events is

$$E_{N-1} = \frac{N-1}{N}\left(\frac{e^2}{2C} - eV\right).$$

The validity condition of the present approach is therefore: $V < e/2C$. More precisely, since $E_i = 0$ for $V = (N-i)e/2C$, the dominant conduction process at $V \in [ie/2C, (i+1)e/2C]$ is the succession of co-tunneling events through $N-i$ junctions and "real" tunnel events through the i junctions left. One should also note that a second validity criterium for this theory is that the thermal population of the leftmost islands must be negligible. Otherwise there would be a contribution to the current via co-tunneling events at a lower order. This condition is satisfied at 20 mK with femtofarad junctions even at very low bias voltages because of the Boltzmann factor

$$\exp(-E_1/k_BT) \simeq \exp(-(e^2/2C)/k_BT) \simeq \exp(-50) \simeq 10^{-22}$$

At $V << e/2C$, the V-term in E_i is negligible and

$$\prod_{i=1}^{N-1} E_i = \left(\frac{e^2}{2C}\right)^{N-1} \frac{N!(N-1)!}{N^N}$$

The matrix element for the transition is therefore independent of the order of the tunnel events: the $N!$ sequences give the same amplitude for the transition. The matrix element for the N-th order transition is finally:

$$M_{\epsilon_1,\epsilon_2,\ldots\epsilon_{2N}} = N! \frac{(\rho_F t)^{N-1} t}{\left(\frac{e^2}{2C}\right)^{N-1} \frac{N!(N-1)!}{N^N}}$$

Final expression of the co-tunneling rate

We substitute the matrix element in the Fermi Golden rule and get the co-tunneling rate through N junctions:

$$\Gamma_N = \frac{2\pi}{\hbar} \left(\frac{R_K}{4\pi^2 R_T}\right)^N \frac{N^{2N}}{(N-1)!^2} \left(\frac{2C}{e^2}\right)^{2N-2} g_N(eV, k_BT) \qquad (A3.2.1)$$

At zero temperature $g_N(eV, k_BT) = (eV)^{2N-1}/(2N-1)!$, hence

$$\Gamma_N = \frac{2\pi}{\hbar} \frac{e^2}{2C} \left(\frac{R_K}{4\pi^2 R_T}\right)^N \frac{N^{2N}}{(N-1)!^2(2N-1)!} \left(\frac{V}{e/2C}\right)^{2N-1} \qquad (A3.2.2)$$

For the sake of comparison, we give the tunneling rate Γ_1 through one voltage biased junction:

$$\Gamma_1 = \frac{V}{eR_T} = \frac{2\pi}{\hbar}\frac{e^2}{2C}\left(\frac{R_K}{4\pi^2 R_T}\right)\left(\frac{V}{e/2C}\right)$$

Hence,

$$\frac{\Gamma_N}{\Gamma_1} = \left(\frac{R_K}{4\pi^2 R_T}\right)^{N-1} \frac{N^{2N}}{(N-1)!(2N-1)!}\left(\frac{V}{e/2C}\right)^{2(N-1)}$$

The exponent N of $(R_K/4\pi^2 R_T)$ is the number of tunneling events necessary to transfer one electron through the array. The power of V reflects the increased number of accessible electronic states when the voltage increases. At finite temperature, extra terms with a lower power of V account for the largest number of accessible states due to a thermal distribution of quasi-particles. Those corrections increase significantly the current at temperatures and voltages such that $eV \simeq \pi k_B T$. Numerically, for 1 femtofarad junctions, the crossover temperature is $T = 300$ mK for $V = e/2C$.

APPENDIX 4.

PAPER 1:

EFFECT OF THE ELECTROMAGNETIC ENVIRONMENT ON THE COULOMB BLOCKADE IN ULTRASMALL TUNNEL JUNCTIONS

Published in: Phys. Rev. Lett. **64**, 1824 (1990)

Referred to as: Devoret *et al.*, 1990a.

Effect of the electromagnetic environment on the Coulomb blockade in ultrasmall tunnel junctions

M. H. Devoret[1], D. Esteve[1], H. Grabert[2],
G.-L. Ingold[2], H. Pothier[1], C. Urbina[1]

[1] *Service de Physique du Solide et de Résonance Magnétique, Centre d'Études Nucléaires des Saclay, 91191 Gif-Sur-Yvette, France*
[2] *Fachbereich Physik, Universität-GHS Essen, 4300 Essen Federal Republic of Germany*

The current–voltage characteristic of an ultrasmall tunnel junction is calculated for arbitrary frequency dependence of the impedance presented to the junction by its electromagnetic environment. It is shown that the Coulomb blockade of tunneling is washed out by quantum fluctuations of the charge on the junction capacitor except for ultrahigh impedance environments. Two simple cases where the environment can be treated as an inductor or resistor are examined in detail. Effects of finite temperatures are discussed.

New effects have been predicted[1] to arise in ultrasmall tunnel junctions with capacitance C such that the charging energy of a single electron $e^2/2C$ exceeds the characteristic energy k_BT of thermal fluctuations. Simple energy considerations suggest that the tunneling of a single electron is completely blocked when the junction capacitor holds a charge less than $e/2$. A large body of experimental data now exists[2-4] that seems to support the theoretical ideas underlying this Coulomb blockade of tunneling. The effect is clearly seen in multi-junction configurations[2] while the existence of elementary charging effects in single tunnel junctions[3,4] is still questionable.

An obvious objection against existing theories of the Coulomb blockade in single junctions comes from considering the effective junction capacitance. Should it not include contributions from the on-chip electromagnetic environment of the junction like the leads and pads? They might easily enlarge the capacitance to values where elementary charging effects become unobservably small. One point of view[5] is that the tunneling electron probes the electromagnetic environment at distances $r < c\tau_t$ where τ_t is the traversal time of the electron passing through the potential barrier and c the speed of charge propagation in the electrical circuit surrounding the junction. On the other hand, recent experimental work[4] suggests that the electron probes distances $r < \hbar c/\Delta E$ where $\Delta E = \max(eV, k_BT)$, V being the dc voltage across the junction.[6]

In this Letter we show that the quantum mechanical nature of the electromagnetic environment can severely reduce Coulomb charging effects in single junctions. For a tunneling electron to change effectively the charge on the junction capacitor and thus lead to the Coulomb blockade effect it has to excite electromagnetic modes of the coupled system formed by the junction and its electromagnetic environment. Since the energy $\hbar\omega$ of these modes is quantized, they will not be excited unless the voltage V across the junction reaches $\hbar\omega/e$. The larger the impedance of the environment the stronger the junction couples to low frequency modes. Thus, charging effects will usually be only observable when the junction is placed in a very high impedance environment or for large voltages. The situation here is reminiscent of the well-known Mössbauer effect[7] where naive reasoning suggests that gamma quanta are emitted with a shifted frequency due to the recoil of the nucleus. An analogy can be drawn between a change of the momentum of the nucleus and a change of the local charge on the capacitor of a tunnel junction so that the occurrence of a frequency shift corresponds to the Coulomb blockade. The Mössbauer effect arises because the probability to excite crystal modes coupled to the nucleus is small when the average recoil energy does not match the energy of the dominant crystal modes. From another point of view the change of the momentum of the nucleus due to recoil is small compared with its spontaneous zero point fluctuations. Hence, recoilless transitions are favored. Likewise, we will find that the Coulomb charging effect in single junctions

is washed out by quantum fluctuations of the electric charge in practical cases where the impedance of the environment is not well above the resistance quantum $R_Q = h/2e^2$.

Our treatment of electron tunneling in a normal junction imbedded in an electrical circuit is based on the assumption that the tunneling Hamiltonian takes the form:

$$H_T = \sum_{\sigma kq} T_{kq} c^\dagger_{k\sigma} c_{q\sigma} \Lambda_e + h.c.$$

where $T_{kq} c^\dagger_{k\sigma} c_{q\sigma}$ is the usual tunneling term[8] which transfers a quasielectron from one side of the junction to the other and where Λ_e is an operator changing the charge Q on the capacitor plates of the junction: $\Lambda_e Q \Lambda_e^\dagger = Q - e$. Here, Q is assumed to be an operator with continuous spectrum. In contrast with the conventional treatment of tunneling, our scheme takes into account — albeit in a minimal fashion — the rearrangement of the electric charge density on the junction during a tunneling event. Introducing the phase [9,10] $\varphi(t) = (e/\hbar) \int_{-\infty}^{t} V(t')dt'$ as the integral over the voltage across the junction, Λ_e can be expressed as $\Lambda_e = e^{i\varphi}$ by making use of the commutation relation $[Q, \varphi] = ie$. We further assume that Q and φ commute with the quasielectron creation and annihilation operators.

As a simple model for the electromagnetic environment we may consider the circuit depicted in Fig. 1a where the leads attached to the junction are represented through a series inductance L and a shunt capacitance C_s. [For the case of a general circuit see below.] The practical observation of Coulomb charging effects requires junction capacitances less than a few femtofarads and the leads attached to such a junction will easily produce shunt capacitances that are several orders of magnitude larger, i.e. $C_s \gg C$. The change of the charge Q_s on the shunt capacitor caused by a tunneling event is therefore entirely negligible and the current-biased junction depicted in Fig. 1a can thus effectively be replaced by the voltage-biased junction shown in Fig. 1b.[11] For this latter model, the total Hamiltonian includes the usual kinetic and chemical potential terms for quasielectrons, the tunneling Hamiltonian H_T, and the Hamiltonian of the electromagnetic environment

$$H_{em} = (Q^2/2C) + (\hbar^2/2e^2L)\varphi^2 - QV$$

which describes the Coulomb charging energy on the capacitor and the magnetic energy of the self inductance of the leads. Then, assuming a constant tunneling matrix element T_{kq}, one finds for the tunneling current along the standard line of reasoning [12]

$$I = \frac{1}{eR_T} \int_{-\infty}^{+\infty} dE \int_{-\infty}^{+\infty} dE' \{ f(E)[1 - f(E')] P(E + eV - E') - [1 - f(E)] f(E') P(E' - E - eV) \} \qquad (1)$$

where $1/R_T$ is the usual tunneling conductance which is proportional to $|T|^2$ and $f(E) = [1 + \exp(\beta E)]^{-1}$ is the Fermi function with $\beta = 1/k_B T$. The novel feature here is the appearance of the function

$$P(E) = (2\pi\hbar)^{-1} \int_{-\infty}^{+\infty} dt \exp[J(t) + iEt/\hbar] \tag{2}$$

in which

$$J(t) = \langle[\varphi(t) - \varphi(0)]\varphi(0)\rangle$$

is the equilibrium phase correlation function. $P(E)$ gives the probability that a tunneling electron creates an excitation with energy E of the electromagnetic environment described by H_{em}. In the conventional treatment where the coupling to the environment is disregarded one has $P(E) = \delta(E)$ and Eq. (1) reduces to the well-known Ohmic law $I = V/R_T$. Because of $C\dot{\varphi} = (e/\hbar)Q$, the equilibrium correlation function $J(t)$ is intimately connected with the spontaneous charge fluctuations on the junction capacitor arising from the coupling to the electromagnetic environment. Using properties of the Fermi function and the detailed balance symmetry obeyed by $P(E)$, the result (1) may be written as

$$I = \frac{1}{eR_T} \int_{-\infty}^{+\infty} dE\, E \frac{1 - e^{-\beta eV}}{1 - e^{-\beta E}} P(eV - E). \tag{3}$$

For the circuit shown in Fig. 1b, we have

$$J(t) = \rho \left\{ \coth\left(\tfrac{1}{2}\beta\hbar\omega_L\right) [\cos(\omega_L t) - 1] - i \sin(\omega_L t) \right\}$$

where $\omega_L = (LC)^{-1/2}$ is the oscillation frequency of the environmental mode described by the Hamiltonian H_{em} and $\rho = \pi/2CR_Q\omega_L$ is the ratio of the single electron charging energy $e^2/2C$ and the mode excitation energy $\hbar\omega_L$. This leads to an I-V-characteristic of the form

$$I = (1/eR_T) \exp\left[-\rho \coth\left(\tfrac{1}{2}\beta\hbar\omega_L\right)\right] \sum_{n=-\infty}^{+\infty} \epsilon_n \frac{\sinh\left(\frac{1}{2}\beta eV\right)}{\sinh\left(\frac{1}{2}\beta\epsilon_n\right)} I_n\left(\rho / \sinh\left(\tfrac{1}{2}\beta\hbar\omega_L\right)\right)$$

where $\epsilon_n = eV - n\hbar\omega_L$ and $I_n(x)$ is the modified Bessel function. Each term corresponds to a tunneling channel where the electron creates or absorbs n quanta of the environmental mode. For zero temperature this result simplifies to read[13]

$$I = \frac{1}{eR_T} e^{-\rho} \sum_{n=0}^{n_{max}} \frac{\rho^n}{n!} (eV - n\hbar\omega_L) \quad \text{for } V > 0$$

where n_{max} is the largest integer below $eV/\hbar\omega_L$. At $T = 0$, a tunneling electron can only excite the environment and create at most n_{max} quanta. It is important to note that the differential conductance dI/dV displays a series of steps at voltages $V_n = n\hbar\omega_L/e$. Usually, for low voltages, the I-V-characteristic will be dominated by the elastic channel ($n = 0$). This behavior is analogous to the presence of a strong elastic line in the Mössbauer gamma spectrum. Inelastic processes are negligible when the mode energy $\hbar\omega_L$ exceeds the single electron charging energy, that is for $\rho \ll 1$. This will mostly be the case since typical series inductances will be well below $(\hbar^2/e^4)C$ even for ultrasmall junctions. At least for low voltages the Coulomb charging effects are then suppressed. Finite temperatures make the deviation from Ohmic behavior even less pronounced. Another way of understanding the suppression of the Coulomb blockade effect is to estimate the spontaneous charge fluctuations on the junction capacitor arising form the coupling to the external circuit. From the Hamiltonian H_{em} we find

$$\langle \delta Q^2 \rangle = \tfrac{1}{2}\hbar\,(C/L)^{1/2} \coth\left(\tfrac{1}{2}\beta\hbar\omega_L\right)$$

which at $T = 0$ exceeds e^2 unless $\rho \gg 1$.

For the case of a general electromagnetic environment with arbitrary frequency dependence the coupled junction-circuit system may be characterized by the diagram in Fig. 1b with the series inductance L replaced by a general frequency dependent impedance $Z(\omega)$. Since the electromagnetic environment is dissipative but linear [there is no other junction in the circuit] we may follow Caldeira and Leggett[14] and treat this environment as if it were an infinite collection of LC-oscillators. The Hamiltonian H_{em} is then replaced by a corresponding Hamiltonian with an infinite number of environmental modes with a spectral density determined by $Z(\omega)$. The result (3) for the I-V-characteristic remains valid for the general case. The environmental influence is again described through the function $P(E)$, Eq. (2), which gives the probability that the tunneling electron transfers the energy E to the circuit. The phase correlation function now takes the form

$$J(t) = \int_0^\infty \frac{d\omega}{\omega} \frac{\mathrm{Re}\, Z_t(\omega)}{R_Q} \{\coth\left(\tfrac{1}{2}\beta\hbar\omega\right)[\cos(\omega t) - 1] - i\sin(\omega t)\} \qquad (4)$$

where

$$Z_t(\omega) = \frac{1}{i\omega C + Z^{-1}(\omega)}$$

is the total impedance of the junction in parallel with the environmental impedance. The formulae (2), (3), and (4) allow for the determination of the I-V-characteristic

for arbitrary frequency dependence of the electromagnetic environment at finite temperatures.

Let us first extract the I-V-characteristic at large voltages. There only the behavior of $P(E)$ for large energies E is relevant which in turn is related to the short time behavior of the phase correlation function. Using $J(t) = -(i\pi/2C)t - (e/\hbar C)^2\langle\delta Q^2\rangle t^2$ for $t \to 0$, we find $I = R_T^{-1}(V - e/2C)$ for $eV \gg k_BT$, $e^2/2C$. This describes an offset of magnitude $e/2C$, the so-called Coulomb gap. For low voltages the behavior of the I-V-characteristic depends on the spectrum of charge fluctuations at frequencies below $eV/\hbar$. Only when the impedance $\mathrm{Re}[Z_t(\omega)]$ in this frequency range exceeds the quantum resistance will the offset still be noticeable.

As a concrete example let us consider a tunnel junction connected to a long dissipative transmission line with characteristic impedance R. In that case $Z(\omega) = R$ [see inset of Fig. 2], and we recognize that the phase correlation function (4) behaves like the mean square displacement of a quantum Brownian particle.[15] At zero temperature the phase correlation grows logarithmically for large t, $J(t) \sim -\alpha \ln(\omega_R|t|)$, where $\alpha = R/R_Q$ and $\omega_R = 1/RC$. This implies a power-law decay proportional to $t^{-\alpha}$ of the Fourier transform of $P(E)$. As a consequence, for $\alpha < 1$, the function $P(E)$ has a singularity at $E = 0$

$$P(E) = \frac{\exp(-\alpha\gamma)}{\Gamma(\alpha)} \frac{1}{E} \left(\frac{E}{\hbar\omega_R}\right)^{\alpha} \Theta(E) \text{ for } E \to 0$$

where $\gamma = 0.5772\ldots$ is Euler's constant. We see that quasi-elastic transitions with small energy transfer E to the environment are most probable. Using (3), this yields for the I-V-characteristic

$$I = \frac{\exp(-\alpha\gamma)}{\Gamma(\alpha+2)} \frac{V}{R_T} \left(\frac{e|V|}{\hbar\omega_R}\right)^{\alpha} \text{ for } V \to 0.$$

which is non-analytic at $V = 0$ and shows a suppression of the Coulomb gap for $\alpha < 1$. The same low-voltage behavior of the characteristic is obtained for a general frequency dependent impedance $Z(\omega)$ with a finite Ohmic component $R = Z(0)$. At finite temperatures, the logarithmic growth of the phase correlation function is replaced by a linear growth, $J(t) \sim -(\pi\alpha/\hbar\beta)|t|$ for $t \to \pm\infty$, and $I(V)$ is now analytic at $V = 0$, but at low temperatures and for voltages between k_BT/e and e/C the behavior is close to the zero temperature case. Fig. 2 displays numerically integrated I-V-curves for various values of R/R_Q at $T = 0$. Clearly, the Coulomb gap only survives at low voltages for resistance values of the order or larger than the resistance quantum R_Q.

In conclusion, by a quantum mechanical treatment of the electromagnetic environment of a tunnel junction we have calculated the I-V-characteristic as a function of

the environment impedance $Z(\omega)$ [Eqs. (2), (3), and (4)]. We have shown that the junction capacitance C will be revealed in the I-V-characteristic as a voltage offset $e/2C$ only if the impedance of the environment $Z(\omega)$ at frequencies below $e^2/2\hbar C$ exceeds the resistance quantum R_Q. The influence of the electromagnetic environment is not associated with the finite duration of the electron tunneling process. In fact, the simple model employed here entirely disregards the finite traversal time. We thus predict that in experimental setups designed to provide a high impedance environment for a single junction[16], the Coulomb gap should be observable. We have stressed that the suppression of the Coulomb gap for a junction in a low impedance electrical circuit occurs for much the same reason as the absence of a frequency shift of gamma radiation from nuclei embedded in a crystal. In linear junction arrays, the presence of islands that can accomodate only an integer number of elementary charges is manifest in a Coulomb gap which can be observed even for low impedance environments.

This work has benefited from fruitful discussions with V. Anderegg, B. Geerligs, U. Geigenmüller, K. K. Likharev, J. E. Mooij, and G. Schön and was partially supported by the Deutsche Forschungsgemeinschaft through Sonderforschungsbereich 237.

References

[1]K. K. Likharev, IBM J. Res. Develop. **32**, 144 (1988) and references therein

[2]T. A. Fulton and G. J. Dolan, Phys. Rev. Lett. **59**, 109 (1987); J. B. Barner and S. T. Ruggiero, Phys. Rev. Lett. **59**, 807 (1987); L. S. Kuz'min and K. K. Likharev, Pis'ma Zh. Eksp. Teor. Fiz. **45**, 389 (1987) [JETP Lett. **45**, 495 (1987)]; L. J. Geerligs and J. E. Mooij, Physica **B152**, 212 (1988); L. S. Kuzmin, P. Delsing, T. Claeson, and K. K. Likharev, Phys. Rev. Lett. **62**, 2539 (1989); R. Wilkins, E. Ben-Jacob, and R. C. Jaklevic, Phys. Rev. Lett. **63**, 801 (1989)

[3]P. J. M. van Bentum, H. van Kempen, L. E. C. van de Leemput, and P. A. A. Teunissen, Phys. Rev. Lett. **60**, 369 (1988); L. J. Geerligs, V. F. Anderegg, C. A. van der Jeugd, J. Romijn, and J. E. Mooij, Europhys. Lett. **10**, 79 (1989)

[4]P. Delsing, K. K. Likharev, L. S. Kuzmin, and T. Claeson, Phys. Rev. Lett. **63**, 1180 (1989)

[5]M. Büttiker and R. Landauer, IBM J. Res. Develop. **30**, 451 (1986)

[6]Yu. V. Nazarov, Zh. Eksp. Teor. Fiz. **95**, 975 (1989)[Sov. Phys. JETP **68**, 561 (1989)]

[7]H. Frauenfelder, *The Mössbauer Effect*, (Benjamin, New York, 1963)

[8]see e.g. M. Tinkham, *Introduction to Superconductivity*, (McGraw–Hill, New York, 1975)

[9]G. Schön, Phys. Rev. **B32**, 4469 (1985); G. Schön and A. D. Zaikin, Phys. Rep. (to appear)

[10]D. V. Averin and A. A. Odintsov, Phys. Lett. **A140**, 251 (1989)

[11]In the Mössbauer problem this corresponds to the fact that the recoil of the entire crystal caused by a gamma emission may be disregarded.

[12]The assumptions made include that $R_T \gg R_Q$, and that the time between subsequent tunneling events is larger than the relaxation time τ_e of the environment, i.e. $I \ll e/\tau_e$. For a study of the R_T-dependence of the I-V-characteristic see: A. A. Odintsov, Zh. Eksp. Teor. Fiz. **94**, 312 (1988) [Sov. Phys. JETP **67**, 1265 (1988)]

[13]Considering the effect of a propagating mode in the junction, a related result was obtained by D. V. Averin and Yu. V. Nazarov (preprint).

[14]A. O. Caldeira and A. J. Leggett, Ann. Phys. (N.Y.) **149**, 374 (1983)

[15]H. Grabert, P. Schramm, and G.-L. Ingold, Phys. Rep. **168**, 115 (1988)

[16]See J. M. Martinis and R. L. Kautz, Phys. Rev. Lett. **63**, 1507 (1989) for such a setup.

Figure Captions

FIG. 1. (a) A current-biased tunnel junction coupled to an external circuit with impedance of leads modeled by a series inductor L and a shunt capacitor C_s. (b) An equivalent voltage-biased junction in the limit $C_s \gg C$.

FIG. 2. The I-V-characteristic of a tunnel junction coupled to an environment characterized by a resistance R (see inset) is shown for $R/R_Q = 0, 0.1, 1, 10$, and ∞.

Fig. 1

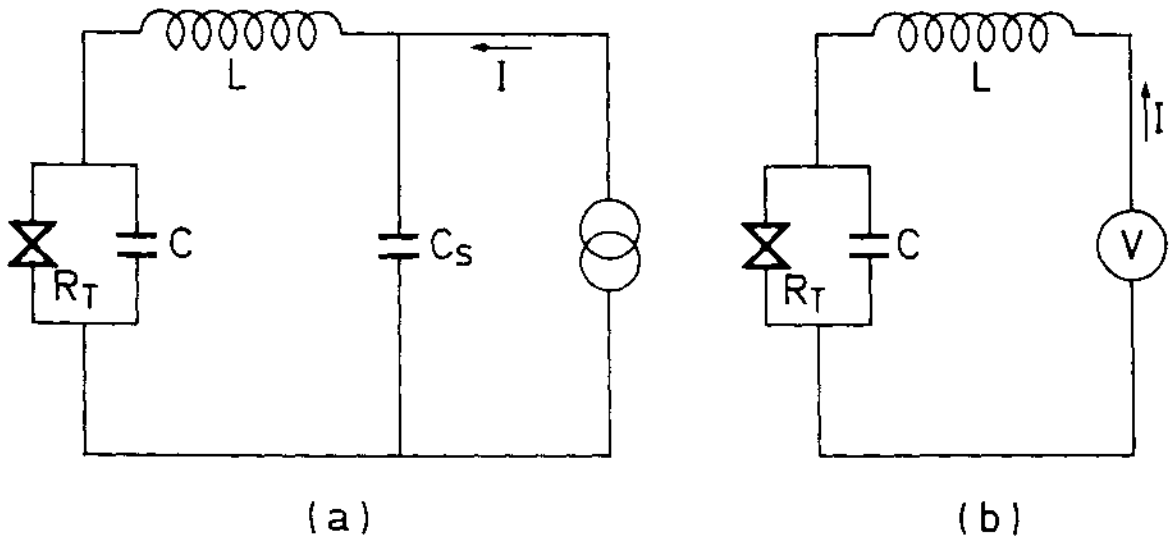

Fig. 2

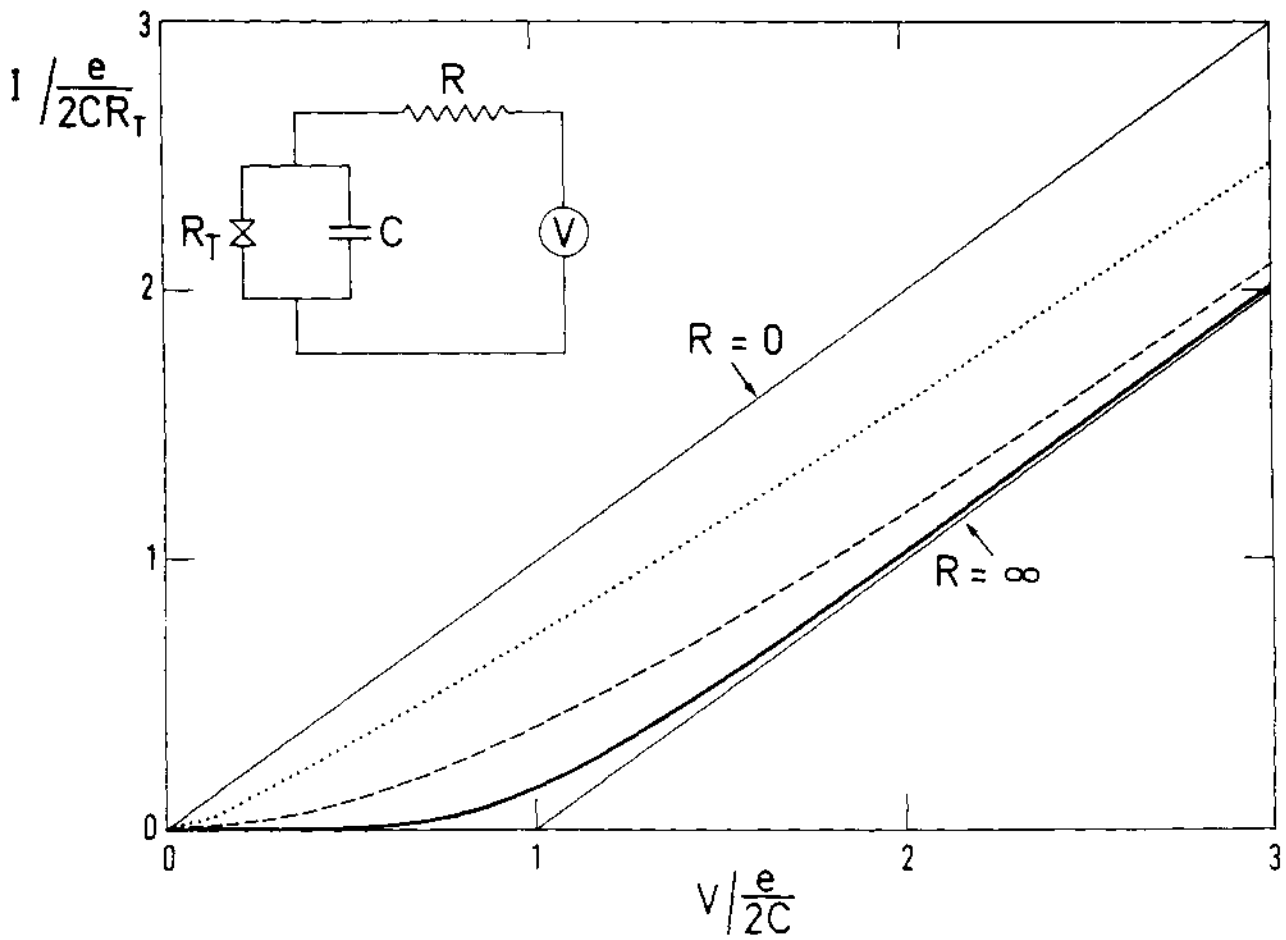

APPENDIX 5.

PAPER 2:

FREQUENCY-LOCKED TURNSTILE FOR SINGLE ELECTRONS

Published in Phys. Rev. Lett. **64**, 2691 (1990)

Referred to as: Geerligs *et al.*, 1990a.

Frequency-locked turnstile device for single electrons.

L.J. Geerligs, V.F. Anderegg, P.A.M. Holweg,[a] J.E. Mooij
Department of Applied Physics, Delft University of Technology,
P.O. Box 5046, 2600 GA Delft, The Netherlands

H. Pothier, D. Esteve, C. Urbina, M.H. Devoret
Service de Physique du Solide et de Résonance Magnétique,
Centre d'Études Nucléaires de Saclay, 91191 Gif-Sur-Yvette, France

We have fabricated an array of ultrasmall tunnel junctions which acts like a turnstile for single electrons. When alternating voltage of frequency f is applied to a gate, one electron is transferred per cycle through the device . This results in a current plateau in the current-voltage characteristic at I=ef. The overall behavior of the device is well explained by the theory of Coulomb blockade of electron tunneling. We discuss the accuracy limitations of this device.

PACS: 73.40.G, 06.20.H, 73.40.R

Submitted to Phys. Rev. Lett. March 2, 1990.

With present-day lithographic techniques it has become possible to fabricate tunnel junctions with capacitance C small enough to make the charging energy of a single electron, $E_C=e^2/2C$, much larger than thermal energies at dilution refrigerator temperatures. Typical capacitances are below 10^{-15} F for junction areas below $(100\ nm)^2$, hence $E_C/k_B>1$ K. Under this condition the discreteness of electron tunneling leads to new phenomena, charging effects, as reviewed by Averin and Likharev.[1] In a pioneering paper Fulton and Dolan [2] confirmed experimentally the existence of charging effects in small circuits of planar tunnel junctions. In linear arrays of small tunnel junctions charge is transferred by mutually repulsing charge-solitons,[3] resulting in time-correlated tunneling events with fundamental frequency I/e. Delsing et al. [4] demonstrated this effect by application of a signal with frequency f, leading to resonances at current levels I=ef and I=2ef. The resonances show up in the differential resistance only. In this paper, we present a new device in which a single electron is transferred per cycle of an externally applied rf signal. In this voltage biased device a current flows which is equal to the frequency times the electron charge. The device is based on a turnstile effect resulting from the Coulomb blockade in linear arrays of tunnel junctions. It opens the possibility of a high accuracy, frequency-determined current standard. In many respects resembling a single electron shift register, the device exemplifies the prospects of using charging effects for practical logic circuits.[5]

The Coulomb blockade of single electron tunneling manifests itself in voltage biased linear arrays as a voltage gap in their current-voltage (I-V) characteristic. This Coulomb gap arises because for an electron to transfer through the array it has to occupy intermediate positions on the metal "islands" between the junctions. For bias voltages well below e/C (C being the junction capacitance) the energy of these intermediate states is higher than the energy of the initial state. Conduction is thus energetically suppressed. Consider the energy of a device constructed, like in our experiment, of both tunnel junctions and true capacitors, biased from several voltage sources. The energy associated with a given electron position is the sum of the capacitive energy for the resulting charge distribution and the work performed by the bias voltage sources.[3] If, under the influence of particular bias conditions, the absolute value of the charge on a junction of the array exceeds a critical charge, an electron can tunnel across this junction. The difference ΔE_k between the final and initial energy for the tunnel event across junction k of the array can be expressed as:

$$\Delta E_k=-e(|Q_k|-Q_{ck})/C_k \qquad (1)$$

where Q_k and C_k are the charge and capacitance of junction k, respectively. The critical charge $Q_{ck}=e/[2(1+C_{ek}/C_k)]$ depends apart from the junction capacitance only on the

equivalent capacitance C_{ek} of the circuit in parallel with junction k. With this concept of a critical charge Q_c the principle of the present experiment can be understood. It is illustrated in Fig. 1. A linear array of 4 junctions of capacitance C is biased by a drive voltage V, which is applied symmetric to ground. The central island, between junctions 2 and 3, is capacitively coupled to a gate voltage V_g.[2,5] If the gate capacitor C_g is chosen to equal C/2, all junctions have the same critical charge for tunneling, Q_c=e/3. For V and V_g within a certain window, the critical charge will be exceeded for the junctions in the left arm, but not for the junctions in the right arm. Once an elementary charge has entered the central island, part of it will polarize the gate capacitor, and the charge on all junctions will be lower than the critical charge. Therefore the elementary charge is trapped on the central island until bias conditions are changed. It is also impossible for another charge to move to the central island. To make the charge leave by the right arm, the gate voltage is decreased. The junctions on the right arm will first exceed the critical charge because of the asymmetry caused by the bias voltage. Cyclically changing the bias conditions by applying an alternating voltage in addition to a dc voltage to the gate capacitor moves one electron per cycle through the chain. We emphasize that after an arbitrary long time, the total charge transferred will be known to within a single electron. The principle will work for a general T-shaped structure of 2n junctions with a gate capacitance of about C/n. However, at least two junctions on each side are needed to avoid the unwanted entering or leaving of a charge.

We will discuss why the stochastic nature of electron tunneling need not perturb the deterministic transfer of electrons through the device. At finite temperature T the tunneling rate is for arbitrary ΔE given by [1]

$$\Gamma=\frac{\Delta E/2E_C}{RC[\exp(\Delta E/k_BT)-1]} \qquad (2)$$

where R is the tunneling resistance of the junction. This shows the two main prerequisites for deterministic electron transfer. The ac cycle should last long enough to let tunneling to and from the central island happen with high probability, i.e. f must be much smaller than $(RC)^{-1}$ to avoid cycles being lost. On the other hand an electron trapped on the central electrode should have a negligible probability to escape by a thermally assisted transfer. At finite temperature there is a tradeoff between the two requirements: a thermally assisted escape will be more probable for lower frequencies. We will discuss the consequences of these limitations more quantitatively below. Finally, we note that eq. (2) is strictly valid only for negligible tunnel conductance. Quantum charge fluctuations associated with a tunnel resistance not much larger than h/e^2 [6,7] generally suppress the charging effects. We have not investigated the consequences of this aspect for the present experiment.

The physical layout of the device is very close to the circuit shown in Fig.1, with 4 junctions of about 0.5 fF and 340 kOhm ($(RC)^{-1}\approx 5$ GHz) and a gate capacitance C_g of 0.3 fF. The values of R and C were determined from the large scale I-V curve,[6] and C_g was determined from the period of the current modulation by the gate voltage. This period ΔV_g yields the gate capacitance as $C_g=e/\Delta V_g$. An important refinement over the circuit of Fig. 1 is the use of two small auxiliary gate capacitances (0.06 fF) to tune out non-integer trapped charges [5] on the remaining two islands. This device was fabricated with nanolithographic methods as described elsewhere,[6] with planar aluminum-aluminum oxide-aluminum junctions. It was thermally anchored to the mixing chamber of a dilution refrigerator, and a magnetic field of 2 Tesla was applied to bring the junctions in the normal (i.e., non-superconducting) state. All leads were low pass filtered by a stage which was also thermally anchored to the mixing chamber. In addition, the gate voltages were strongly attenuated. The gate voltages were applied by room temperature dc voltage sources referenced to cryostat ground. In addition, an ac voltage could be applied to the central gate capacitor. The voltage bias was symmetric with respect to cryostat ground. The measurement was performed with a two-wire method: a FET-opamp circuit with virtually shorted input terminals, in series with voltage source and sample, was used to measure the current.

Fig. 2 shows I-V curves of the device, without ac gate voltage applied (dotted curve) and with ac gate voltage of different frequencies between 4 and 20 MHz. Without ac gate voltage, a large zero-current Coulomb gap is present. With ac gate voltage of frequency f, wide current plateaus develop inside the Coulomb gap at a current level I=ef. The plateaus even extend to voltages outside the gap. In Fig. 2 the dc gate voltages were the same for each curve, the ac amplitude was adjusted for the widest plateau, which required more power at higher frequencies. Thermometer temperature varied from 10 to 40 mK, depending on applied ac power. Good plateaus were observed up to 40 Mhz, but only for frequencies below about 10 MHz were part of the plateaus flat within experimental current noise (about 0.05 pA, DC to 1 Hz). Fig. 3 shows the dependence of the I-V curve on ac amplitude at a frequency of 5 MHz. Clearly, the height of the plateaus is not dependent on the ac amplitude, although the width is. For high amplitudes, we have observed a tendency to form plateaus at I=2ef. Another sample with n=3 junctions in each arm showed the same behavior, although with somewhat rounded plateaus. We attribute this rounding to the larger capacitances (about 2 fF) of the junctions in this device.

A gate voltage adjustment was necessary to obtain wide plateaus. A suitable procedure was to maximize the Coulomb gap without ac voltage, using the auxiliary gate voltages. Next the current versus dc gate voltage would be recorded at fixed bias voltage, with ac gate voltage applied. This shows an oscillating behavior with minima

and maxima at I=ef, I=2ef or even higher multiples, depending on the ac amplitude. An example is shown in the inset of Fig. 2. The I-V curves of Fig. 2 were obtained with dc gate voltage in the middle of a I-V_g plateau at I=ef, corresponding to half the elementary charge induced on the gate capacitor. When misadjusting both auxiliary gates on purpose, we could still obtain plateaus in the I-V curve, but not as wide as in Fig. 2.

The dependence of the I-V curves on ac amplitude, as shown in Fig. 3, are very well simulated by numerical calculations based on eq. (1) and (2). Results are shown in the same figure as dashed curves on the right of the measurements. No fitting parameters were used. The only adjustments made were assuming 1 dB attenuation in the ac voltage line to be present in addition to the known attenuators, and introducing a higher temperature (50-75 mK) than the thermometer indicated during the experiments (10-20 mK) to roughly account for remaining noise or heating of the sample.

In Table 1 we compare the current step height I_s, obtained by taking half the measured current distance between the positive and the negative plateaus, with the prediction I_s=ef. Up to 10 MHz, regions could be found (around 0.15 mV) where the plateau was flat within the current noise. In those cases about 50 points were taken in the central parts of these regions to determine the average current with its standard deviation σ_m. Above 10 MHz, the current level at the inflexion point was taken in a similar way. The measured current step coincides with ef within experimental accuracy, which is around 0.3 %. We attribute the deviation of more than $3\sigma_m$ at 20 and 30 MHz to the difficulty of determining the inflexion point. To discuss the expected intrinsic accuracy of the current step height, we return to the example shown in Fig. 1. For an electron transfer in the circuit shown in Fig. 1 the first tunnel event of each half of the cycle ($\Delta E=-0.1e^2/C$) can occur in two junctions with a rate $\Gamma=(10RC)^{-1}$. For a square wave modulation this yields a probability to miss a cycle of about $\exp(-\Gamma/f)=\exp(-1/10fRC)$. For the device used in the experiments, $(RC)^{-1}\approx 5$ GHz, so at 5 MHz this probability is $\exp(-100)\approx 10^{-44}$, while at 50 MHz it is already about 10^{-5}. Obviously, the required accuracy puts an upper limit to the allowed frequency. Next, to estimate the effect of thermal fluctuations, we compare the rate for unwanted tunneling events, $\tilde{\Gamma}$, with the one for favorable events, Γ. From eq. (2) we find that the ratio is of order $\exp(-\Delta E/k_BT)$. For an accuracy of e.g. 10^{-8}, it is necessary to have $\tilde{\Gamma}/f\approx 10^{-8}$, which combined with the requirement $\Gamma/f=10^3$ yields $\exp(-\Delta E/k_BT)=10^{-11}$, or $k_BT\approx\Delta E/25$. Since typically ΔE is on the order of $0.1e^2/C$, for the present device this corresponds to temperatures of about 15 mK. Comparable problems with unwanted transitions could arise from insufficient screening from noise and interference in the experiments. The simulations in Fig. 3 suggest that in the present experiment these disturbances seem to be described well by a temperature of not more than 50 mK, which is already close to the temperature requirement derived above. More careful

screening is possible. These limitations are relaxed by the use of smaller junctions. For junctions of 0.1 fF with the same resistance, the requirement that $f<10^{-3}/RC$ corresponds to f<30 MHz and $k_BT<0.1e^2/C$ to T<75 mK.

In conclusion, we have fabricated a device producing a current clocked by an externally applied high frequency voltage. Charge transfer is controlled at the level of single electrons. The theoretical limitations on the accuracy are very promising. The good agreement between the I-V curves and the theory shows that the dc and ac behavior of small capacitance normal metal tunnel junctions is well understood, and that device behavior can be reliably predicted.

Acknowledgements

This work was supported by the Dutch Foundation for Fundamental Research on Matter (FOM) and the Commissariat à l'Energie Atomique (CEA). We thank U. Geigenmüller, K. Likharev, M. Peters and G. Schön for valuable discussions, and P.F. Orfila for technical assistance.

[a]affiliation: Centre for Submicron Technology

References

1. D.V. Averin and K.K. Likharev, in "Quantum Effects in Small Disordered Systems", edited by B. Al'tshuler, P. Lee, and R. Webb (Elsevier, Amsterdam, to be published).

2. T.A. Fulton and G.J. Dolan, Phys. Rev. Lett. **59**, 109 (1987).

3. K.K. Likharev, N.S. Bakhvalov, G.S. Kazacha, and S.I. Serdyukova, IEEE Trans. Magn. **25**, 1436 (1989).

4. P. Delsing, K.K. Likharev, L.S. Kuzmin, and T. Claeson, Phys. Rev. Lett. **63**, 1861 (1989).

5. K.K. Likharev, IBM J. Res. Develop. **32**, 144 (1988).

6. L.J. Geerligs, V.F. Anderegg, C.A. van der Jeugd, J. Romijn, and J.E. Mooij, Europhys. Lett. **10**, 1 (1989).

7. G. Schön and A.D. Zaikin, Quantum Coherent Effects, Phase Transitions, and the Dissipative Dynamics of Ultra Small Tunnel Junctions, preprint submitted to Physics Reports, and references therein.

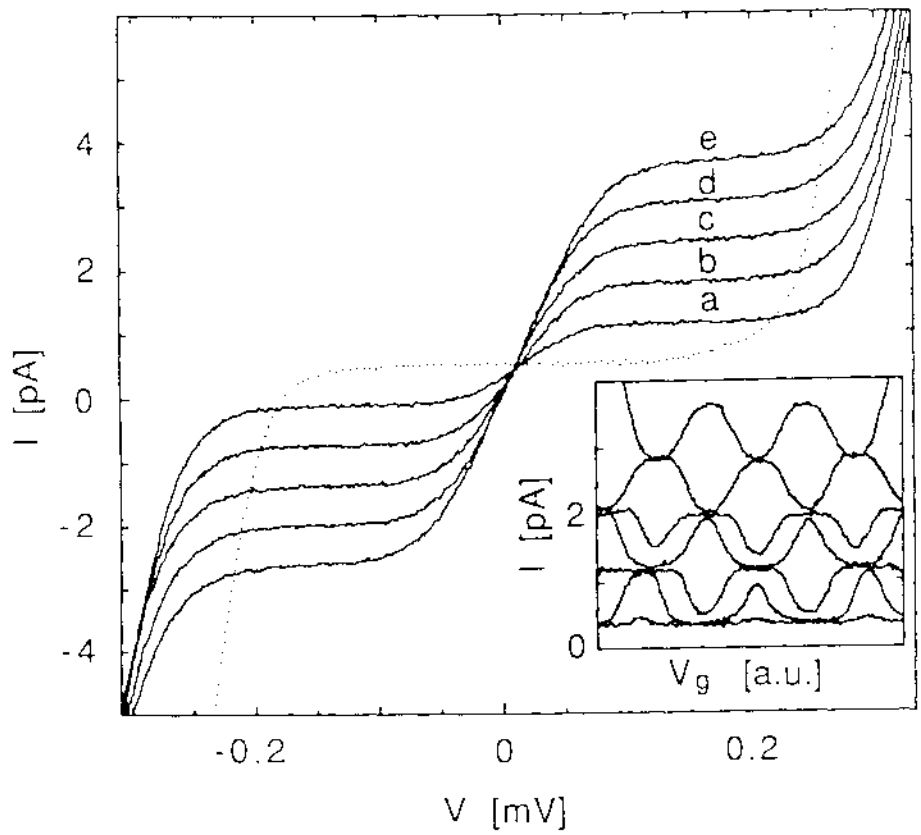

Figure 2.

Current-voltage characteristics without ac gate voltage (dotted) and with applied ac gate voltage at frequencies f from 4 to 20 Mhz in 4 Mhz steps (a-e). Current plateaus are seen at I=ef. The inset shows current versus dc gate voltage characteristics for f=5 MHz. The curves tend to be confined between levels at I=nef and I=(n+1)ef, with n integer. The bias voltage was fixed at 0.15 mV. For the bottom curve, which is nearly flat, the ac gate voltage amplitude is 0. For the other curves the calculated ac amplitude at the sample increases from 0.60e/C for the lowest one to 3.4e/C for the upper one, where e/C=0.30 mV.

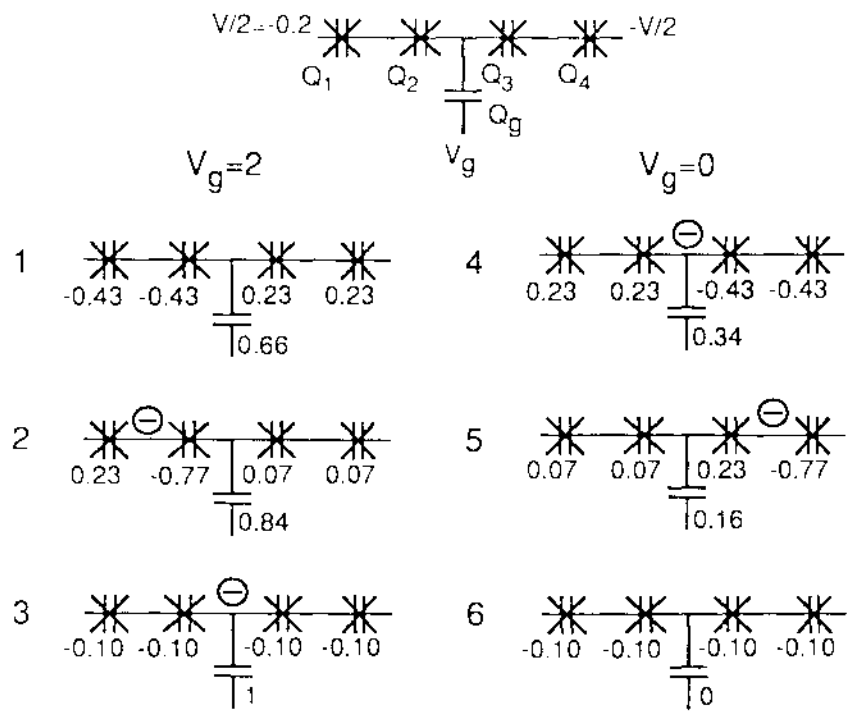

Figure 1.

Principle of controlled single electron transfer through a linear array of small tunnel junctions. Junctions, with capacitance C, are denoted by crossed capacitor symbols, the gate voltage V_g is applied via a true (non-tunneling) capacitance C_g. If $C_g=C/2$, tunneling across any junction can only occur if for that junction $|Q|>Q_c$, with $Q_c=e/3$. The voltages and charges are indicated in units of e/C and e. 1-6 indicate consecutive times in the cycle. Left: First half of the cycle, $V_g=2$. An elementary charge (- in a circle) ends up trapped on the central electrode. Right: Second half of the cycle, $V_g=0$. The charge can only leave on the right hand side. No further tunneling can occur in the emptied array .

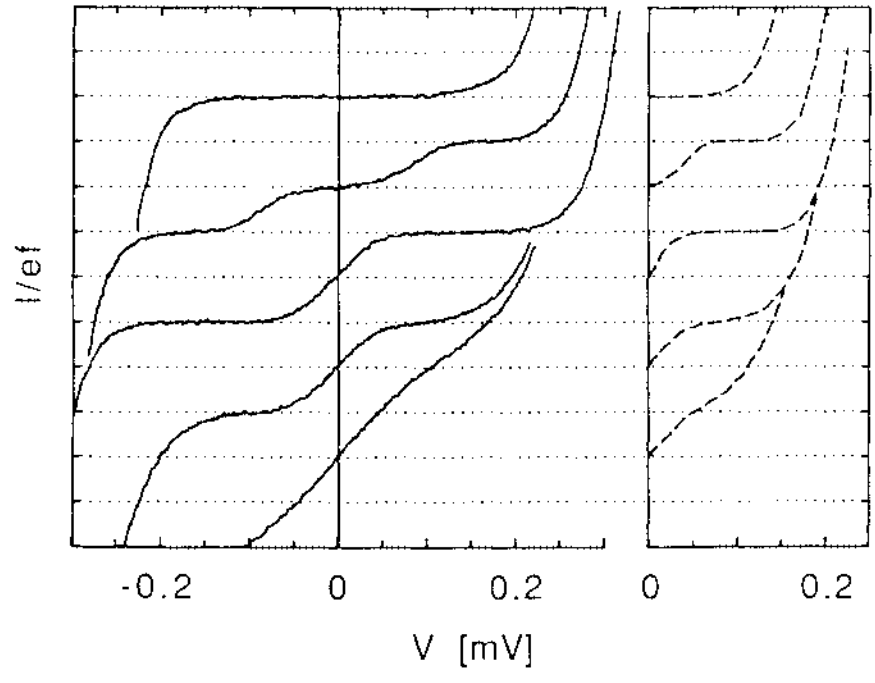

Figure 3.

Current-voltage characteristics at f=5 Mhz for different levels of applied ac gate voltage. The dotted horizontal lines are at intervals ef=0.80 pA.The I-V curves have all been offset in x-direction by 15 μV to compensate for opamp voltage offset in the current measuring circuit, and individually in y-direction to display them more clearly. From top to bottom the calculated ac voltage amplitudes at the sample are 0, 0.60, 0.95, 1.50, and 1.89, expressed in units of e/C=0.30 mV. On the right, the corresponding simulated I-V curves are shown as dashed lines. For these calculations, 1 dB extra ac attenuation was assumed, and temperatures of 50 mK (upper 3 curves) and 75 mK (lower 2) were used.

Table 1. Comparison of the measured current plateau I_s with the relation I_s=ef. σ_m is the standard deviation of I_s.

f (MHz)	I_s (fA)	σ_m (fA)	ef-I_s (fA)
4.012	635	2	8
6.011	967	2	-4
8.031	1287	2	0
10.040	1610	2	-1
12.029	1930	2	-3
14.028	2243	2	5
16.026	2560	3	7
18.063	2890	3	4
20.011	3196	3	10
30.036	4856	3	-44

REFERENCES

Abragam, A., 1961, *The principles of Nuclear Magnetism*, Clarendon Press, p. 93-96.

Anderegg, V.F., L.J. Geerligs, J.E. Mooij, H. Pothier, D. Esteve, C. Urbina and M.H. Devoret, 1990, Physica **B 165& 166**, 61.

Averin, D.V., and K.K. Likharev, 1986, J. Low Temp. Phys. **62**, 345.

Averin, D.V., and K.K. Likharev, 1991, in *Quantum effects in Small Disordered Systems*, B.L. Altshuler, P.A. Lee, R.A. Webb (eds), Elsevier, to appear.

Averin, D.V., and A.A. Odintsov, 1989, Sov. Phys. JETP **69**, 766; Averin, D.V., and A.A. Odintsov, 1989, Phys. Lett. **A 140**, 251.

Averin, D.V., and Yu. V. Nazarov, 1990, Phys. Rev. Lett. **65**, 2523.

Averin, D.V., Yu. V. Nazarov and A.A. Odintsov, 1990, Physica **B 165& 166**, 945.

Beenakker, C.W., H. van Houten and A.A.M. Staring, 1991, in *Granular Nanoelectronics*, D.K. Ferry (ed), NATO ASI Series B, Plenum Press, to appear.

Büttiker, M., and R. Landauer, 1986, IBM J. Res. Devel. **30**, 451.

Büttiker, M., Phys. Rev. **B 36**, 3548 (1987).

Cleland, A.N., J.M. Schmidt and J. Clarke, 1990, Phys. Rev. Lett. **64**, 1565.

Cohen, M.H., L.M. Falicov and J.C. Phillips, 1962, Phys. Rev. Lett. **8**, 316.

Cohen-Tannoudji, C., B. Diu, F. Laloë, 1973, *Mécanique Quantique*, Hermann.

Delsing, P., K.K. Likharev L.S. Kuzmin and T.D. Claeson, 1989, Phys. Rev. Lett. **63**, 1180.

Delsing, P., K.K. Likharev, L.S. Kuzmin and T. Claeson, 1989, Phys. Rev. Lett. **63**, 1861

Delsing, P., 1990, *Single Electron Tunneling in Ultrasmall Tunnel Junctions*, PhD Thesis, Göteborg.

Delsing, P., D.B. Haviland, T. Claeson, K.K. Likharev and A.N. Korotkov, 1991, submitted for publication to Proceedings of SQUID'91, H. Koch (ed), Springer, Heidelberg.

Devoret, M.H., D. Esteve, H. Grabert, G.-L. Ingold, H. Pothier and C. Urbina, 1990a, Phys. Rev. Lett. **64**, 1824.

Devoret, M.H., D. Esteve, H. Grabert, G.-L. Ingold, H. Pothier and C. Urbina, 1990b, Physica **B 165& 166**, 977.

Devoret, M., D. Esteve, Ph. Lafarge, P.-F. Orfila, H. Pothier and C. Urbina, 1991, Pour la Science **159**, 86; to be published in Images de la Physique.

Dolan, G.J., and J.H. Dunsmuir, 1988, Physica **B152**, 7.

Eigler, D.M., and E.K. Schweizer, 1990, Nature **344**, 524.

Falci, G., V. Bubanja and G. Schön, 1991, preprint.

Fulton, T.A., and G.J. Dolan, 1987, Phys. Rev. Lett. **59**, 109.

Fulton, T.A., P.L. Gammel, D.J. Bishop, L.N. Dunkleberger and G.J. Dolan, 1989, Phys. Rev. Lett. **63**, 1307.

Geerligs, L.J., V.F. Anderegg, C.A. van der Jeugd, J. Romijn and J.E. Mooij, 1989, Europhys. Lett. **10**, 79.

Geerligs, L.J., V.F. Anderegg, P. Holweg, J.E. Mooij, H. Pothier, D. Esteve, C. Urbina and M.H. Devoret, 1990a, Phys. Rev. Lett. **64**, 2691.

Geerligs, L.J., V.F. Anderegg, J. Romijn and J.E. Mooij, 1990b, Phys. Rev. Lett. **65**, 377.

Geerligs, L.J., D.V. Averin and J.E. Mooij, 1990c, Phys. Rev. Lett. **65**, 3037.

Geerligs, L.J., 1990, *Classical and Quantum Charge Dynamics in Small Tunnel Junctions*, PhD Thesis, T.U. Delft.

Geerligs, L.J., S.M. Verbrugh, P. Hadley and J.E. Mooij; H. Pothier, P. Lafarge, C. Urbina, D. Esteve and M.H. Devoret, 1991, submitted for publication to Z. Phys. B.

Geigenmüller, U., and G. Schön, 1989, Europhys. Lett. **10**, 765.

Glattli, D.C., C. Pasquier, U. Meirav, F.I.B. Williams, Y. Jin and B. Etienne, 1991, submitted for publication to Z. Phys. B.

Glazman, L.I., and R.I. Shekhter, 1989, J. Phys. Condensed Matter, **1**, 5811.

Goy, P., J.M. Raymond, M. Gross and S. Haroche, 1983, Phys. Rev. Lett. **50**, 1903.

Grabert, H., G.-L. Ingold, M.H. Devoret, D. Esteve, H. Pothier and C. Urbina, 1991a, in Proceedings of the Adriatico Research Conference on *Quantum Fluctuations in Mesoscopic and Macroscopic Systems*, Triest, July 1990, H.A. Cerdeira *et al.* (eds), World Scientific, Singapore, p. 199.

Grabert, H., G.-L. Ingold, M.H. Devoret, D. Esteve, H. Pothier and C. Urbina, 1991b, Z. Phys. **B 84**, 143.

Haviland, D.B., L.S. Kuzmin, P. Delsing, K.K. Likharev and T. Claeson, 1991, submitted for publication to Z. Phys. B.

Ingold, G.L., and H. Grabert, 1991, Europhys. Lett. **14**, 371.

Ingold, G.L., P. Wyrowski and H. Grabert, 1991, submitted for publication to Z. Phys. B.

Josephson, B.D., 1969, in *Superconductivity*, R.D. Parks (ed), Marcel Dekker, New York, p. 423.

Kittel, C., 1963, *Introduction to Solid State Physics*, John Wiley.

Klauder, J.R., and B.-O. Skagerstam, 1985, *Coherent States*, World Scientific, Singapore.

von Klitzing, K., 1986, Rev. Mod. Phys. **58**, 519.

Kouwenhoven, L.P., A.T. Johnson, N.C. van der Vaart, A. van der Enden, C.J.P.M. Harmans and C.T. Foxon, 1991, submitted for publication to Z. Phys. B.

Lafarge, P., H. Pothier, E.R. Williams, D. Esteve, C. Urbina and M.H. Devoret, 1991, submitted for publication to Z. Phys. B.

Likharev, K.K., and A.B. Zorin, 1985, J. Low Temp. Phys. **59**, 347.

Likharev, K.K., 1988, IBM J. Res. Dev. **32**, 144.

Likharev, K.K., N.S. Bakhalov, G.S. Kazacha and S.I. Serdyukova, 1989, IEEE Trans. Mag. **25**, 2.

Martinis, J.M., and R.L. Kautz, 1989, Phys. Rev. Lett. **63**, 1507.

Nazarov, Yu.V., 1989, Zh. Eksp. Teor. Fiz. **95**, 975.

Nazarov, Yu.V., 1991, Phys. Rev. **B 43**, 6220.

Niemeyer, J., 1974, PTB-Mitt. **4**, 251.

Niu, Q., 1990, Phys. Rev. Lett. **64**, 1812.

Pothier, H., P. Lafarge, P.F. Orfila, C. Urbina, D. Esteve and M.H. Devoret, 1991a, Physica **B 169**, 573.

Pothier, H., P. Lafarge, P.F. Orfila, C. Urbina, D. Esteve and M.H. Devoret, 1991b, submitted for publication to Europhys. Lett.

Roman, P., 1965, *Advanced Quantum Theory*, Addison-Wesley, p. 254.

Roukes, M.L., M.R. Freeman, R.S. Germain, R.C. Richardson and M.B. Ketchen, 1985, Phys. Rev. Lett. **55**, 422.

Shields, J.Q., R.F. Dziuba and H.P. Layer, 1989, IEEE Trans. Instrum. Meas. **38**, 249.

Schiff, L.I., 1955, *Quantum Mechanics*, Mc-Graw Hill.

Urbina, C., H. Pothier, P. Lafarge, P.F. Orfila, D. Esteve and M.H. Devoret; L.J. Geerligs, V.F. Anderegg, P.A.M. Holweg and J.E. Mooij, 1991a, IEEE Trans. Mag. **27**, 2578.

Urbina, C., P. Lafarge, H. Pothier, D. Esteve and M.H. Devoret, 1991b, submitted for publication to Proceedings of SQUID'91, H. Koch (ed), Springer, Heidelberg.

Van Dyck, R.S. Jr., P.B. Schwinberg, and H.G. Dehmelt, 1986, Phys. Rev. **D 34**, 722.

Wellstood, F.C., 1988, *Excess Noise in the dc SQUID; 4.2 K to 20 mK*, PhD Thesis, Berkeley; F.C. Wellstood, C. Urbina and J. Clarke, 1989, Appl. Phys. Lett. **54**, 2599.